ERRATUM

In de figuren op de pagina's 34 t/m 37 zijn bij het vermenigvuldigen enkele grijze lijntjes weggevallen.
Daarom treft u deze hierbij nogmaals in een verbeterde versie losbladig aan.

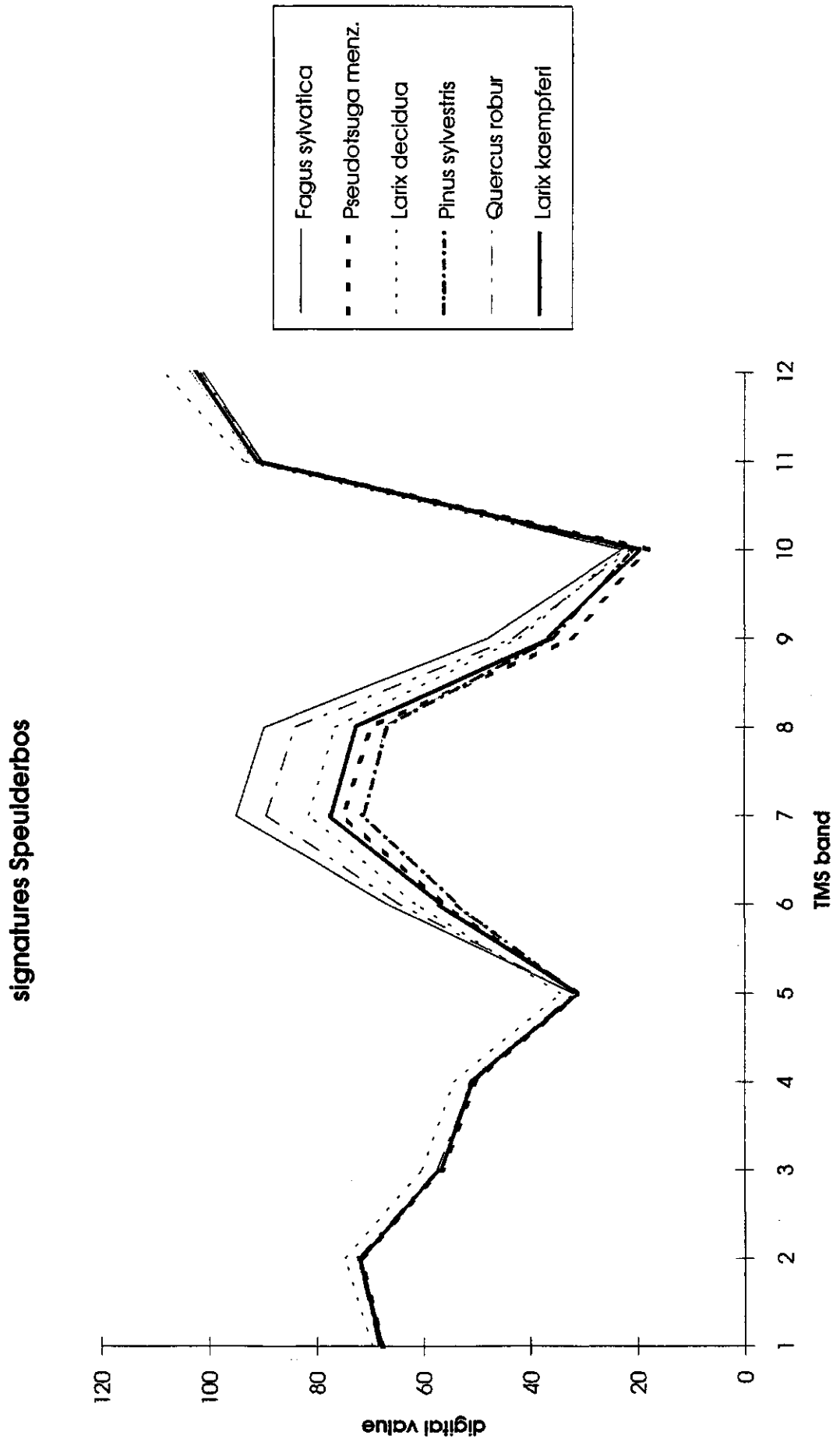

Figure 6.1a. Signatures Speulderbos for the optical data.

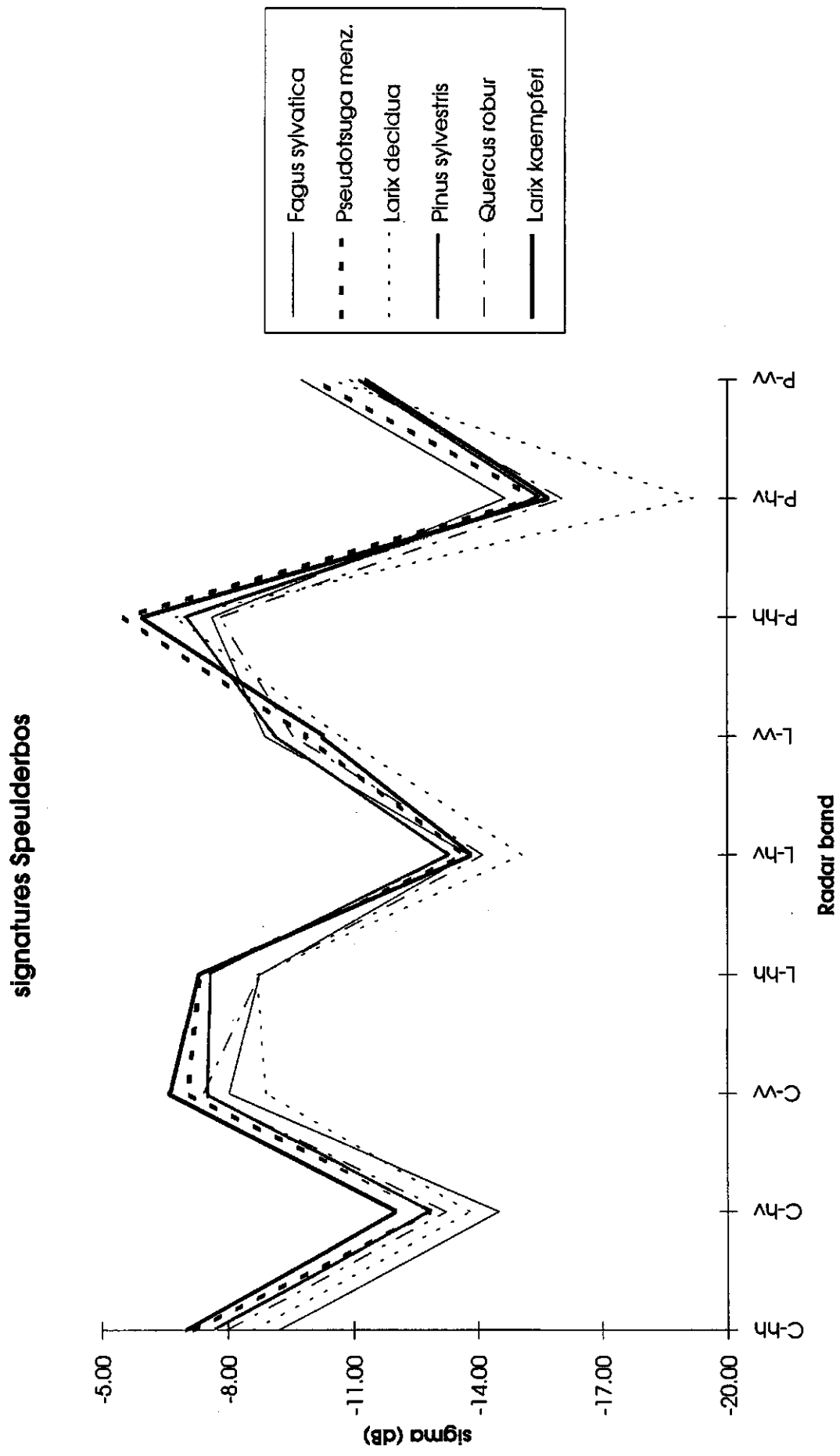

Figure 6.1b. Signatures Speulderbos for the microwave data.

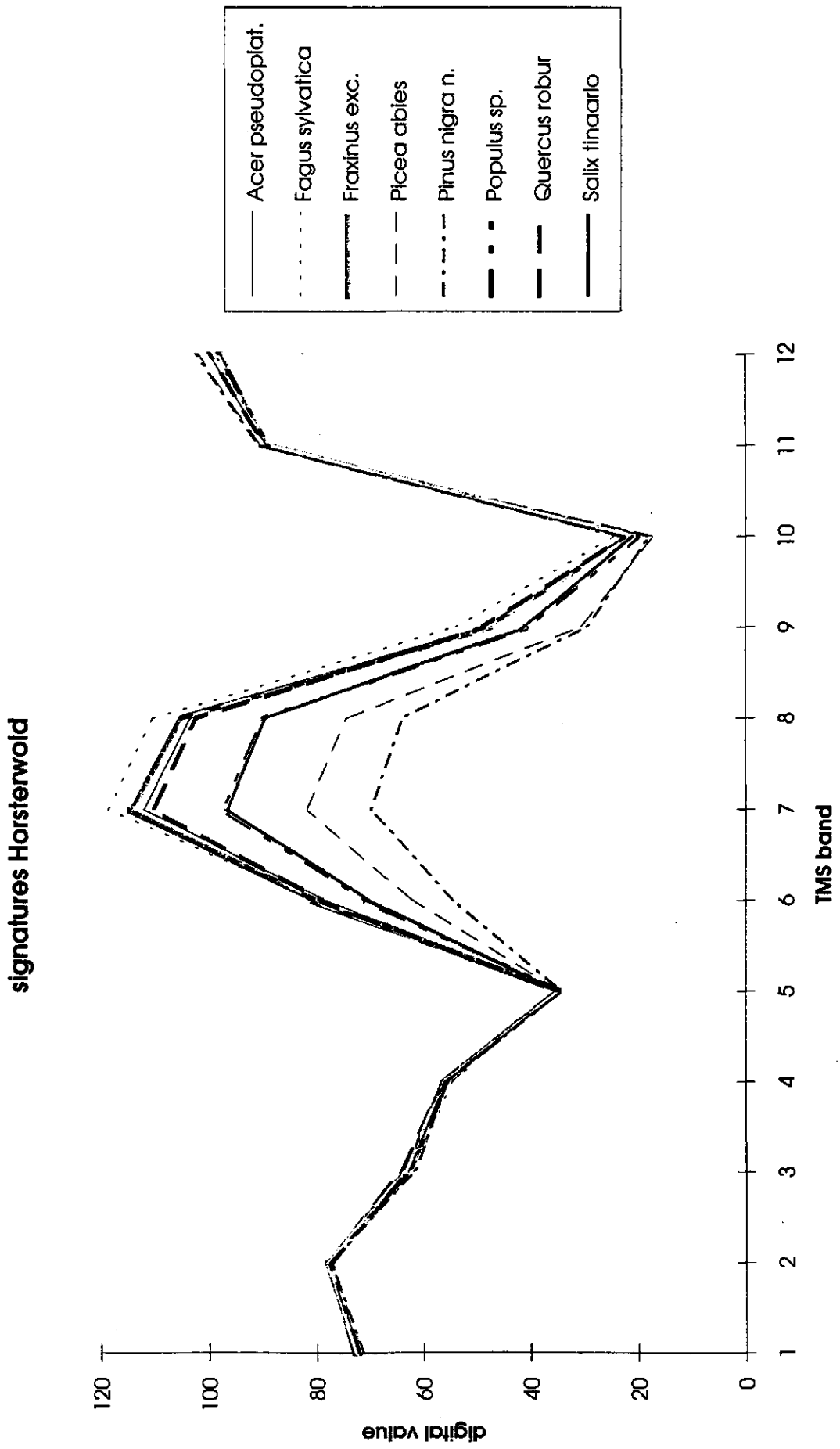

Figure 6.2a. Signatures Horsterwold for the optical data.

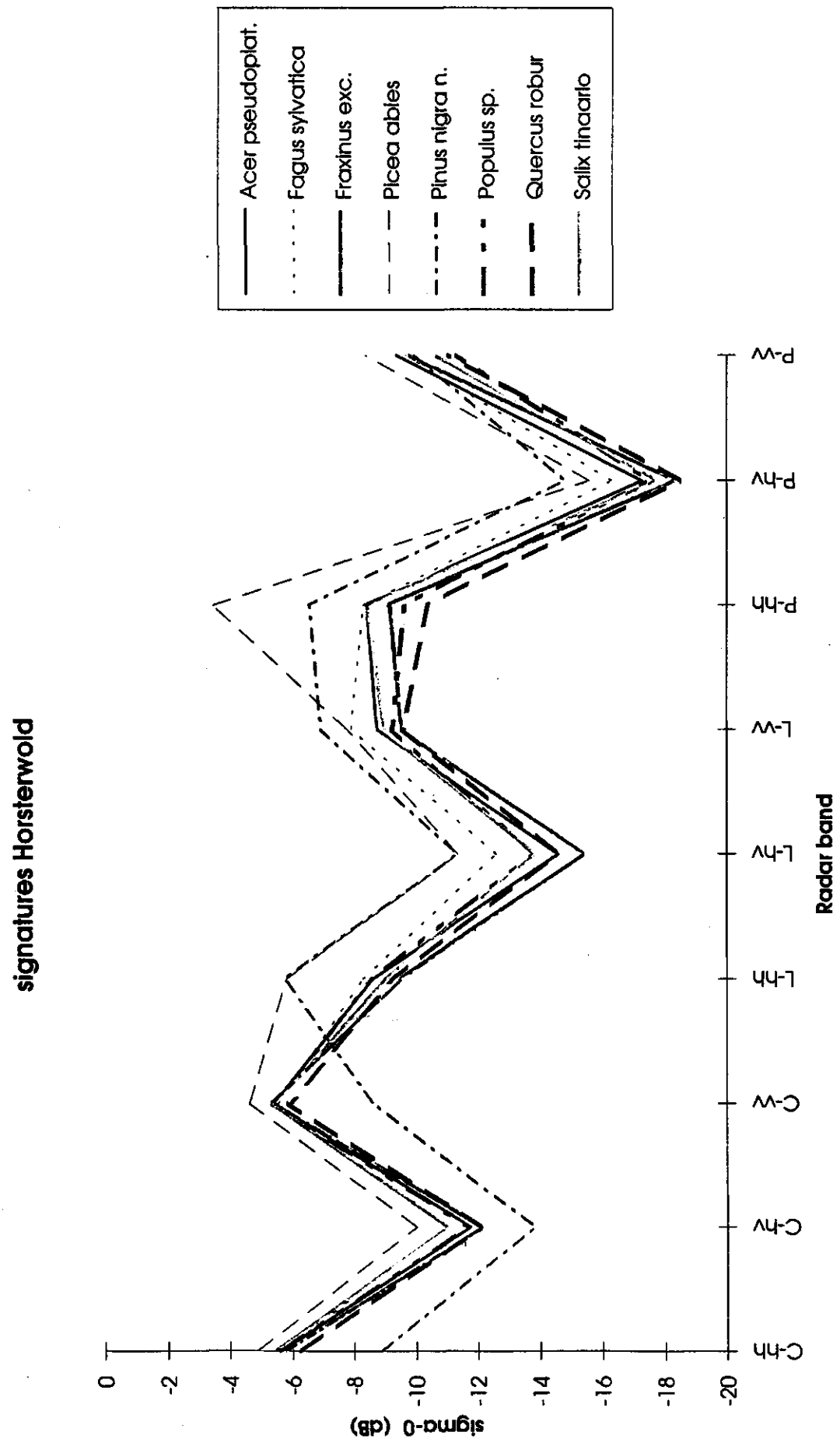

Figure 6.2b. Signatures Horsterwold for the microwave data.

Combining optical and microwave remote sensing data of forest vegetation

MAC Europe 1991

G. van Maren
C. Varekamp

Supervisors: D.H. Hoekman
J.J. van der Sanden

RAPPORT 33

Februari 1993

Vakgroep Waterhuishouding
Nieuwe Kanaal 11, 6709 PA Wageningen

ISSN 0926-230X

CONTENTS

Part II: Literature study on optical and microwave models

Preface

This report is the result of a 5 months thesis subject in Remote Sensing carried out at the Department of Water Resources. The thesis has been written in English because researchers abroad are also interested in the subject.

We would like to thank our supervisors dr.ir. D.H. Hoekman and ir. J.J. van der Sanden for their comments on this report. We are also grateful to ir. M. Vissers for his technical support and ir. Otten of the departement of Mathematics for helping us with the SAS system. Finally we would like to thank Mrs L. Roepke for helping us with the English language.

Summary

In this study the possibilities for a combined (synergetic) use of optical and microwave remote sensing data of forest vegetation were examined.

Within the framework of the MAC Europe campaign, airborne TMS (Thematic Mapper Simulator) and airborne C-L-P band SAR (Synthetic Aperture Radar) data over two forest areas in the Netherlands were registered.

First variance analysis, signature analysis and discriminant analysis were performed in order to assess the usefulness of each band and combinations of bands for discriminating forest classes. Combining optical and microwave data improved forest classification results in most cases.

Next the empirical relationships between optical/microwave data and forest parameters were examined. Microwave P-band data gave some relationships with forest parameters for all stands independent of forest class. Optical data were highly correlated with forest parameters but for Fagus sylvatica only.

Also a literature study on optical and microwave remote sensing models was conducted. One microwave scattering model was used to model the interaction of microwaves with two Populus species.

Part I:

Analysis of optical and microwave data

1 INTRODUCTION

During the summer of 1991 a Multisensor Airborne Campaign, designated MAC Europe '91, was carried out by the National Aeronautics and Space Administration (NASA). The joint scientific aims for MAC Europe were to use advanced remote sensing techniques to document Earth surface properties and to better understand the processes determining those properties.
Specific objectives for MAC Europe include characterizing the radar response of forests in order to infer biomass and other structural properties of the forest, relating high spectral resolution reflectances to surface chemical composition and vegetation stress, mapping surface geology, examining ocean circulation patterns, investigation of soil moisture and surface hydrological properties, exploring the multispectral properties of volcanic terrains, and calibrating and inter-calibrating airborne remote sensing instruments.

The main objective of this study is to investigate the possibilities of a combined (synergetic) use of optical and microwave remote sensing data for forest vegetation studies.

Within the framework of the MAC Europe campaign, a DC-8 aircraft carrying the three frequency (C-,L- and P-band), full polarimetric Synthetic Aperture Radar (SAR) and the ER-2 aircraft carrying the Thematic Mapper Simulator (TMS) performed overflights over the Horsterwold and the Speulderbos sites in the Netherlands. SAR-images acquired on the 3rd of July 1991 and TMS-images acquired on the 5th of July 1991 of both the Horsterwold and the Speulderbos are used in this study.

Synergy has been studied for its significance in the following:

1. Classification of forest classes.
2. Estimation of biophysical forest parameters by means of empirical relationships.
3. Microwave and optical remote sensing models.

On microwave and optical remote sensing models a separate literature study has been conducted to get an overall idea of the possibility of merging radar data with optical data to derive biophysical information about forest vegetation.

This report consists of two parts. Part I contains an analysis of the MAC-Europe data. Here chapter 2 provides an introduction to the basic principles of optical and microwave remote sensing. Chapter 3 describes the possible use of optical and microwave remote sensing. In chapter 4 a description is given of the Horsterwold and Speulderbos study areas as well as specifications of the TMS and AIRSAR systems. Chapter 5 provides the methods used in this study. In chapter 6 the results are presented and discussed. Finally in Chapter 7 conclusions are drawn.
Part II contains the literature study on microwave and optical remote sensing models.

2 PRINCIPLES OF OPTICAL AND MICROWAVE REMOTE SENSING

A remote sensing system using electromagnetic radiation has four components:

- a source
- interaction with the earth's surface
- interaction with the atmosphere
- a sensor (figure 2.1).

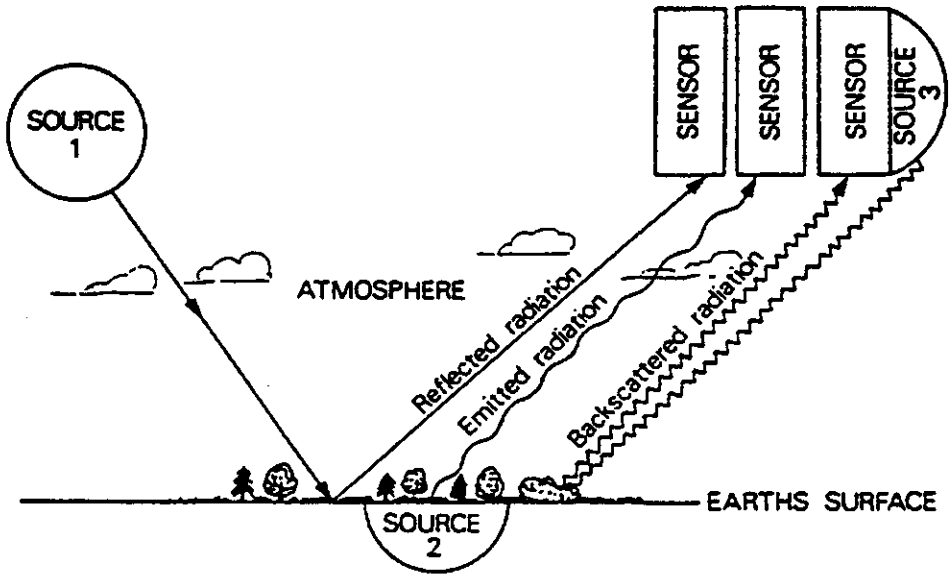

Figure 2.1. A remote sensing system (Curran, 1985).

The link between the components of the remote sensing system is electromagnetic radiation. This radiation occurs as a continuum of wavelengths and frequencies from short wavelength, high frequency cosmic waves to long wavelenght, low frequency radio waves (figure 2.2).

The TMS (Thematic Mapper Simulator) operates in the optical region of the electromagnetic spectrum. This region includes visible and near infrared radiation in the waveband 0.4 μm - 3 μm.

The SAR (Synthetic Aperture Radar) operates in the microwave region of the electromagnetic spectrum. No firm definition exists for the microwave region of the electromagnetic spectrum. A reasonable convention is that it extends from 0.3 to 300 GHz or 1m to 1mm in wavelength (Ulaby, 1981).

Optical and microwave remote sensing will be treated in further detail in sections 2.1 and 2.2.

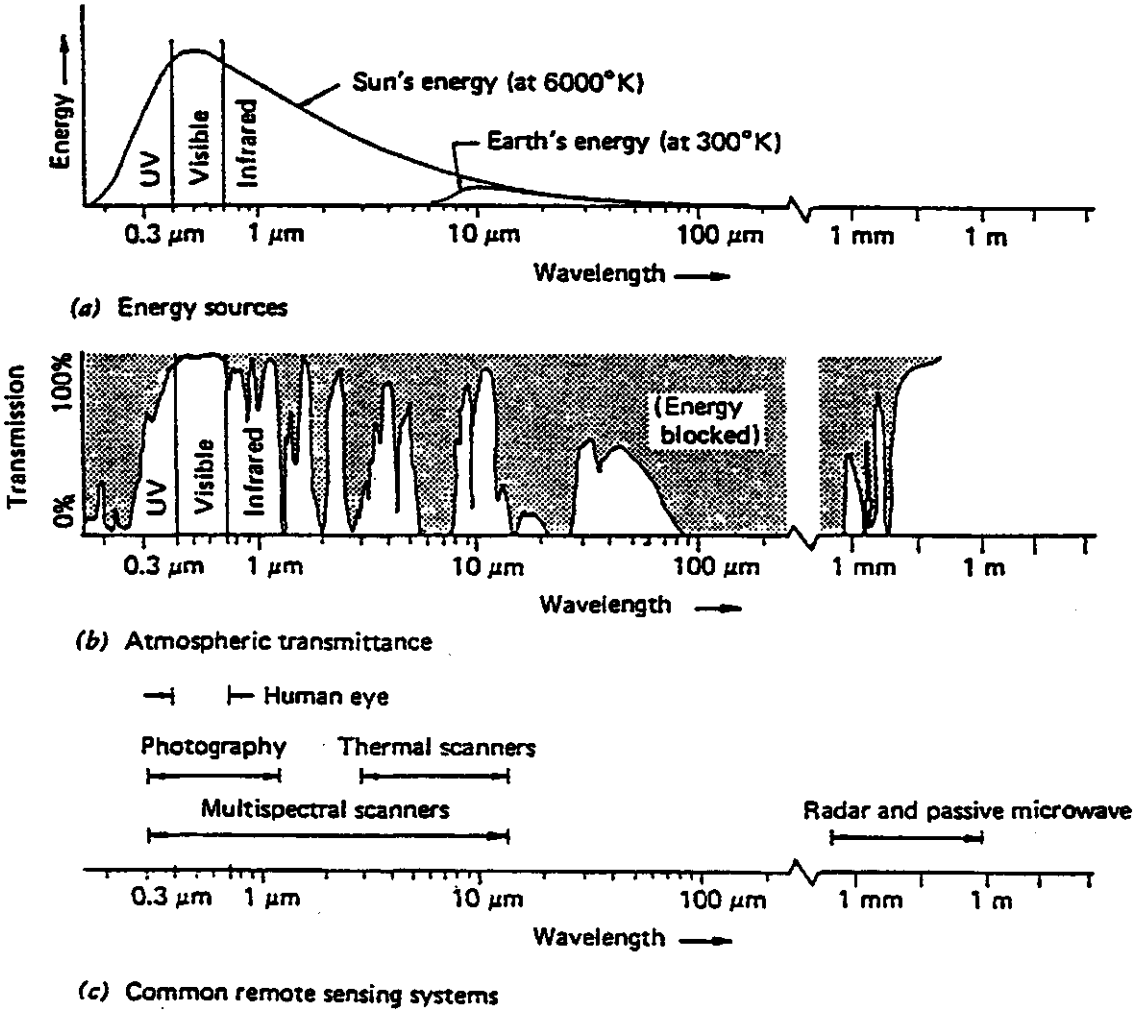

Figure 2.2. Spectral characteristics of (a) energy sources, (b) atmospheric effects, (c) sensing systems (Lillesand, 1987)

2.1 Optical remote sensing

Source

The source in an optical remote sensing system is the sun. The sun radiates high frequency short wavelengths of electromagnetic radiation and radiation at these wavelengths is high in energy (figure 2.2a).

Interaction with vegetation

The electromagnetic radiation interacts with vegetation, soil, water and urban areas. The radiation is either reflected, absorbed or transmitted. Since this report is concerned with forest vegetation, only the interaction with the vegetation is discussed.

The spectral reflectance of a vegetation canopy varies with wavelength. This is due to the reflectance properties of the leaves. A leaf is built of layers of structural fibrous organic matter, containing pigmented, water-filled cells and air spaces.
Because of the pigmentation (chlorophyl), blue and red light (≈ 0,44 μm and ≈ 0.65 μm) are absorbed strongly for photosynthesis. Green light (≈ 0.55 μm) is also absorbed but less than blue and red. In the near infrared spectrum reflection of the leaf is controlled by the structure of the spongy mesophyll tissue. Very little of this infrared energy is absorbed internally. Most of it (up to 60%) is reflected or transmitted (figure 2.3).

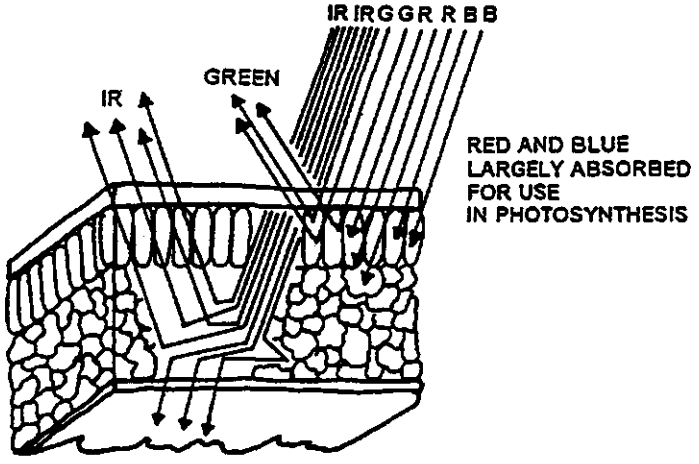

Figure 2.3. Interaction of structure with visible and near-infrared radiation. (Campbell, 1987)

The combined effects of leaf pigments and physiological structure give all healthy green leaves their characteristic reflectance properties: low reflectance of red and blue light, medium reflectance of green light and high reflectance of near infrared radiation (figure 2.4).

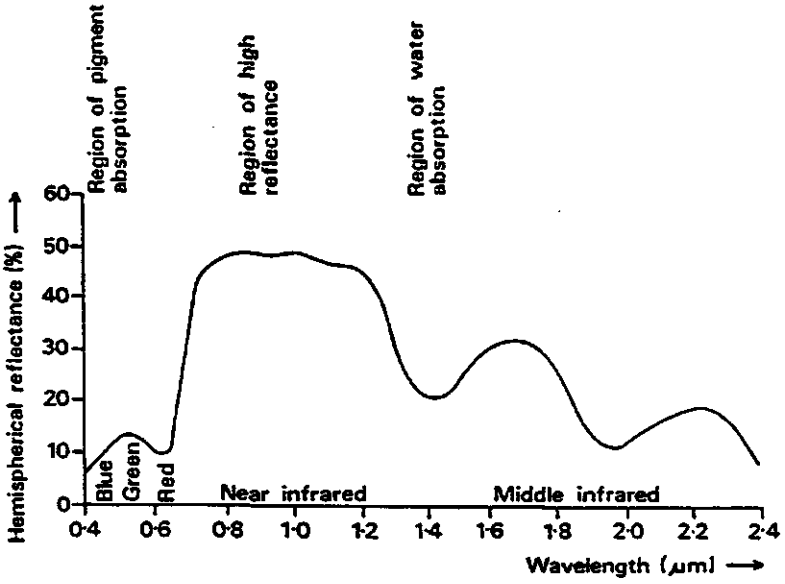

Figure 2.4. Reflectance of a leaf. (Curran, 1985)

Leaf reflectance is also strongly reduced as a result of absorption by three major water absorption bands that occur near wavelengths of 1.4 μm, 1.9 μm and 2.7 μm (figure 2.4). Within the remaining optical bands, electromagnetic radiation is also sensitive to leaf moisture but to a lesser degree.

Knowledge of spectral behaviour of individual leaves cannot completely explain reflectance from vegetation canopies. A vegetation canopy is composed of a mosaic of leaves, other plant structures, background and shadow. The overall reflectance is formed by a combination of leaf reflectance, background reflectance and shadow (Curran, 1985).
On analyzing the bidirectional reflectance recorded by a sensor the effects of:

- soil background,
- angular elevation of the sun and sensor and
- canopy geometry

have to be taken into account.

The bidirectional reflectance of the soil has a considerable effect on the bidirectional reflectance of the canopy. Curran (1983a) found that the relationship between LAI and near infrared reflectance is different on dark and light soils.
The elevation of the sun and sensor in relation to a vegetation canopy will affect the reflectance because a vegetation does not reflect radiation equally in all directions.
Solar elevation is also related to the amount of canopy shadow which tends to decrease the early morning and late evening reflectance. This is most noticeable in the visible region up to the optical band of 0.7 μm.
The angular elevation of the sensor determines the amount of soil that is visible: when the angle of elevation moves from the vertical, less soil and more vegetation is seen.
This effect is particulary severe when the angle of elevation varies by only a few degrees around the vertical.

The effect of solar and sensor azimuth is also important. The bidirectional reflectance of a canopy is usually higher when the sensor is looking into, as opposed away from, the sun.
The geometry of the canopy will determine the amount of shadow seen by the sensor and will therefore influence the sensitivity of bidirectional reflectance measurements to angular variations in sun and sensor. (Curran, 1985)

Interaction with the atmosphere

All electromagnetic radiation before and after it has interacted with the earth's surface, has to pass through the atmosphere prior to its detection by a sensor. This passage will alter the radiation's intensity as function of frequency and thus spectral scattering. These effects are most severe in the optical region (figure 2.2b). When analyzing remote sensing data these interactions have to be taken into account. For further details refer to Chahine (1983).

Sensor

The TMS is an airborne multispectral scanner. Multispectral scanners are used in aerial and satellite sensor imagery. A multispectral scanner measures the radiance of the earth's surface along a scanline, perpendicular to the line of aircraft flight (figure 2.5). The radiation from the earth's surface passes through a telescope (1), to be focussed onto a rotating mirror (2), which reflects the radiation onto a set of optics (3), where it is passed on to a dichroic grid (4), to be split into reflected and emitted radiation. The reflected radiation is divided into its spectral components using

a prism (5) and is detected and amplified by the detectors and pre-amplifiers (6), while the emitted thermal radiation goes straight to the thermal recorders and pre-amplifiers (6). All information is in electronic form and is controlled by the electric control console (7), into which can be plugged one or several recording devices.

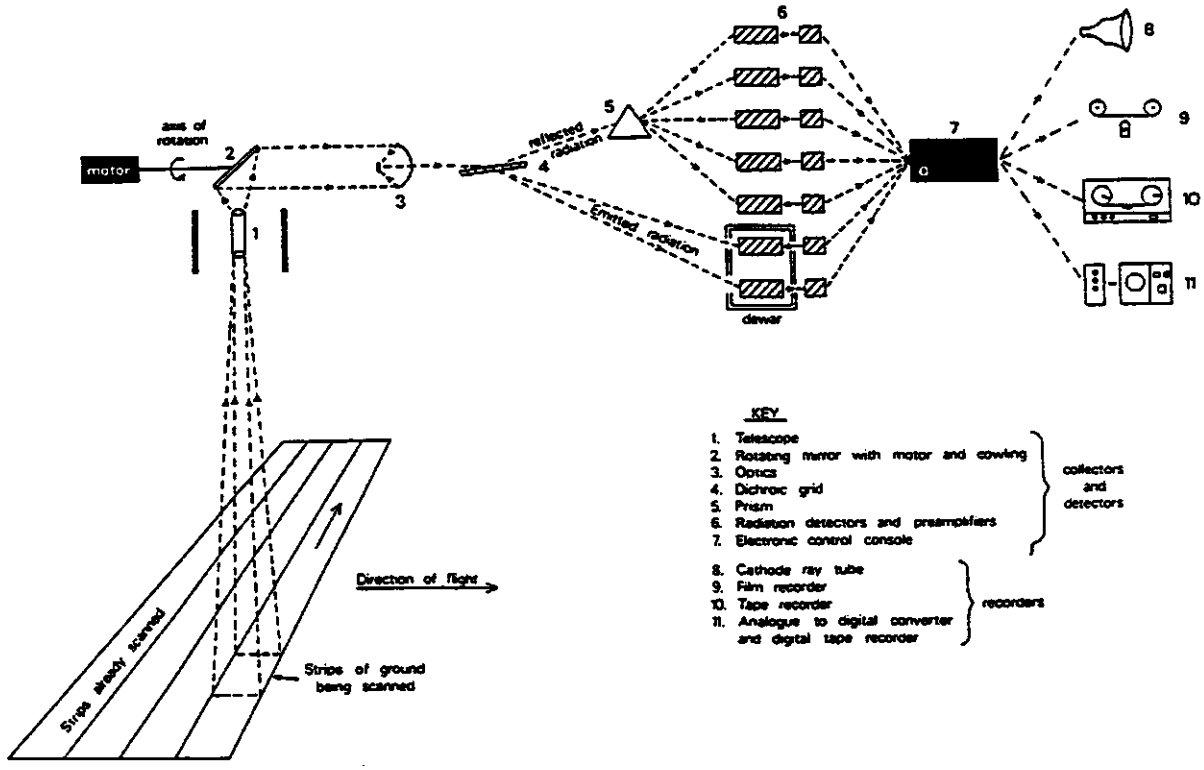

Figure 2.5. A diagrammatic representation of a multispectral scanner (Curran 1985).

2.2 Microwave remote sensing

Source and sensor

The microwave portion of the spectrum includes wavelengths within the approximate range of 1 mm to 1m. Microwaves are capable of penetrating the atmosphere under virtually all conditions. Radar is an active microwave sensor, which means that it supplies its own source of energy or illumination.

A conventional imaging radar system measures the scattered wave as a scalar quantity and any additional information about the scattering process contained in the polarization properties of the scattered signals is lost. The NASA/JPL AIRSAR is a full polarimetric system. To ensure that all information in the scattered wave is retained, a full polarimetric system measures the polarization of the scattered wave through a vector measurement process.
Radar signals can be transmitted and/or received in different modes of polarization. That is, the signal can be filtered in such a way that its electrical wave vibrations are restricted to a single plane perpendicular to the direction of wave propagation. (Unpolarized energy vibrates in all directions perpendicular to that of propagation). The objective of radarpolarimetry is to utilize the information conveyed in the polarization transformation properties of an object. The polarization concept can be visualized by the polarization ellipse given in figure 2.6 (Groot, 1991).

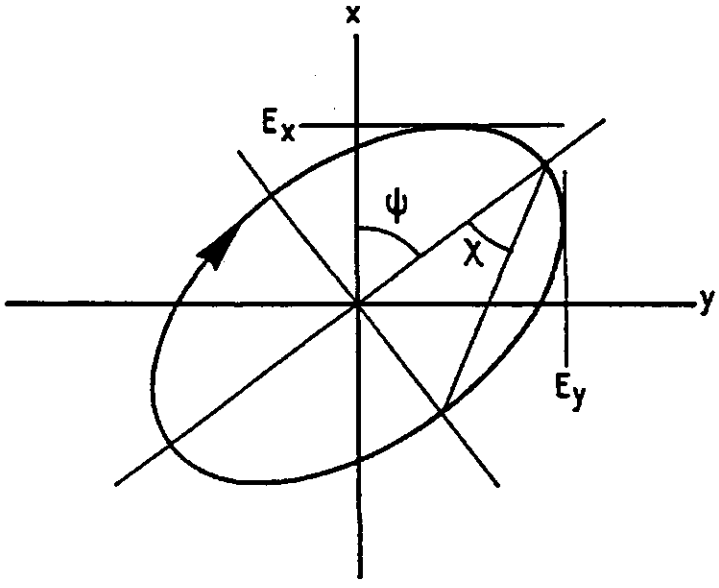

Figure 2.6. Polarization ellipse.

The polarization is characterized by two parameters:

1. <u>orientation</u> ψ . This is the orientation of the longer axis of the ellipse with respect to the positive x-axis.

2. <u>ellipticity</u> χ . This is a measure for the 'fatness' of the ellipse.

When the polarization ellipse is degenerated to a straight line ($\chi = 0$) the wave is called linearly polarized. Special cases of linear polarizations are horizontal ($\psi = 0°$) and vertical ($\psi = 90°$) linear polarizations. When χ equals $\pm$ 45° the wave is called circularly polarized.

When an electromagnetic wave is scattered by an object its polarization generally changes. The change depends on the kind of object. It can be useful to study these changes and relate them to object features. The **Scattering matrix S** describes the way in which the polarization of a wave is altered by scattering. The scattering matrix describes the scattering by a single stationary target; it cannot be used to describe the scattering by a time-varying or distributed target. A time-varying or distributed object is represented by an average Stokes matrix. A Stokes matrix formulation uses Stokes vectors. The **Stokes vector F** expressed in terms of the geometrical parameters ψ and χ is given below:

$$F = \begin{pmatrix} S_0 \\ S_1 \\ S_2 \\ S_3 \end{pmatrix} = I_0 \begin{pmatrix} 1 \\ cos2\psi cos2\chi \\ sin2\psi cos2\chi \\ sin2\chi \end{pmatrix}$$

with: ψ = polarization orientation angle
χ = ellipticity angle

The power received by a radar with identical receive and transmit antennas depends on the Stokes matrix and the send and receive polarizations. To visualize the contents of a given Stokes matrix a three dimensional plot of the received power as a function of orientation and ellipticity can be made. These plots are called "(co)-polarization responses". There are two kinds of response: in the case of co-polarization responses, the transmitting and receiving antennas have the same polarization; in the case of cross-polarized responses, the receiving antenna is polarized orthogonally to the transmitting antenna. As an exemple the polarization responses of a conducting trihedral corner reflector are given in figure 2.7 (Ulaby, Elachi, 1990).

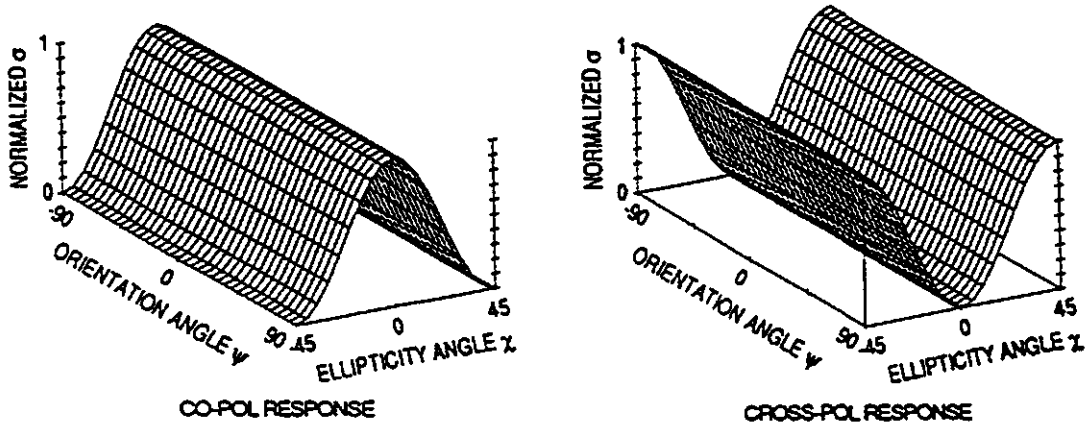

Figure 2.7. Polarization responses of a conducting trihedral corner reflector.

As can be seen, the polarization responses are independent of the polarization ellipse orientation angles. This makes the corner reflector a useful target for the calibration of polarimetric images (Zyl, 1990).

There are two types of imaging Sideways Looking Radar (SLR) systems. The first is the Sideways Looking Airborne Radar (SLAR), and the second, the Synthetic Aperture Radar (SAR), a high resolution refinement of the SLAR. The SLAR looks to one side of the flight direction with a beam that is wide vertically and narrow horizontally. The image is produced by motion of the aircraft past the area being covered. The SLAR transmits short pulses of radio frequency energy, rather than a continuous wave. The resolution in the direction parallel to the platform's direction of motion (the azimuth or along track) direction is achieved by virtue of the length of the antenna. The resolution in the perpendicular (range or cross track) direction is determined by the pulse length of the radar only (independent on fleight height). A main drawback of the SLAR is that the azimuth resolution is proportional to the platform altitude. This is the reason for the development of SAR systems (Rees, 1990).

In external appearance, a SAR system is indistinguishable from a SLAR. Higher resolution in the azimuth (along track) direction is achieved by greater sophistication in the processing of the return signal (Rees, 1990). Unlike the SLAR the SAR relies on the motion of the platform to achieve high resolution in the azimuth direction. If, over an interval of time T, the signal returned to the antenna is stored as amplitudes and phases, it is in principle possible in principle to reconstruct the signal which would have been obtained by an antenna of length v.T , v being the platform speed. Since T can be made large, this 'synthetic aperture' can also be made large, thus achieving a high resolution (figure 2.8).

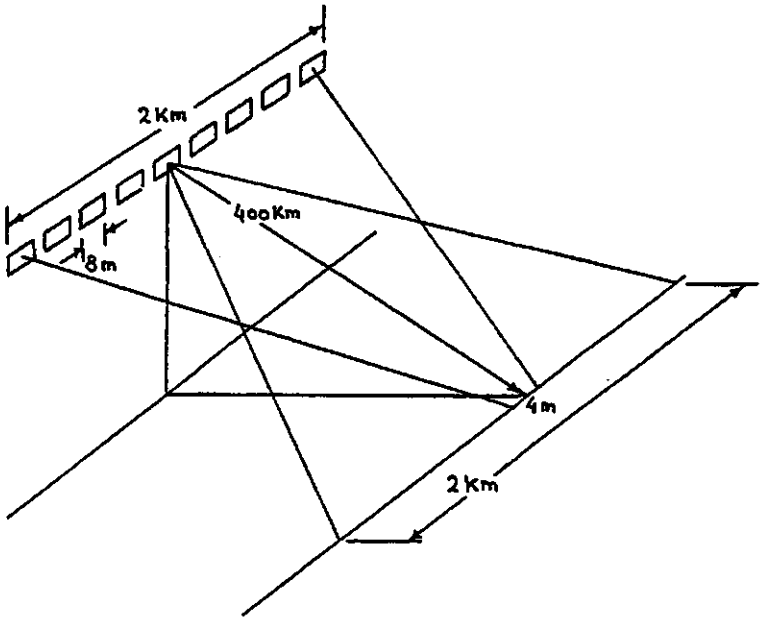

Figure 2.8. Advantage of a SAR system over a SLAR system in a space application. The length (L) of the Real Aperture is 8m. The length (L) of the Synthetic Aperture is 2km. In this example the wavelength is 4cm and R is 400km. The resolution of the Real Aperture in the along-track direction is 2km. The resolution of the Synthetic Aperture in the along-track direction is 4m.

When analyzing radar images the following features inherent to a radar system have to be considered:

- distortion of the image in the across track direction
- layover and shadowing
- speckle

A SAR system measures the range to the various scattering objects. In the simplest form of processing the image is presented in such a way that this range (the slant range) increases uniformly across the image. This is a form of distortion since we actually require that the ground range increases uniformly.

Two further problems are caused by the topography of the surface being sensed. These are layover and shadowing, which are consequences of the oblique angle of incidence. Layover arises because the top of a vertical object is closer to the radar than the bottom of the object. Layover is relatively significant at small values of the incidence angle θi. Shadowing is more of a problem at large values of θi. In this case, one part of the surface is hidden from the view of the radar by another part (Rees, 1990).

Radar images contain some degree of speckle, a grainy or salt and pepper pattern. Speckle arises from the coherent nature of radar waves, causing random constructive and destructive interference and, hence, random bright and dark areas in radar imagery. A technique useful to reduce speckle is multiple look processing. For the AIRSAR system the number of looks is 16. This means that 16 samples are taken per pixel having a size of e.g. 6.66m in range direction and 12.1m in azimuth direction (Zyl et al., 1990).

Interaction with vegetation

Radar waves interact with a vegetation canopy as a group of volume scatterers composed of a large number of discrete plant components. The vegetation canopy is underlain by soil that may result in surface scattering of energy that penetrates the vegetation canopy. In general shorter wavelengths (2 to 6 cm) are best for sensing crop canopies and tree leaves. At these wavelengths, volume scattering predominates and surface scattering from the underlying soil is minimal. Longer wavelengths (10 to 30 cm) are best for sensing tree trunks and limbs. In addition to plant size and radar wavelength, many other factors affect radar backscatter from vegetation (Lillesand, 1987).

3 USE OF OPTICAL AND MICROWAVE REMOTE SENSING

3.1 Classification

Classification is the process whereby an image is converted into some kind of thematic map, in which regions with similar properties are indicated in the same way (Rees, 1990).

Optical images can be used for classification purposes. The proportion of radiance that is reflected, absorbed or transmitted is dissimilar for different features on the earth's surface. This means that it is possible to identify features on the basis of their spectral properties.

There have been several investigations concerning the use of microwave data to map earth terrain types and landcover (Zyl, 1989). These investigations can be grouped into four approaches:

- mapping based on textural information in radar images
- mapping based on multiple incidence angle images
- mapping based on multiple polarization parameters, such as amplitude (i.e. HH, VV and HV) images, or the phase difference between the HH and VV elements of the scattering matrix.
- mapping based on the use of both amplitude and phase information (Zyl, 1989).

The following two polarimetric features can be useful tools to relate the received signal to scene properties:

1. Polarization Phase Difference (PPD).
The PPD can be defined as the like-polarized phase difference, or the phase difference between the recorded HH-polarized and VV-polarized signals (Ulaby et al., 1987). The PPD is related to the main biophysical parameters of a forest stand. The PPD is induced by three sources:

- scattering from the ground (negligible)
- bistatic scattering from the trunks (related to the cylinder radius of the trunks).
- Two way propagation in the canopy (affected by density and height of cylinders).

The PPD may provide additional information for determination of the vegetation type and structure.

2. Degree of polarization (d).
The degree of polarization is a measure for the variability of the polarization in time (or in space, when the Stokes vector is a space average). The degree of polarization is defined as the ratio of the intensity of the completely polarized part and the intensity of the total wave. It can be determined from the field-averaged scattered Stokes vectors.
In case of surface scattering the return wave is strongly polarized; d is close to 1. On the other hand, scattering from thick vegetation results in an almost completely unpolarized return wave; d is close to 0 (Groot, 1991).

3.2 Estimation of biophysical parameters

Remote sensing data have been found useful in characterizing homogeneous forests quantatively.

Studies have demonstrated the relationship between tree parameters such as Leaf Area Index (LAI), age, height, basal area, canopy closure, biomass, and radiation recorded in different channels of various airborne and spaceborne remote sensing systems. Such relationships can be described by models. These can be developed for the optical as well as for the microwave region of the electromagnetic spectrum. A literature study on models has been carried out and can be found in part II of this report.

3.3 Combination of optical and microwave remote sensing

The properties of objects in the optical and microwave region are completely different. The optical spectral response of vegetation canopies results from molecular resonances and scattering at the micrometer scale, whereas radar backscatter results from plant morphology, i.e. the geometric and bulk dielectric properties of the canopy constituents. Multi-sensor observations in which data from complementary windows of the electromagnetic spectrum are combined may yield an improvement in information content (Baker, 1992).

No algorithms or models exist that can really merge microwave data with optical data to derive biophysical information about the canopy. It is therefore critical that studies be conducted to develop these models and algorithms.

4 STUDY AREA AND SYSTEM SPECIFICATIONS

4.1 Study area

The forest sites selected for this research are located in the central part of The Netherlands. One test site has been selected in Flevoland and one at the Veluwe (figure 4.1). The province of Flevoland comprises two polders reclaimed from Lake IJsselmeer. This fresh water was formed in 1932 when the Zuiderzee, a large bay containing brackish to salt water, was enclosed. The topsoil of Flevoland originates from marine sediments. The Veluwe region is part of the province of Gelderland and features the largest forested region in The Netherlands. The soils have been developed in coarse and fine Pleistocene sands.

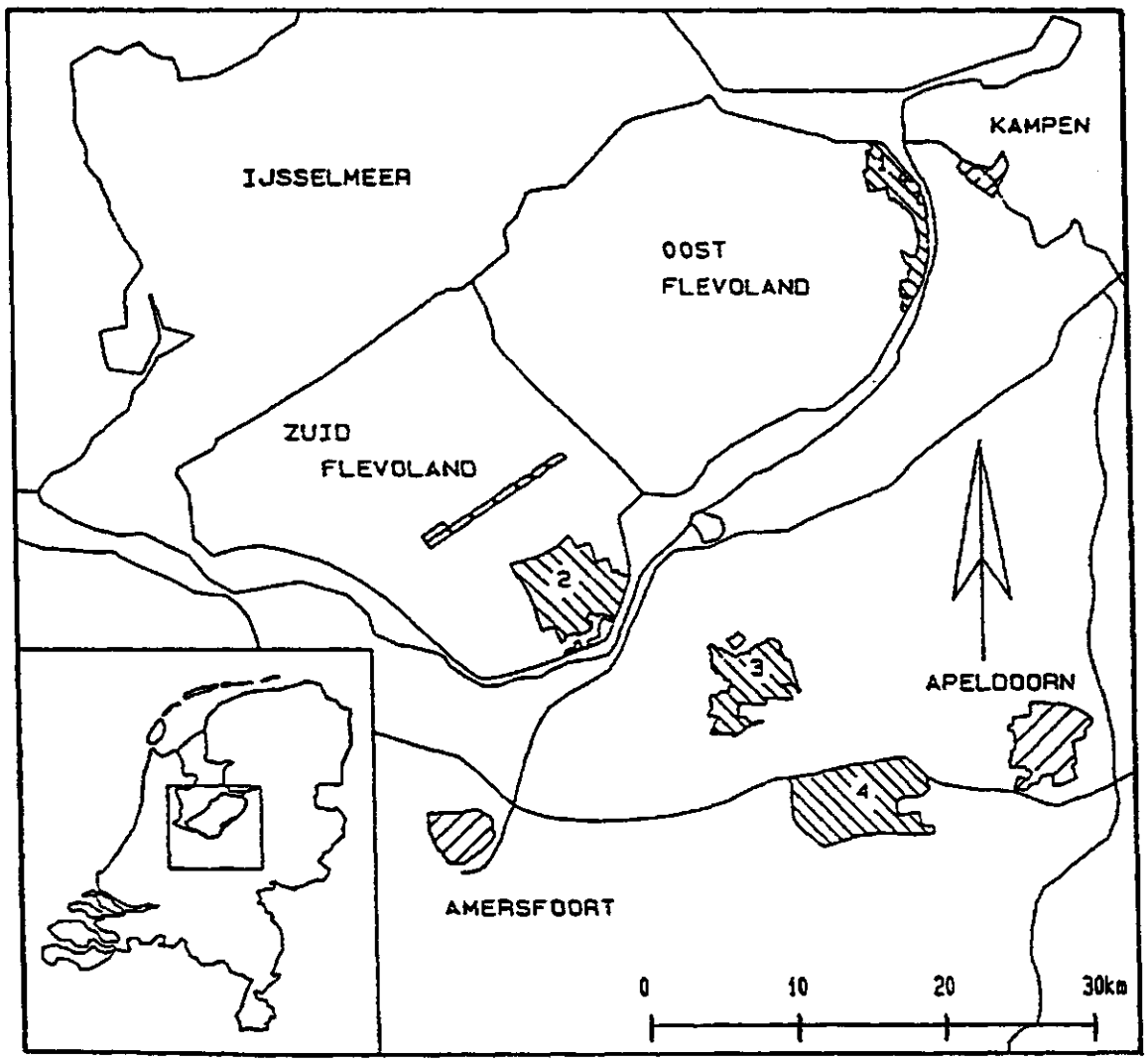

Figure 4.1. Location of the forest test sites: (2) Horsterwold (3) Speulderbos.

The Horsterwold site

The forest site in Flevoland, the 'Horsterwold', is located in the polder Southern Flevoland, reclaimed in 1966. The forest is still managed by the 'Directie Flevoland'. Planting started in 1973. When completed, the forest will be 4000 ha large,becoming the largest deciduous forest in the country. The site comprises large numbers of poplar stands and stands of other deciduous species like: willow, elm, beech, oak, alder, maple, and ash. A small number of spruce and pine stands is also present. The soil consists of fine loamy sand that originates from reworked pleistocene sands. It can be classified as a Calcaric Fluvisol (World Soil Map). The ground water level varies in depth between 80 cm (winter) and 180 cm (summer) during the year. The digging of ditches and canals locally changed the original profile due to upbringing of fine to coarse sands. The thickness of this layer varies between 0 and 20 cm.

The Speulderbos site

The Forest District "Speulder- en Sprielderbos", located at the Veluwe, is managed by the State Forest Service. The area is 2390 ha large and contains many species in many age classes. Scots pine, Douglas fir, Japanese larch, beech and oak stands prevail. Corsican pine, European larch, Norway spruce and grand fir stands occur less frequently. Within the Speulderbos some large and old beech forests, with a total area of 345 ha, can be found. These forests have been managed for hundreds of years. The structure in some parts of the beech forests resembles the structure of natural forests to some extent. North and east of the Forest District heathlands are present. The forest district comprises areas with loamy fine sands and areas with coarse sands. The sands belong mainly to preglacial fluviatile sediments shaped into low hills by the Saale ice sheet (ice-pushed ridge of Garderen). Soil classification (World Soil Map) distinguishes in this district a Leptic Podzol and Humic Podzol. The level of the ground water is in excess of 2 to 3 m depth. Since research in this forest district was focussed on the Speulderbos part, this site, throughout the report, will be referred to as 'the Speulderbos'.

These two test sites comprise a fair range of species, age classes, soils and other environmental conditions. Stand areas typically range from one to several hectares, which is quite small but normal for large parts of Europe.

4.2 TMS and AIRSAR system

The optical data were acquired on 5-7-1991 with the ER-2 aircraft carrying the Daedalus airborne Thematic Mapper Simulator (TMS). Specifications of the TMS are given in table 4.1.

The microwave data were acquired on 3-7-1991 with a DC-8 aircraft carrying the three frequency (C-,L- and P-band), full polarimetric Synthetic Aperture Radar (SAR). Specifications of the SAR are given in table 4.2.

Here we have to make some remarks about the quality of the SAR-images. Over the Horsterwold the DC-8 aircraft suffered from excessive plane motion. Beside this the P-band signal was influenced by interference. The quality of the Speulderbos images was good.

Table 4.1. TMS specifications (source: Nasa, 1992).

Channels:

Daedalus channel	TM band	wavelength, μm
1	A	0.42 - 0.45
2	1	0.45 - 0.52
3	2	0.52 - 0.60
4	B	0.60 - 0.62
5	3	0.63 - 0.69
6	C	0.69 - 0.75
7	4	0.76 - 0.90
8	D	0.91 - 1.05
9	5	1.55 - 1.75
10	7	2.08 - 2.35
11	6	8.5 - 14.0 low gain
12	6	8.5 - 14.0 high gain

Sensor/aircraft parameters:

IFOV	: 1.25 mrad
Ground resolution	: 81 feet (25 meters) at 65,000 feet
Total scan angle	: 42.5°
Swath width	: 8.3 nmi (15.4 km) at 65,000 feet
Pixels/scanline	: 716
Scan rate	: 12.5 scans/second
Ground speed	: 400 kts (206 m/second)

Table 4.2. AIRSAR specifications (source: Zyl et al., 1991)

Flight hardware characteristics:			
Parameter	P	L	C
Wavelength(cm)	68	24	5.7
Chirp bandwith(MHz)		20(or 40)	
Chirp freq.(MHz)	448.75-428.75	1258.75-1238.75	5308.75-5288.75
Chirp duration(μsec)		10(or 5)	
Peak transmit power(dBm)	60	67	59
Ant. polarization		H/V dual microstrip patch array	
Ant. gain(dBi)	14	18	24
Azimuth beamwith(°)	19.0	8.0	2.5
Elevation beamwith(°)	38.0	44.0	50.0
Ant. dim. (elev*azimuth, cm)	91.4*182.9	45.7*161.3	16.5*135.9
Receiver gain(dB)	58	50	62
Receiver gain control(dB)		> 80	
Receiver inst. dyn range(dB)		> 40	
Sys. noise temperature(K)		500-3000 (receiver gain dependent)	
Bits/sample		8	
Relevant NASA/ARC DC-8 characteristics:			
Nominal altitude(ft)		26,000	
Nominal velocity(knots)		420	
Image characteristics:			
Multi-look (Standard)		16-look compressed Stokes matrix	
Image size(rg*az,pixels)		1280*1024 per freq	
Bytes/pixel		10	
Pixel size(rg*az,m)		6.66*12.1	

5 METHODS

The following chapter describes the methodology used in this study. The way in which the training areas were defined is explained in section 5.1. Data extraction and the database are described in section 5.2. A review of the methods used for the statistical analysis of the spectral data and for classification purposes is given in sections 5.3 and 5.4. In section 5.5 empirical relationships of the spectral data with forest biophysical parameters are investigated. Finally in section 5.6 a microwave scattering model is described.

5.1 Definition of training areas

The Horsterwold forest and the Speulderbos forest were used for the collection of the spectral data. On the basis of a forest map and a standlist we selected 183 training areas (> 1 ha.) in the Horsterwold and 65 training areas (> 1 ha.) in the Speulderbos. The training areas in the Horsterwold represent 10 forest classes. The training areas in the Speulderbos represent 6 forest classes. The extent of the training data was set to 10 areas per class as far as possible. Table 5.1 lists the classes and the number of polygons wich make up each class. The Poplar clones were grouped into three classes (according to their taxonomic groups). This was done because previous research (Hoekman, 1990) showed that taxonomic properties affect the radar backscatter level in C-band and X-band. Only for the signature analysis the three Populus sections were grouped into one class. Forest class Larix decidua, comprising only one stand was not included in the classification dataset.

Table 5.1. Forest classes in the Horsterwold and the Speulderbos.

Forest classes Horsterwold	*# Polygons (total=183)*
Acer pseudoplatanus	10
Fagus sylvatica	10
Fraxinus excelsior	10
Picea abies	11
Pinus nigra nigra	9
Populus section Aigeiros	66
Populus section Aigeiros x Tacamahaca	27
Populus section Tacamahaca	19
Quercus robur	11
Salix 'Tinaarlo'	10
Forest classes Speulderbos	*# Polygons (total=65)*
Fagus sylvatica	13
Larix decidua	1
Larix kaempferi	10
Pinus sylvestris	20
Pseudotsuga menziesii	10
Quercus robur	11

The polygons representing the forest classes were defined with the use of the DSPARE utility of the DISIMP Image processing software. Outlining of the polygons was done with the help of a

forest map and based on visual interpretation of the TMS imagery only. Previous research (Butera 1986, Hildebrandt et al. 1988, Thunnissen et al. 1992, v/d Sanden 1988, Schardt 1990) and personal experience showed that the TM bands 3,4,5 (TMS bands 5,7,9) were best suited for visual interpretation of the imagery. Figures 5.1 and 5.2 show the composite TMS images we used for outlining the polygons.

Figure 5.1. TMS-bands 5,7,9 composite image of the Horsterwold (TMS5:blue, TMS7:green, TMS9:red).

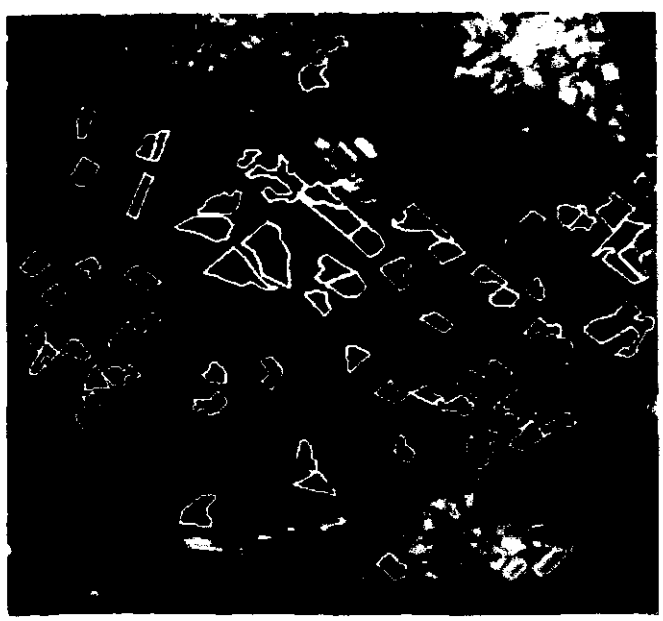

Figure 5.2. TMS-bands 5,7,9 composite image of the Speulderbos (TMS5:blue, TMS7:green, TMS9:red).

The polygons defined on the TMS image were co-registered with the radar image through the use of ground control points. A first order polynomal transformation was applied with the use of the modules COORDN and DIGUTIL of the ERDAS image processing software.

5.2 Data extraction and database

With the use of the program EXTRACT, reflectance data were extracted for the areas defined by the polygons from the TMS imagery. The program DECOSTOKEXTRACT provided the SAR data. Two databases, one for the Horsterwold and one for the Speulderbos were created, containing for each polygon the following parameters:

- mean spectral data and standard deviation
- polygon number, number of pixels
- incidence angle (for the SAR data only)
- the forest biophysical parameters: age, dbh, height, basal area, volume/Ha and Mean Annual Increment (MAI).

The TMS bands were internally calibrated to obtain radiance values from digital numbers. It was not possible to correct for atmospheric influences because the necessary information was not available.

From the SAR images the "differential cross section", σ°, was calculated by multiplying the Stokes vectors with the Stokes scattering operator. σ° is defined as the expectation of the radar cross section per unit area:

$$\sigma^\circ = \frac{\langle \sigma \rangle}{Ares}$$

with: σ° = "radar cross section" (m^2)
Ares = resolution cell area (m^2)

Another measure in which the radar backscatter is often expressed is gamma. Gamma is calculated by deviding σ° values by the cosine of the incidence angle:

$$\gamma = \frac{\sigma^\circ}{\cos(\theta inc)}$$

with: σ° = "differential cross section" (m^2/m^2)
θinc = incidence angle (°)

In this research the measure σ° is adopted, because it is used most commonly in literature. The σ° values are expressed in Decibels (dB). This is done by taking the logarithm of σ°, and then multiplying it by the factor ten.

The grounddata of the Speulderbos and the Horsterwold already available in a database were updated with the help of stand registers.

5.3 Feature selection

In order to find out if combining optical and microwave data is more promising for classification than using either one of the two information sources alone, several subsets of bands were selected. Such a subset of most informative bands represents the wavebands which are required in the classification procedure to obtain satisfactory results. The selection of an optimal set of wavebands is known as feature selection. The motive for feature selection is the reduction of data dimensionality and thus the cost of classification. These selections of subsets were based on several procedures:

- variance analysis
- signature analysis
- discriminant analysis

Variance analysis

First of all the potential information content of each spectral band was examined. The potential information content, according to Sadowski et al. (1985), may be directly related to the range of digital values and backscatter values. If there are no band-dependent sources of noise within a sensor system, the range of data values (and other statistical parameters such as variance) will provide a straightforward measure for the information content which is readily comparable among several bands. The variance as a measure of the spread or dispersion about the mean was determined for each band (calculated as the variance of a sample).

Signature analysis

In order to get a first impression of the capabilities of optical and radar bands for discriminating among the forest classes, signatures of the different forest classes were examined. This was done for the set of twelve visible/infrared and nine radar bands. Signatures of the different forest classes are represented by the complete datasets of polygons. The signature analysis of the dataset included the calculation of mean digital values, mean σ°(dB) values and variances for each forest class. Examination of the signatures of the different Populus clones showed that the overall range in digital values and σ°(dB) values was not very large. Therefore we decided to group the clones into one seperate class, for the signature analysis only.

Discriminant analysis

Discriminant analysis is a statistical technique for classifying individuals or objects into mutually exclusive and exhaustive groups on the basis of a set of independent variables (Dillon, 1984). We used discriminant analysis to:

- find the best subsets of original bands
- find linear combinations of the original variables having the property that the ratio of between-groups to within groups variability is as large as possible
- succesfully assign the polygons representing the forest classes to one of the several groups.

In the context of this method it is important to note that the sampling units are the training areas as a whole (pooled data) and not the pixels within the training areas. The data were pooled in attempt to reduce the effect of scene noise in the optical data and speckle in the radar data. This improves the separability of the classes and the classification accuracy.

First the procedure STEPDISC in the SAS statistical package was used. STEPDISC uses stepwise selection to produce a discriminating model that best reveals differences among the forest classes. The variables (all optical and radar bands) are chosen to enter or leave the model according to one of two criteria:

- the significance level of an F-test from an analysis of covariance, where the variables already chosen act as covariates and the variable under consideration is the dependent variable.
- the squared partial correlation (R**2) to predict the variable under consideration from the CLASS variable, controlling for the effects of the variables already selected for the model. R**2 is the percentage of the total variation that is explained by the variable under consideration.

Stepwise selection begins with no variables in the model. At each step the model is examined. If the variable in the model that contributes least to the discriminating power of the model fails to meet the criterion to stay, then that variable is removed. Otherwise, the variable not in the model that contributes most to the discriminating power of the model is entered (Dillon, 1984).

The STEPDISC procedure was performed for three different cases both for the Speulderbos and the Horsterwold:

- using only optical bands (TMS1-TMS12)
- using only radar bands (C-HH,C-HV,C-VV,L-HH,L-HV,L-VV,P-HH,P-HV,P-VV)
- using all bands (TMS1-TMS12/C-HH,C-HV,C-VV,L-HH,L-HV,L-VV,P-HH,P-HV,P-VV)

It is important to realize that in the selection of variables for entry, only one variable can be entered into the model at each step. The selection process does not take into account the relationships between variables that not yet have been selected. Thus, some important variables could be excluded in the process. However STEPDISC can be a valuable aid in selecting the bands which best reveal the differences among the forest classes (SAS Institute Inc., 1989).

To improve the classification results the procedure CANDISC (CANononical DISCriminant analysis) in SAS was used. This procedure is related to principal component analysis and canonical correlation. It derives canonical variables that summarize between-class variation in much the same way that principle components summarize total variation. Given two or more groups of observations with measurements on several variables (optical and radar bands), CANDISC derives a linear combination of the variables that has the highest possible multiple correlation with the groups. This is accomplished by maximizing the between group variance relative to the within group variance. This maximal multiple correlation is called the first canonical correlation. The coefficients of the linear combination are the canonical coefficients. The variable defined by the linear combination is the first canonical variable. The second canonical correlation is obtained by finding the linear

combination uncorrelated with the first canonical variable that has the highest possible multiple correlation with the groups (SAS Institute Inc., 1989). The CANDISC procedure was performed for the same cases as the STEPDISC procedure.

Variance analysis and signature analysis gave us a general idea of the bands which would be most discriminating. Discriminant analysis provided specific subsets of bands which would be most discriminating among the forest classes of the Speulderbos and the forest classes of the Horsterwold.

5.4 Classification

In order to find out if the combination of optical and microwave data is more promising than one of the data sources alone, classification was carried out on several subsets of data for the Horsterwold and the Speulderbos:

- classification based on a subset of optical bands.
- classification based on a subset of radar bands.
- classification based on a subset of all available bands.

The DISCRIM procedure in SAS was used as classification procedure. DISCRIM develops a discriminant function or classification criterion using a measure of generalized square distance (Mahalanobis distance) assuming that each class has a multivariate normal distribution. Each observation is placed in the class from which it has the smallest generalized distance (Dillon, 1984; SAS Institute Inc., 1989).

First the classification was performed using the subsets of bands coming out of the STEPDISC procedure. In order to improve the classification results classification was also done with canonical variables derived from the CANDISC procedures.

Because the STEPDISC procedure on the optical data of the Speulderbos produced only a subset of four bands we decided to use subsets of four bands in all the classification procedures in order to be able to compare the results of the different strategies. To determine if increasing the number of bands in the subset would increase the classification results, subsets of 1 to 7 bands were entered in the classification procedure. This was carried out for the Horsterwold data with subsets containing optical bands, radar bands and subsets containing a combination of optical and radar bands. The STEPDISC procedure provided these subsets.

It is important to note that the classification accuracies will be artificially high because the same set of training areas was used in the design of the classifier. However comparison of the different strategies used for the classification of the Speulderbos and the Horsterwold will not be hindered by the bias in the classification accuracies. Also the effects of different band combinations will still be valid.

5.5 Empirical relationships with forest parameters

The relationships of the spectral data with the forest biophysical parameters: age, dbh, height, basal area, volume/Ha and MAI (Mean Annual Increment) were investigated. For the total of 183 stands in the Horsterwold relationships were studied mainly with age because the ground dataset is far from

complete. For the total of 64 stands in the Speulderbos (Larix decidua was not included in the analysis) a complete ground data collection was available. We related the following spectral variables to the biophysical forest parameters:

1. C-,L-,P-band mean $\sigma°$(dB) values for HH,HV and VV polarization
2. Single band reflectance of optical data
3. Ratios of radar band polarizations
4. Radar biophysical indices
5. Optical indices

Table 5.2 lists the ratios and indices we used. A literature study showed that these indices may give good results.

The radar like-polarized backscattering magnitude is strongly affected by incidence angle. For example, there is a noticeable decrease of backscatter magnitude from near to far range (Pope et al. 1992). This incidence angle effect presents a problem for finding relations between the microwave data and forest biophysical parameters. The incidence angle effect is examined in section 6.3.2.

Pope et al. (1992) state that radar biophysical indices based on ratios of normalized differences are largely independent of local incidence angle and therefore unaffected by changes in incidence angle. Furthermore, with the design of these indices general knowledge of scattering mechanisms derived from microwave models was used. So next to single radar bands, biophysical indices were related to forest parameters.

Regression analysis is largely based upon fitting preconceived mathematical expressions to different sets of data. In order to get an idea of the possible use of a regression model for the estimation of forest parameters, first relationships between the spectral data and forest parameters were examined in scatter diagrams. We performed straight line regression on the sets of data which showed a clear trend in a scatter diagram.

The Pearson product-moment correlation as a numerical measure of the direction and degree of closeness of the linear relationship was determined:

$$r = \frac{cov(x,y)}{\sqrt{(var(x) \cdot var(y))}}$$

with: X = forest biophysical parameter
Y = spectral variable

For testing the null hypothesis that the correlation equals 0 Student's t-value was calculated. The p-value for the t-value gives the possibility that the true value of the correlation coefficient is zero.

One has to be careful with the interpretation of the results of the regression analysis for the following reasons:

- A significant correlation between two variables X and Y does not necessarily indicate that X causes Y. There is a possibility that the correlation has no physical significance at all, but represents an accidental parallelism between the two variables.

- There is the possibility that the correlation is badly distorted by other unexamined variables such as; undergrowth, biomass distribution, soil roughness, soil structure, soil texture, soil moisture content (with its influence on the radar backscatter) and other environmental parameters. Also in some cases the incidence angle effect may cause the relationship to be seriously distorted.

- A further reason for careful interpretation of the results is the possibility of inaccurate positioning of the polygons. Because the outline of some forest stands was quite hard to recognize small displacements may have occured.

- The reliability of the ground data (stand registers) has also to be taken into account. Most of the ground data were collected in October 1988 by the State Forest Service.

Table 5.2. Ratios and indices.

Ratio P-band HV & P-band VV (dB)	
Ratio P-band HV & C-band VV (dB)	
Ratio L-band HV & C-band VV (dB)	
CSI (canopy structure index)	$= \frac{vv}{vv + hh}$
VSI (volume scattering index)	$= \frac{hv}{hv + \left(\frac{vv + hh}{2}\right)}$
BMI (biomass index)	$= \frac{vv + hh}{2}$
ITI (interaction type index)	= HH, VV phase-angle difference
Vegetation index 1	$= \frac{tms9}{tms7}$
Vegetation index 2	$= \frac{tms7}{tms5}$
Vegetation index 3	$= \frac{tms5}{tms3}$
Normalized difference vegetation index 1	$= \frac{tms9 - tms7}{tms9 + tms7}$
Normalized difference vegetation index 2	$= \frac{tms7 - tms5}{tms7 + tms5}$

5.6 A microwave scattering model

Since no suitable optical model was available at the time, modeling was done in the microwave region only. Backscatter modeling was done for two Populus species of the Horsterwold. The Microwave Scattering Model for Layered Vegetation (Karam et al., 1992) was used as described in Part II of this report.

In the first case the interaction of microwaves with an 18 years old Populus 'Oxford' stand (PZ_8_C2) was modeled using data from an extensive set of ground data collected for the MAESTRO-1 campaign, of August the 16th 1989 (Droesen et al., 1990). For Populus 'Oxford' (stand PZ_8_C2) the scatterers were grouped into 4 diameter classes: 1 class for the trunks and 3 classes for the branches. Total tree biomass and biomass of branches in a certain diameter class were estimated. The number densities of the different branch scatterers, we needed as input for the microwave backscatter model, were then calculated from estimations of the total branch biomass. Other input parameters such as: dielectric constants, leaf radius, leaf thickness, leaf volume fraction, stem number density and height of the scatterers were all taken from the MAESTRO-1 ground data.

In the second case, the model is run for 9 years old, 12 years old, and 18 years old Populus 'Robusta' stands. Here a more intensive approach based on the use of the "TREE" simulation programm built by Peter Leersnijder, was adopted for finding certain input parameters needed for the microwave backscatter model. For two 20 years old Populus 'Robusta' trees the following tree data were collected:

- total tree height
- stem diameter at different heights
- height where living crown begins
- order of branches and twigs
- lengths of branches and twigs for 5 orders
- diameters at the basis of branches and twigs for 5 orders
- branch angle/rotation relative to the previous branch order
- number of branches in each branch order

These data were used to calibrate the "TREE" simulation programme for Populus 'Robusta'. A computer printout of the 20 years old simulated Populus 'Robusta' tree is shown in figure 5.3. All 5 branch orders were drawn. This simulated tree resembles the real Populus 'Robusta' tree quite well.

The "TREE" simulation programm was able to generate the branch number densities for 6 branch diameter classes in 18 angular ranges of 5° each. The input parameters needed for the "TREE" simulation programme were tree age and tree height. Because relationships between tree age and other tree parameters where included in the "TREE" simulation programm, we were able to obtain this information for 9 years old, 12 years old and 18 years old Populus 'Robusta' trees. However, the possibilities of rather large errors occuring with such extrapolations with age have to be taken into account. So for 9 years old and 12 years old Populus 'Robusta' trees one has to realize that errors can be large. The Populus 'Robusta' trees could be displayed on a personal computer screen. For the ages of 9 years old, 12 years old and 18 years old Populus 'Robusta' we generated three trees per age. Figure 5.4 shows in all 9 photos, representing three trees per age. Only the first two branch orders were drawn.

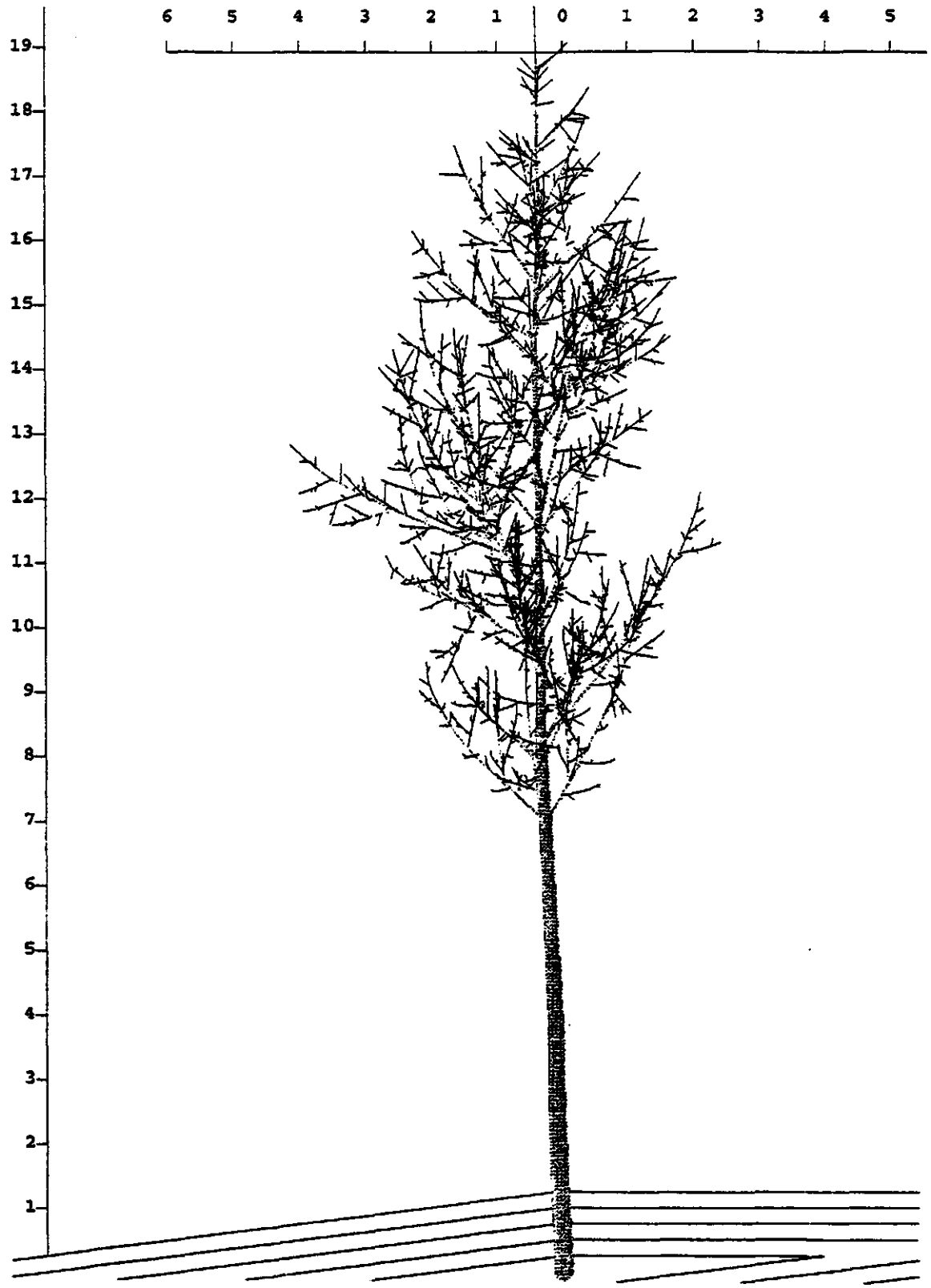

Figure 5.3. 20 years old Populus 'Robusta' tree, simulated by the "TREE" simulation programm of Peter Leersnijder. All 5 branch orders are shown.

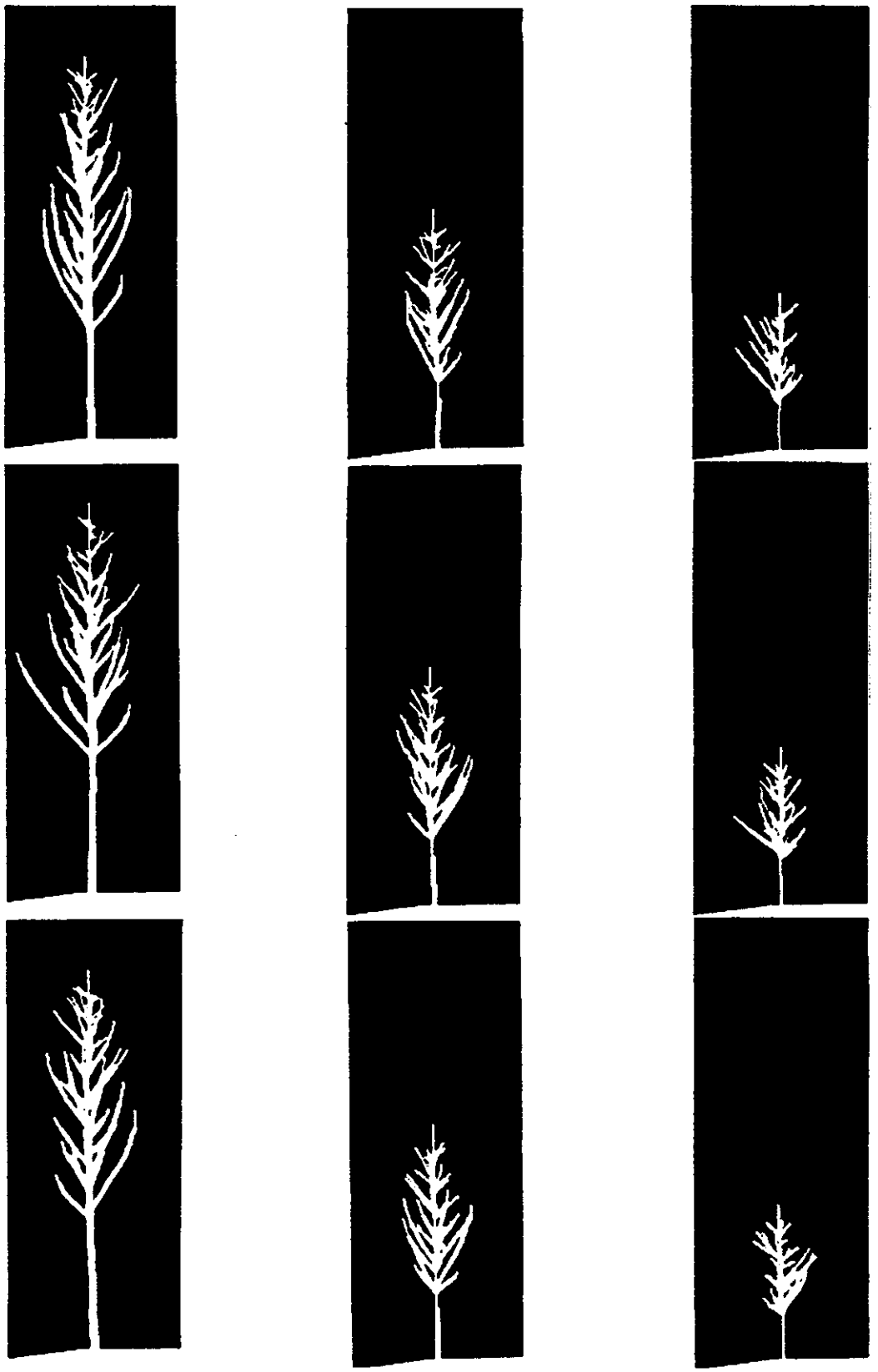

18 years old *12 years old* *9 years old*

Figure 5.4. Photos of Populus 'Robusta' trees drawn by the "TREE" simulation programm on a personal computer screen. Per age three trees were randomly generated. Only branch order 1 and branch order 2 are shown.

Input data were sent to the Wave Scattering Research Centre of the University of Texas, USA. In Texas the model was run and the output data were returned to us as σ°(dB) values in HH-, HV- and VV polarizations.

The input parameters needed for the model are given in table 5.3. In this table input parameters for 18 years old Populus 'Robusta' at C-band are given in the format they were sent to Texas. Second-order (2nd order) scattering within the canopy has been accounted for. Each group of scatterers is a collection of identical scatterers with a number density and a probability density function (PDF) for the scatterer inclination destribution. By adjusting the values of B0, B1, B2, BM and n, the probability density function can vary. These values are different for leaves and for the specific branch diameter classes. The leaves volume fraction was calculated from the LAI (Leaf Area Index) information listed in MAESTRO-1 ground data report. For the leaves the PDF was not measured but esimated from field observations. For the branches the scatterer inclination distribution information (number density) was calculated by the "TREE" simulation programm of Peter Leersnijder, and was put at the bottom of each file we sent to Texas.
Table 5.4 lists these data for four 18 years old Populus 'Robusta' at C-band. The branches were divided in angular ranges of 5°. For the ground, leaves and branches dielectric constants were taken to have the same values as for Populus 'Oxford'. Each dielectric constant consists of a real part (Re) and an imaginary part (Im). The dielectric constants are the only input parameters which differ for C-, L- and P-band. For more detailed information about the input parameters consult Karam et al. (1992).

Fieldwork showed that in most of the Populus 'Robusta' stands an understory consisting of Alnus glutinosa trees was present. We made therefore a second set of data for Populus 'Robusta' in which the Alnus glutinosa trees where modeled as a third layer. However we received a message from Texas, saying that the model could not cope with this second set of data. The problem was that when the diameter of the trunks of Populus 'Robusta' in the second layer becomes comparable to its half height, the approximation of "dielectric cylinders" is not valid. Modeling a third undergroth layer made the trunks of Populus 'Robusta' in the second layer to short.

At the moment we are working on a third set of data in which the understory of Alnus glutinosa trees is modeled in the second layer. The second layer will thus contain the trunks, one branch scatterer type and leaves.
The following changes of the input data were applied:

- The addition of one branch scatterer type in the second layer with radius of 7.0e-3 m and half height of 1.8e-1 m. The PDF was taken continuous and equal to the PDF of branches with the same size present in the crown layer of 18 years old Populus 'Robusta' trees (see also table 5.4).
The number density was also taken the same as for 18 years old Popolus 'Robusta' (5.5e-1 m^{-3}).

- The addition of leaves in the second layer with volume fraction half of the value taken for the leaves in the crown layer of 18 years old Populus 'Robusta' (2.5e-5). The PDF of the leaves was left unchanged.

Table 5.3. Model input parameters with data for 18 years old Populus 'Robusta' at C-band.

Populus Robusta, age 18y, C-band, MAC-EUROPE

robc18z.mul							First Output File
robc18z.sct							Second Output File
robc18z.lef							Leaf Contribution
robc18z.bch							Branch Contribution to 1st order
5.30							Frequency (MHz)
1							2nd order (1) or 1st order (0)
2							PDF continuous (1),discrete (0) or mixed (2)
18		8					Gauss Quadrature
1.2e-2		2.4e-1					Surface Roughness: sigma & l
20		60		9			Start, Stop and Step Angle (°)
0.							Phi Incident (°)
3.20e-2		1.1e-4					Leaves Radius & Half-height (m)
4.9.e-5	0.	0.					Leaves Volume Fraction (m^{-3})
(24.7,	-9.8)						Leaves Dielectric Constant
(14.1,	-2.8)						Ground Dielectric Constant
120.	0.	90.	30.	1.			PDF Leaves: B0,B1,B2,Bm,n (°)
11.4	6.20	0					Canopy Layer Height:upper,middle,lower (m)
7							Number of (Cylinder) Scatterer Types
1.8.e-3	3.5.e-3	7.0.e-3	1.4.e-2	2.8.e-2	5.6.e-2	1.3.e-1	Radii of Scatterers (m)
2.e-2	7.e-2	1.8.e-1	2.9.e-1	4.6.e-1	5.8.e-1	3.1.e-0	Half-heights of Scatterers (m)
14.1	14.1	14.1	14.1	14.1	14.1	13.2	Re(Eps)
5.5	5.5	5.5	5.5	5.5	5.5	5.1	Im(Eps)
4.16	2.4	5.5.e-1	1.4.e-1	2.1.e-2	7.5.e-3	3.5.e-3	number Density (m^{-3})
*	*	*	*	*	*	4.	B0
*	*	*	*	*	*	0.	B1
*	*	*	*	*	*	4.	B2
*	*	*	*	*	*	0.	Bm
*	*	*	*	*	*	6.	Power n
6							Number in upper layer
1							Number in middle layer
0							Number in lower layer

Table 5.4. Branch scatterer inclination distribution information. The number of branches within each angular range of 5° for 4 trees is given.

	diameter classes; ranges in mm					
	<5	5-10	10-20	20-40	40-80	80-160
angular ranges						
0- 5	622	364	34	3	0	0
5-10	506	313	24	2	0	0
10-15	480	288	33	4	0	0
15-20	537	279	39	2	0	0
20-25	487	300	29	4	0	0
25-30	444	304	40	0	0	0
30-35	541	328	49	6	1	0
35-40	461	378	79	18	1	0
40-45	448	351	109	29	3	0
45-50	444	301	110	41	5	0
50-55	442	302	107	50	17	0
55-60	379	312	78	40	3	0
60-65	277	317	88	27	3	0
65-70	213	251	84	19	0	0
70-75	153	196	70	21	0	0
75-80	45	192	89	10	0	0
80-85	13	184	60	7	0	0
85-90	2838	194	51	9	12	16
total number	9330	5154	1173	292	45	16

6 RESULTS/DISCUSSION

In this chapter the results of the study are described. The results of the different feature selection strategies are described in section 6.1. The classification results of the Speulderbos and the Horsterwold using the output of the discriminant analysis are presented in section 6.2. Section 6.3 contains the results of the regression analysis. Finally in section 6.4 the simulated outputs of the microwave scattering model are compared with measured backscatter values.

6.1 Feature selection

6.1.1 Variance analysis

For the Speulderbos as well as for the Horsterwold optical bands 6 to 9 seemed the most promising for discrimination between forest classes. Table 6.1 shows the average digital number per band and its variance.

Table 6.1. Average digital numbers per band (optical data), average σ°(dB) values per band (microwave data) and variances.

	HORSTERWOLD		SPEULDERBOS	
digital number				
	variance	average	variance	average
tms 1	2.07	72.00	0.61	68.02
tms 2	3.08	77.37	1.04	72.12
tms 3	5.17	62.78	1.34	56.91
tms 4	4.64	55.39	1.34	50.61
tms 5	2.34	34.74	0.66	31.69
tms 6	57.74	71.14	38.15	59.09
tms 7	159.00	98.43	114.83	80.58
tms 8	137.87	90.69	108.15	75.70
tms 9	45.18	41.04	37.00	39.32
tms10	5.09	20.38	3.77	20.53
tms11	1.45	88.76	1.14	90.63
tms12	6.15	98.63	4.86	102.41
sigma nought (dB)				
	variance	average	variance	average
C HH	1.01	-5.79	1.14	-7.87
C HV	0.85	-11.62	1.42	-13.09
C VV	1.05	-5.54	0.86	-7.40
L HH	2.54	-8.40	0.58	-7.95
L HV	3.42	-13.60	0.34	-13.68
L VV	2.61	-8.96	0.48	-9.48
P HH	7.09	-8.96	1.21	-6.88
P HV	4.14	-17.27	0.78	-15.48
P VV	4.25	-10.78	0.76	-10.67

Sadowski (1985) showed that the range of data values (and statistical parameters such as variance) will provide a straightforward measure of information content that is readily comparable among several bands. Bands 6 to 9 have a clearly higher variance than the rest of the optical bands. So apparently bands 6 to 9 in the optical region contain most of the information.

The variance analysis of the radar bands showed that there are remarkable differences between the Horsterwold data and the Speulderbos data. Table 6.1 shows that for the Horsterwold data P-band HH has the highest variance, followed by P-band VV and P-band HV.

In the Speulderbos C-band HV has the highest variance, followed by P-band HH and C-band HH. The high P-band variance in the Horsterwold could be understood by the fact that the P-band is sensitive to age differences between forest stands. This is especially true for relatively young forest like the Horsterwold (Hoekman, 1992 , personal communication).

The backscattering in C-band mainly originates from the upper layer of the canopy. The high variance of C-band in the Speulderbos is probably due to the fact that the Speulderbos contains more species than the Horsterwold, and therefore has a more heterogeneous canopy. This means that scatter elements of many different sizes and shapes are present, causing the overall variance to be relatively high.

6.1.2 Signature analysis

The Speulderbos data

The signature analysis of the optical Speulderbos data showed that coniferous stands could be separated from deciduous stands by using signature differences in bands TMS7 and TMS8. In these bands coniferous species gave much lower digital values than any of the deciduous species (figure 6.1a). Larix decidua has a remarkable different signature curve than the rest of the coniferous species. Field work showed that the Larix decidua stand recently had been cut and replanted with Pinus sylvestris.
So it was not possible to separate among the coniferous species because the within forest class variances are very high for bands TMS7 and 8 (Appendix I). Neither was this possible for the deciduous species. The reason for this could be the large difference in age class of the selected plots which shows up especially in these bands. Analysis of the signatures of the microwave data of the Speulderbos also showed that coniferous stands could be seperated from deciduous stands by using L-band HH σ°(dB) values (figure 6.1b). Deciduous stands showed lower backscatter values than coniferous stands. Other radar bands showed no better possibilities for separating the forest classes.

The Horsterwold data

The signature analysis of the optical Horsterwold data showed that coniferous stands have a lower reflectance than the deciduous stands (figure 6.2a) in TMS-band 6,7,8. Among the different deciduous species no classes could be clearly separated due to the high variance within the forest classes (Appendix I). The two conifer species, however, could be separated rather well from one another. Remarkable is the signature difference in TMS-bands 7 and 8 between Salix 'Tinaarlo', Populus sp. and the rest of the deciduous stands. The signature analysis of the microwave Horsterwold data showed that all C-band polarizations and P-band HH can be used to separate Picea abies from Pinus nigra (figure 6.2b). P-band HH could also separate deciduous stands from coniferous stands.

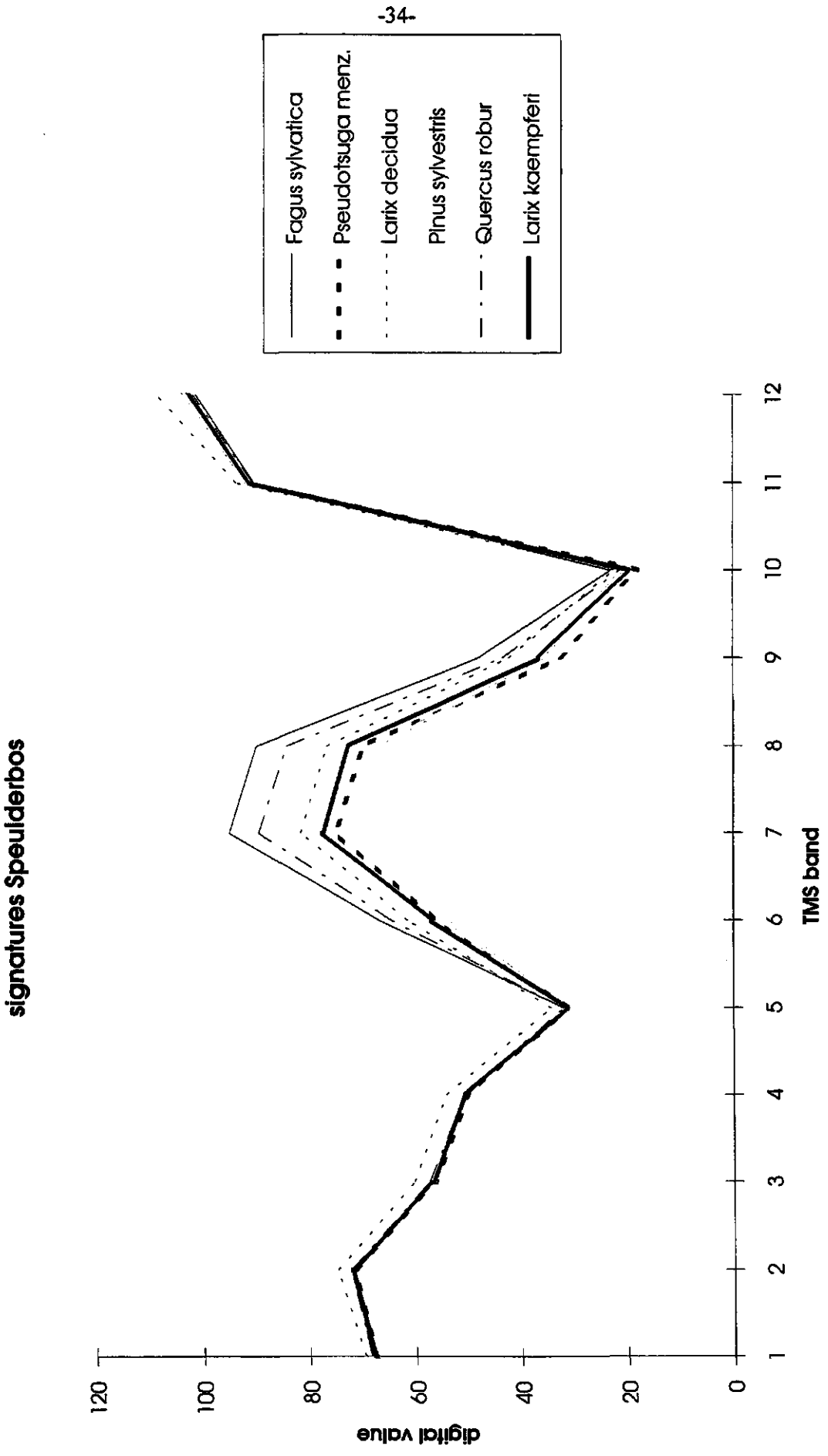

Figure 6.1a. Signatures Speulderbos for the optical data.

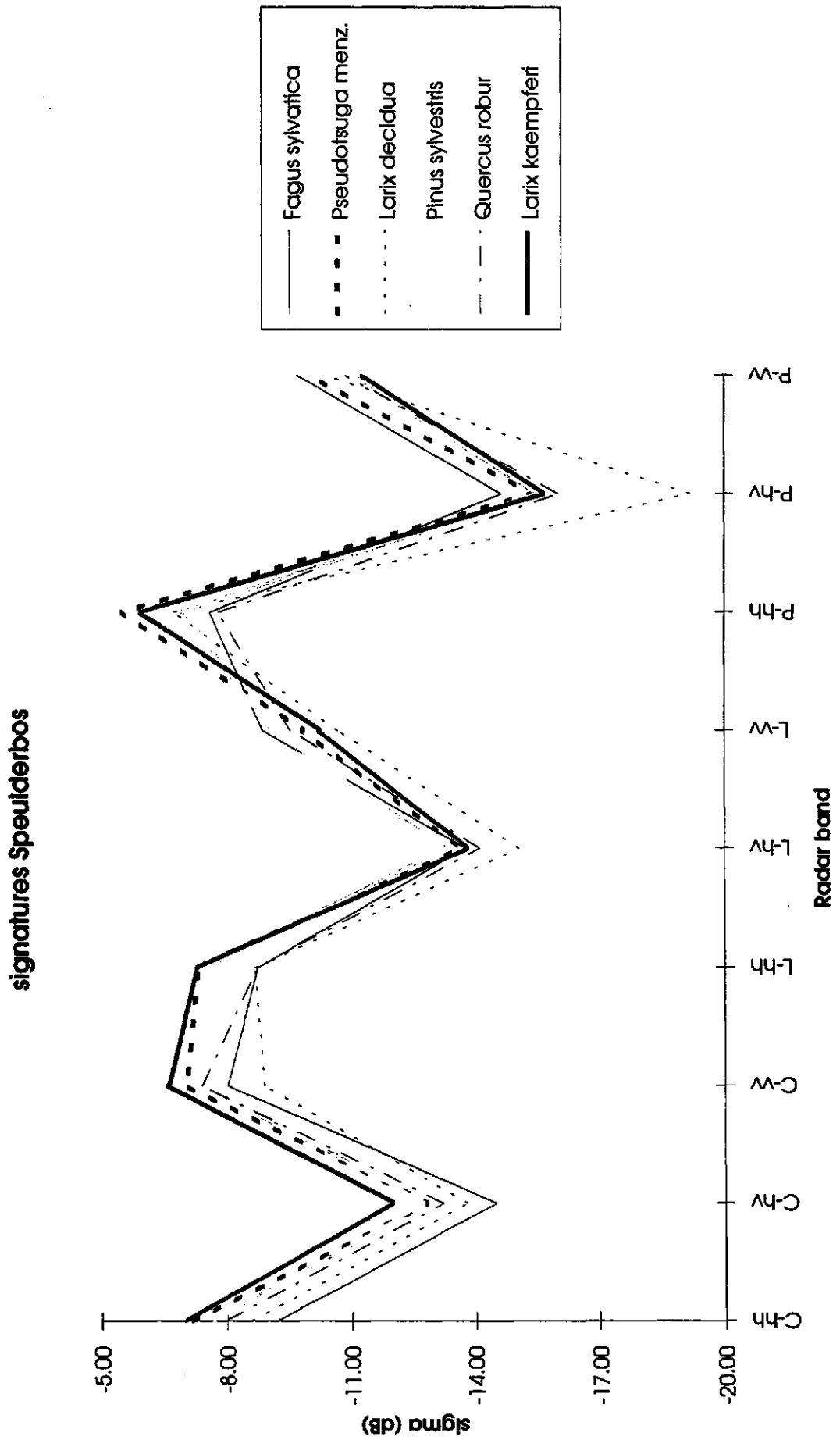

Figure 6.1b. Signatures Speulderbos for the microwave data.

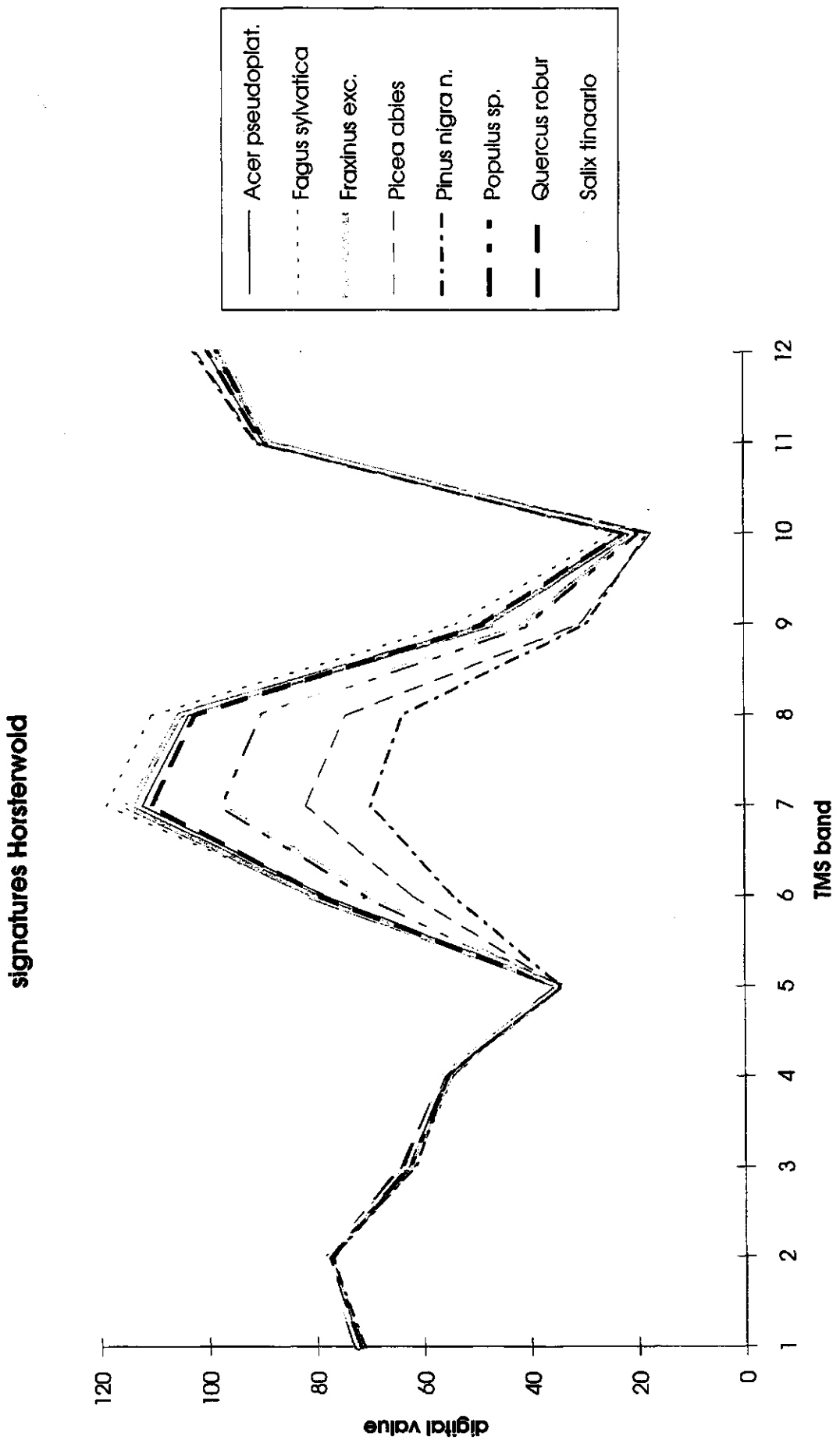

Figure 6.2a. Signatures Horsterwold for the optical data.

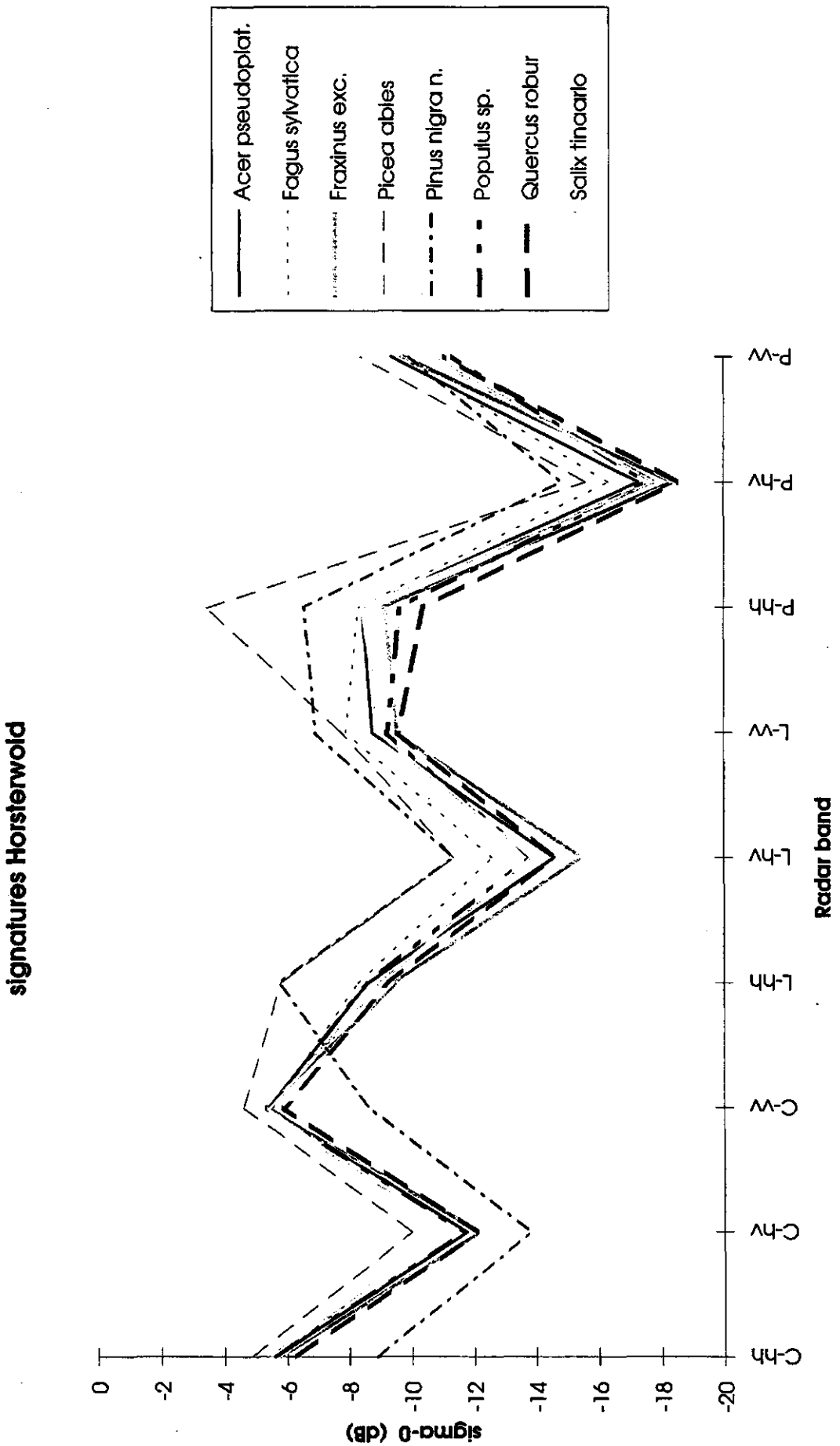

Figure 6.2b. Signatures Horsterwold for the microwave data.

The signature analysis indicated - in this case - that the best separation of classes could be expected using bands 7 and 8 in the optical region and L-band HH, P-band HH or C-band HH,HV,VV in the microwave region.
Hildebrandt (1988) and Schardt (1990) also found that TM 4 (TMS 7) contained the most information for separation of forest classes. Leckie (1990) concluded that radar bands were greatly superior to visible/infrared bands for differentiating one softwood species from another. The signature analysis in this study showed that near infrared bands 7 and 8 do have possibilities for separating softwood species. Leckie(1990) also found that radar C-band had difficulties in separating coniferous species from deciduous species. We found that HH-polarized radar bands L and P were able to separate between coniferous and deciduous species.

6.1.3 Discriminant analysis

The STEPDISC procedure selects a specific subset of bands that can be useful for discriminating among the forest classes. The STEPDISC procedure was performed for three different cases both for the Speulderbos and the Horsterwold:

- using optical bands (TMS1-TMS12)
- using only radar bands (C-HH,C-HV,C-VV,L-HH,L-HV,L-VV,P-HH,P-HV,P-VV)
- using all bands (TMS1-TMS12/C-HH,C-HV,C-VV,L-HH,L-HV,L-VV,P-HH,P-HV,P-VV).

The Speulderbos data

The stepwise discriminant analysis of the optical data showed that TMS8 is the most discriminating band (R**2 = 0.7832) followed by TMS9, TMS11 and TMS12 (table 6.3). Analysis of the radar data showed that L-HH (R**2 = 0.7314) discriminates best among the forest classes, followed by P-VV, L-VV and C-HH.

Using all bands in the stepwise discriminant analysis TMS8 appears to be the most discriminating band, followed by P-HV, TMS9 and L-VV (table 6.3). Surprisingly L-HH being the best radar band ends up as number 5. In each step of the discriminant analysis new squared partial correlation factors have been calculated, considering the effects of the variables already entered in the model. Apparently L-HH is stronger correlated with TMS8 than with P-HV.

The Horsterwold data

The analysis of the optical data showed that in the Horsterwold TMS8 is also the most discriminating band (R**2 = 0.7437), followed by TMS6, TMS9 and TMS11 (table 6.3). C-HV (R**2 = 0.6470) followed by L-HH, C-HH and L-VV are the most discriminating radar bands.
Using all bands again TMS8 appears to be the most discriminating band, followed by C-HH, L-HH and TMS6. Again the best discriminating radar band (C-HV) is not so good when using all bands in the discriminant analysis.

TMS8 seems to be the most discriminating optical band at both sites. L-band HH appears to be the most discriminating radar band. However table 6.3 shows that in the Speulderbos the longer radar wave bands (L-band VV and P-band VV) are better in discriminating among the classes. In the Horsterwold C-band HH and C-band HV are better in discriminating.

Table 6.3. STEPDISC results.

	SPEULDERBOS				HORSTERWOLD		
	Optical	partial R^2	F statistic		Optical	partial R^2	F statistic
1	TMS8	0.7832	53.279	1	TMS8	0.7437	55.767
2	TMS9	0.4887	13.860	2	TMS6	0.4676	16.782
3	TMS11	0.4835	13.341	3	TMS9	0.5576	23.949
4	TMS12	0.2442	4.524	4	TMS11	0.5427	22.414
	Radar	partial R^2	F statistic		Radar	partial R^2	F statistic
1	L-hh	0.7314	40.170	1	C-hv	0.6470	35.226
2	P-vv	0.6518	27.146	2	L-hh	0.6450	34.721
3	L-vv	0.5953	20.963	3	C-hh	0.5628	24.455
4	C-hh	0.2374	4.353	4	L-vv	0.3820	11.674
	Combination	partial R^2	F statistic		Combination	partial R^2	F statistic
1	TMS8	0.7832	53.279	1	TMS8	0.7437	55.767
2	P-hv	0.5597	18.436	2	C-hh	0.6839	41.344
3	TMS9	0.5026	14.399	3	L-hh	0.6219	31.249
4	L-vv	0.5692	18.494	4	TMS6	0.5534	23.402

The STEPDISC procedure does not take into account the relationships between variables that not yet have been selected. Thus, some important variables could be excluded in the process (SAS Institute Inc., (1989). The CANDISC procedure was used trying to improve the classification results. CANDISC derives a linear combination of the variables that has the highest possible multiple correlation with the groups. The CANDISC procedure was performed for the same cases as the STEPDISC procedure.

The Speulderbos data

The pooled within canonical structure of the three cases of the Speulderbos data are given in Appendix II. It is clear that using only optical bands, the old variables TMS6-TMS9 contribute most to the first two canonical variables. Using only the radar bands especially L-HH is most contributing followed by C-HH, C-HV, and P-HH. In the combination the same bands are important.

The Horsterwold data

Appendix II also shows the pooled within canonical structure of the three cases of the Horsterwold data. Again TMS6-TMS9 contribute most to the first two canonical variables. However here C-HH, C-HV, C-VV contribute most especially to the second canonical variable.

CANDISC showed that TMS6-TMS9 are the most important bands for classification purposes at both sites. L-band HH is the best band for discrimination among the forest classes in the Speulderbos and C-HH, C-HV and C-VV for the Horsterwold. These results also came out of the signature analysis and the STEPDISC procedure.

Variance analysis and signature analysis gave us a general idea of the bands that would be most discriminating. Discriminant analysis provided specific subsets of bands that would be most discriminating among the forest classes of the Speulderbos and the Horsterwold.
STEPDISC provided six specific subsets of original bands. CANDISC provided six subsets of canonical variables.
These twelve subsets were used as input for the classification procedure.

6.2 Classification

6.2.1 STEPDISC

First the classification procedure DISCRIM was performed with the subsets of bands coming out of the STEPDISC procedure for the three cases of the Speulderbos data and the Horsterwold data. Because the STEPDISC procedure on the optical data of the Speulderbos produced only a subset of four bands we decided to use subsets of four bands in all classifications in order to be able to compare the results of the different strategies.

The Speulderbos data

The STEPDISC procedure using optical data provided a subset of bands consisting of TMS8, TMS9, TMS11 and TMS12. The confusion matrix (Appendix III) shows the number of observations and percent classified into variable SOORT.

The polygons representing the forest classes Fagus sylvatica and Larix kaempheri were classified correctly. Problems occured classifying Pinus sylvestris, Pseudotsuga menz. and Quercus robur. Using these four bands 87.5% of the polygons was classified correctly.
The STEPDISC procedure using radar microwave data provided a subset of bands consisting of L-HH, P-VV, L-VV and C-HH. In this case Fagus sylvatica and Quercus robur were classified correctly. Here also 87.5% of the polygons was classified correctly.

Radar bands had less problems discriminating Pinus sylvestris and Quercus robur than the optical bands. (85%,100% versus 75%,90.91%). The optical bands were better in discriminating Larix kaempferi (100% versus 70%). Using the subset of bands consisting of optical and microwave data (TMS8, TMS9, Lvv, Phv) 89.1% of the polygons was classified correctly (table 6.5).
Here a combination of optical and microwave data has a minor effect on the classification result.

The Horsterwold data

The STEPDISC procedure using optical data provide a subset of bands consisting of TMS8, TMS6, TMS9 and TMS11. With these bands a classification result of 63.4% was achieved. After grouping the three Populus sections into one class the percentage of polygons classified correctly increased to 79.8%. Problems occured especially classifying Quercus robur and Salix 'Tinaarlo' (Appendix IV). Classification using the subset of radar bands (C-HV, L-HH, C-HH, L-VV) gave slightly worse results (57.4%, 65%).
Using the subset of all bands (TMS8, C-HH, L-HH, TMS6) the classification result did not improve.

63.4% of the polygons was classified correctly at first and after grouping the Populus sections 75.4% was classified correctly.

These six classification results, using the subsets coming out of the STEPDISC procedures, show that the combination of optical bands and radar band does not provide much better classification results.

6.2.2 CANDISC

Now the classification procedure DISCRIM was performed with the subsets of bands coming out of the CANDISC procedure for the three cases in the Speulderbos data and the Horsterwold data.

The Speulderbos data

The first four canonical variables (optical) were used as input for the classification procedure. The confusion matrix (Appendix V) shows the number of observations and percent classified into SOORT. The polygons representing the forest classes Fagus sylvatica and Larix Kaempferi were classified correctly. Again problems occurred classifying Pseudotsuga menz., Pinus sylvetris and Quercus robur. However the percent of polygons classified correctly is now higher than the percent using the original optical bands derived from the STEPDISC procedure (93.7% vs 87.5%).
Using canonical variables derived from the original radar bands the classification result is even higher (95.3% vs 87.5%). Fagus sylvatica, Pseudotsuga menz. and Quercus robur were classified correctly (Appendix V).
All polygons were classified correctly using canonical variables derived from all available bands (100% vs 89.1% using original bands). These figures show that a higher classification accuracy is obtained using canonical variables. More important is the fact that the combination of optical and radar bands produces a better classification result (optical 93.7%, radar 95.3%, combination 100%).

The Horsterwold data

Here we found for the canonical variables derived from the original optical bands an overall classification accuracy of 64.5%. This figure increased dramatically when the three Poplar sections were grouped into one class (81.4%).
Using the four canonical variables derived from the original radar bands the result was 75.4%. Appendix VI shows that radar bands discriminate better among the several Poplar sections than the optical bands (64.5%). This suggests that taxonomic properties influence the radar backscatter level. Hoekman (1990) found differences in the backscatter level of several Populus sections for X-band and C-band. Grouping the Poplar sections in one class gave a result of 81.4%. The classification results for the four canonical variables derived from all available bands were 81.9% and 90.1%

Here the results were also better using canonical variables.
The combination of optical bands and radar bands again proved to be significantly better than one of the sources alone (optical 64.5%/81.4%, radar 75.4%/81.4%, combination 81.9%/90.1%).

It is important to note that the classification accuracies will be artificially high because the training areas were used in the design of the classifier. However comparison of the different strategies used in the classification of the Speulderbos and the Horsterwold will not be hindered by the bias in the classification accuracies.

Overall classification results:

Speulderbos	
Data type	Overall classification accuracy
TMS bands	87.5%
Radar bands	87.5%
Combination	89.1%
Horsterwold	
	*
TMS bands	63.4% / 79.8%
Radar bands	57.4% / 65.0%
combination	63.4% / 75.4%
Speulderbos	
Canonical components (optical)	93.7%
Canonical components (radar)	95.3%
Canonical components (combination)	100 %
Horsterwold	
	*
Canonical components (optical)	64.5% / 81.4%
Canonical components (radar)	75.4% / 81.4%
Canonical components (combination)	81.9% / 90.1%

* = 1 Populus class

Leckie (1990) also showed that combining visible/infrared and radar bands improved forest class discrimination. He found that MSS bands 9 (835 nm), MSS 5 (575 nm) and MSS 11 (2150 nm) combined with X-band VV and C-band HH provided close to the maximum classification accuracy. We found TMS6 (720 nm), TMS 8 (980 nm) and TMS9 (1650 nm) to be the best optical bands in the combination at both sites. The best radar bands in the combination were different for the Speulderbos and the Horsterwold:

- Speulderbos data L-band VV, P-band HV
- Horsterwold data C-band HH, L-band HH

Except for P-band HV, like-polarized radar bands classify best. For P-band HV we found a reasonable relationship with dbh in the Speulderbos (see further in section 6.3.3). Because P-band HV backscattering results primarily from volume scattering in the crown it is possible that the discriminating power of P-band HV is the result of differences in size and orientation of the branches between the forest classes.
Classification of forests using co-registered Landsat MSS and SIR-B radar data (Skidmore et al., 1986) also proved to be better than using either of the sources alone. They found a slight increase of overall classification accuracy. Popella (1988) concluded that radar data (SIR-B) can support optical data in seperating forest areas but only to a certain extent. He found that TM band 4 offered excellent possibilities of differentiation between the forest areas. Radar showed less possibilities. Our

research indicated that for separate cases different radar bands should be used for classification purposes.

Because the STEPDISC procedure on the optical data of the Speulderbos produced only a subset of four bands we decided to use subsets of four bands in all the classification procedures in order to be able to compare the results of the different strategies.
To determine if increasing the number of bands in a subset would increase the classification result, subsets of 1 to 7 bands were entered into the classification procedure. Figure 6.3 shows that the overall classification accuracy can be improved by increasing the number of bands in the classification procedure. For radar bands and for the combination of optical bands and radar bands, there is a steady increase in classification accuracy with the number of bands, up to seven. For the optical bands, there is only marginal improvement in classification accuracy after four bands.

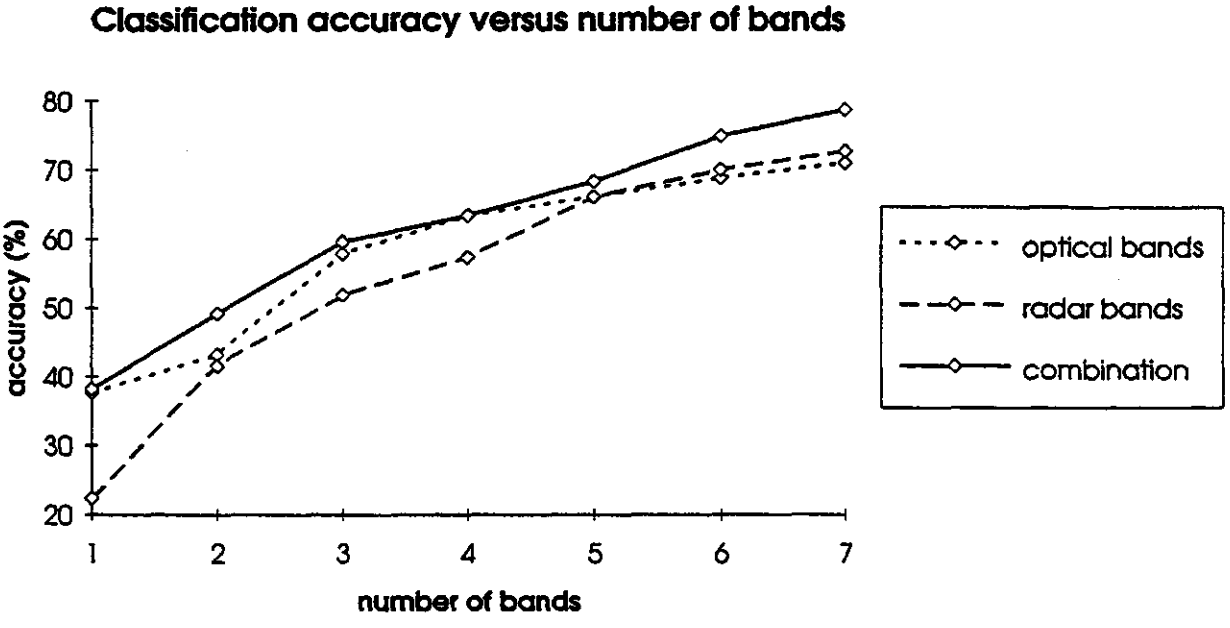

Figure 6.3. Classification accuracy versus number of bands

6.3 Empirical relationships with forest parameters

6.3.1 Regression analysis with optical data

Regression analysis was used to explore relationships between stand reflectance in the TMS bands and stand age, dbh, height, basal area, volume/ha and MAI.

First the relationships between the single band reflectances and the forest parameters were investigated.
Ardö (1992) found that spectral radiance in Landsat TM band 5 (TMS9) had the largest correlation with field measurements of volume (r=-0.79). Franklin (1986) showed that the spectral feature most strongly related to vegetation amount is visible reflectance (TM bands 1,2 and 3), which decreases

as the conifer basal area increases. None of the optical bands we used were highly correlated with any of the forest parameters.
Oza (1989) concluded that band ratios TM 3/2, TM 4/2, and TM (3-2)/(3+2) gave higher correlations than simple radiance values in various bands for mean dbh, height and age.

So various band ratios and indices (table 5.2) were correlated with mean tree parameters of the stands in the Speulderbos and the Horsterwold. It is generally accepted that such indices characterize the green vegetation quantatively (Richardson and Wiegand 1977, Tucker 1979). A response in TMS5 is believed to be related to chlorophyll absorption, TMS7 to reflectance and transmittance of the internal leaf structure and TMS9 to leaf water absorption (Swain and Davis, 1978).

The correlation coefficient (r) as a numerical measure of the direction and the degree of closeness of the linear relationship is given in table 6.4. Also the p-value for Student's t-value (the possibility that the true value of the correlation coefficient is zero) is given in table 6.4. We found that only for Fagus sylvatica in the Speulderbos strong relationships exist. Especially Vegetation index 1 (r=+0.91) had a strong relationship with the dbh of Fagus (figure 6.4).

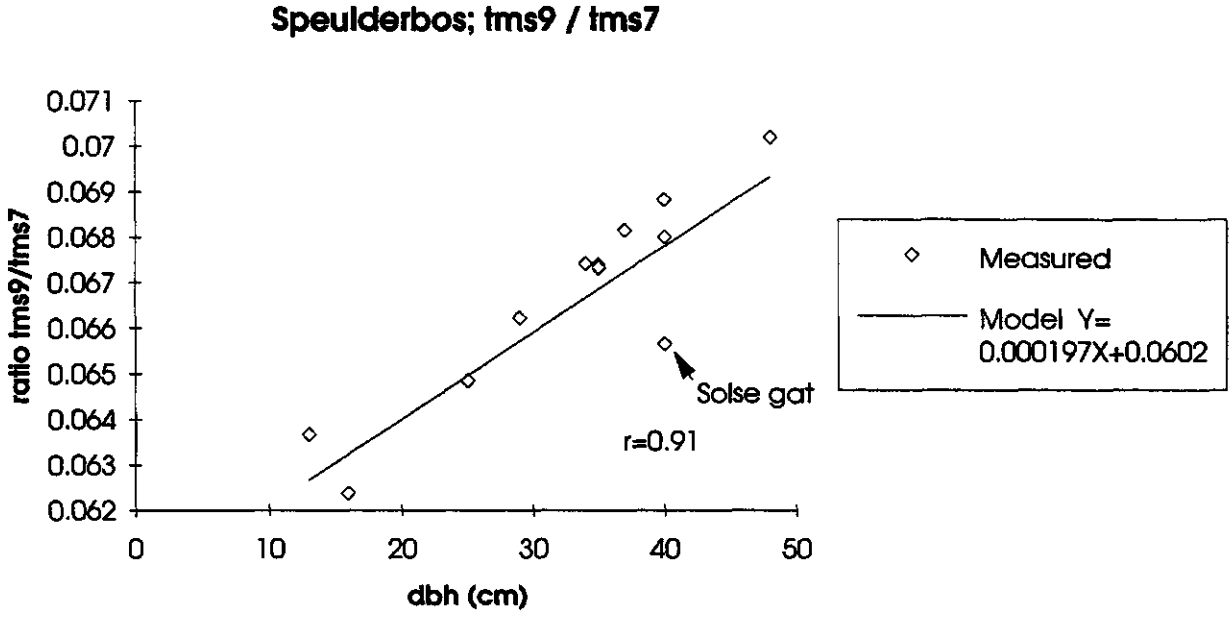

Figure 6.4. Vegetation index 1 as a function of dbh for Fagus sylvatica in the Speulderbos.

Fieldwork of the Fagus stands showed that there was a large depression in the middle of one stand (Solse Gat, figure 6.4), containing grass vegetation and open water. It is obvious that this depression had influenced the mean reflectance in all bands. After removing this particular stand from the regression analysis the correlation increased to r=+0.98.

Also good relationships were found between Vegetation index 1 and vol/ha (r=+0.81), age (r=+0.94), MAI (r=-0.81) and basal area (r=+0.64). Peterson et al. (1986) also showed that various linear ratios of TMS bands could be used to predict total basal area in certain forest types (red fir, Vegetation index 1, r=+0.76; lodgepole pine, Vegetation index 2, r=+0.82). Vegetation index 2 and Vegetation index 3 in our study were less correlated with the tree parameters of Fagus than Vegetation index 1.

The Normalized difference vegetation index 1 showed a good correlation with height (r=+0.85) and MAI (r=-0.82) for Fagus sylvatica. The Normalized difference vegetation index 2 had strong negative correlations with dbh (r=-0.83), vol/ha (r=-0.83) and height (r=-0.89).

Blanchard (1980), Butera (1986) and Tucker (1978) found that an index containing TMS7 and TMS5 is the optimum for biomass estimation. We showed that TMS9 is an important band also. Since TMS9 reacts to leaf moisture content apparently strong relationships exist between the stand parameters and the leaf moisture content of the leaves 'seen' by the sensor. Older Fagus stands had higher reflection in TMS9 indicating a lower leaf moisture content than younger stands. Unfortunately no ground truth data were available to verify this.

Surprisingly we only found good relationships for Fagus sylvatica. Additional fieldwork showed that all the Fagus stands had no understory vegetation. All the other forest stands had considerable understory vegetation. Apparently this understory vegetation has a large influence on the mean reflectance in the optical bands that were used for the indices.
Butera (1986) and Spanner (1990) also concluded that understory vegetation has a tremendous effect on the mean reflectance. Dottavio (1981) concluded that the percent of canopy closure and so the amount of understory vegetation seen by the sensor, was the most significant variable affecting the received radiation.

These results indicate that optical data might be helpful in estimating forest parameters. However since the spectral response in the optical region is a direct response to all leaf mass (trees, shrubs, grasses etc.), optical remote sensing can only be used for forest parameter estimation if the canopies of the forest classes of interest are closed (e.g. nearly closed).

Table 6.4. Correlation coefficients and p-values.

Spectral variable	Forest par.	Corr. coeff.	P-val.
RELATIONSHIPS SPEULDERBOS (ALL CLASSES)			
P-band HV	height	0.63	0.0001
	dbh	0.73	0.0001
P-band ratio HV and VV	basal area	0.42	0.0006
P-band VSI	dbh	0.59	0.0001
	basal area	0.49	0.0001
RELATIONSHIPS SPEULDERBOS (ONE CLASS)			
P-band HH	height (Pinus s.)	-0.61	0.0041
P-band ratio HV and VV	basal area (Fagus)	0.62	0.0231
	vol/ha (Larix k.)	0.62	0.0541
	vol/ha (Fagus)	0.71	0.0068
C-band CSI	dbh (Pseudotsuga)	0.8	0.0052
tms9-tms7/tms9+tms7	basal area (Fagus)	0.64	0.0183
	vol/ha (Fagus)	0.81	0.0008
	dbh (Fagus)	0.9	0.0001
	height (Fagus)	0.85	0.0003
	MAI (Fagus)	-0.82	0.0012
tms7-tms5/tms7+tms5	dbh (Fagus)	-0.83	0.0004
	height (Fagus)	-0.89	0.0001
	vol/ha (Fagus)	-0.83	0.0004
tms9/tms7	vol/ha (Fagus)	0.81	0.0008
	dbh (Fagus)	0.91	0.0001
	dbh (Fagus)	0.98	0.0001
	age (Fagus)	0.94	0.0001
	basal area (Fagus)	0.64	0.0184
	MAI (Fagus)	-0.82	0.0012
RELATIONSHIPS HORSTERWOLD (ALL CLASSES)			
P-band HV	age	0.52	0.0001
P-band HH	age	0.54	0.0001
P-band BMI	age	0.42	0.0001
RELATIONSHIPS HORSTERWOLD (ONE CLASS)			
P-band BMI	height (Pop.Geneva)	-0.82	0.0036
L-band BMI	height (Pop.Geneva)	-0.81	0.0045
C-band VSI	height (Pop.Geneva)	0.66	0.0362
P-band HH	height (Pop.Geneva)	-0.81	0.0044

6.3.2 Incidence angle effect radar

For three polarizations, σ°(dB) values as a function of incidence angle were examined in scatter diagrams for the Speulderbos and the Horsterwold (only one example is shown in this report).

First the like-polarized (HH) σ°(dB) values as a function of incidence angle were examined. In the Horsterwold only the three Populus sections (different taxonomic groups) showed a decrease in σ°(dB) in all bands of more than 1 dB with an increasing incidence angle. The remaining classes of the Horsterwold either showed a decrease in σ°(dB) in all bands within the range of 1 dB or showed a σ°(dB) which seemed indifferent of changing incidence angle. In the Speulderbos most classes showed a slight decrease in σ°(dB) of 0.5 dB to 1 dB at the most with increasing incidence angle.

Then for the Speulderbos the behaviour of cross-polarized (HV) σ°(dB) values was considered. There seemed to be little to no incidence angle dependence of cross-polarized σ°(dB) values. P-band HV backscatter magnitude, of all bands showed the least dependence of changing incidence angle.

From the foregoing we concluded that only in the case of the three Populus sections in the Horsterwold the incidence angle effect resulted in the radar backscatter magnitude showing a clear trend as a function of changing incidence angle. Figure 6.5 gives and example of a scatter diagram of C band HH backscatter as a function of incidence angle for the three Populus sections in the Horsterwold.

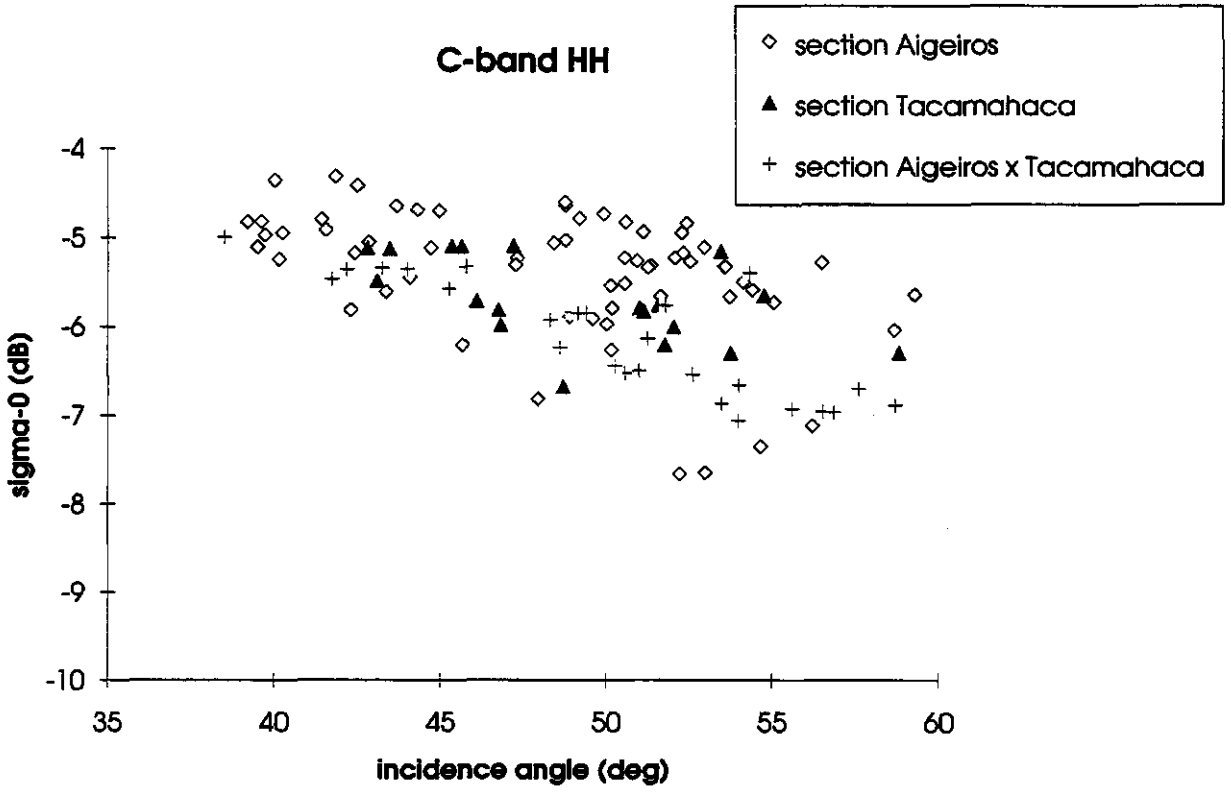

Figure 6.5. C band-HH as a function of incidence angle.

Dividing the Populus sections into several datasets covering angular ranges of 5° did not result in better relationships with forest parameters. Therefore we decided to use the entire incidence angle

range for the following regression analysis. This large incidence angle range was necessary to include a sufficient number of stands in the analysis, at the expense of higher data dispersion.

6.3.3 Regression analysis with microwave data

Regression analysis with radar data was first carried out for C-, L- and P-band for the three polarizations. Then the ratios and indices listed in table 5.2 were related to forest parameters. Table 6.4 lists the correlation coefficients (r) and the p-values.

The relations between the C-, and L-band spectral variables and all forest parameters are poor. For C-band only the CSI showed a promising relationship in a scatter diagram. C-band CSI had a positive correlation with dbh for Pseudotsuga menz. (r=+0.8). The CSI is a measure of vertical versus horizontal structure in the vegetation. Ecosystems dominated by nearly vertical elements will have high CSI values, while ecosystems dominated by horizontal or near horizontal elements will have lower CSI values (Pope et al.,1992). In C-band most of the backscattering originates from the tree crowns. Apparently older stands of Pseudotsuga menz. (with a higher dbh) are dominated by vertical oriented twigs and branches.

For P-band spectral variables, some relationships with forest parameters were found. For P-band the HV polarized backscatter gave higher positive correlations with forest parameters than both like polarized signals. The correlation of P-band HV backscatter with height (r=+0.63) and with dbh (r=+0.73) for the total number of stands in the Speulderbos looks quite promising. This result is in agreement with Hussin et al. (1991) and Sader (1987) who found positive, but higher correlations of HV polarized data with forest parameters (e.g. with biomass) than we did.

The P-band like-polarized backscatter mainly originates from the stems and the ground. Stands with a large dbh combined with a wet soil will give a relatively high backscatter level. This effect, often termed 'trunk-ground scattering mechanism' is particularly strong for HH-polarization. This can e.g. be seen from table 6.1 in section 6.1.1 where the average P-band HH backscatter in the Speulderbos is about 4dB higher than the average P-band VV backscatter. Richards et al. (1987) found that enhancements of 10dB in L-band HH backscatter were possible after flooding the forest floor in a natural eucalypt forest. Their results were based on a theoretical backscatter model for forest at L-band.

Cross-polarized (HV) backscattering mainly originates from multiple scattering within the tree crown and is less influenced by the surface condition. The relationship of P-band HV with dbh (figure 6.6) can be understood by assuming a close relationship between branch biomass and dbh for the tree species in the Speulderbos.

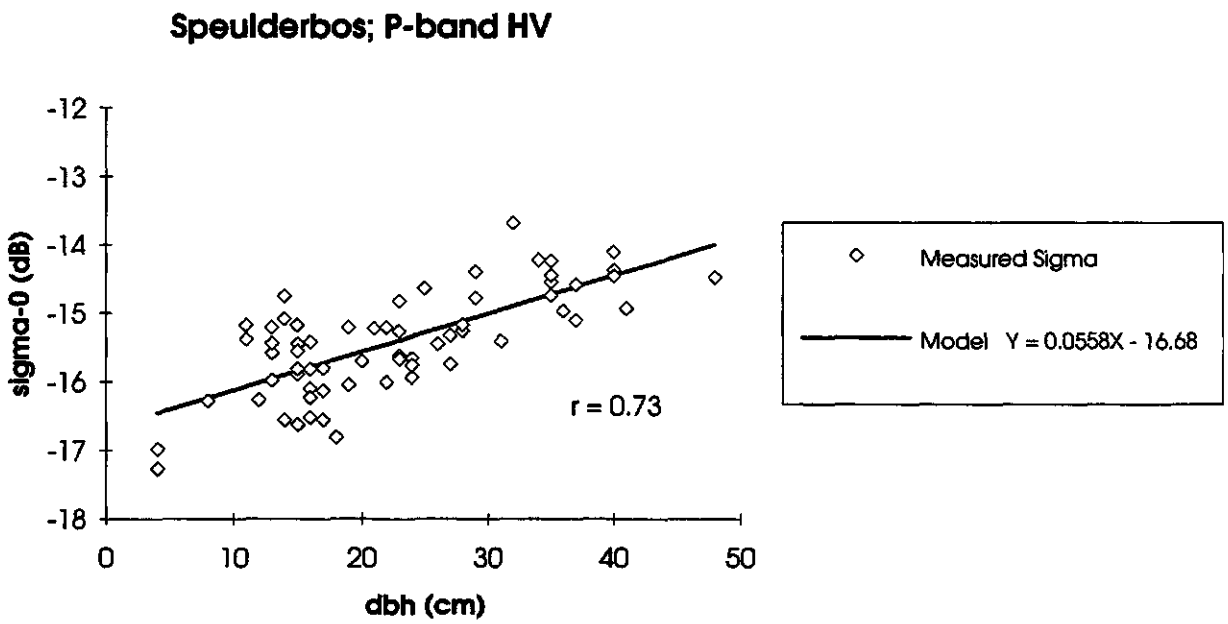

Figure 6.6. P-band HV σ°(dB) values as a function of dbh for the total number of stands in the Speulderbos.

P-band HH showed negative correlations with height for Pinus sylvestris in the Speulderbos (r=-0.61) and with height for Populus 'Robusta' in the Horsterwold. Rooij (1991) found more negative correlations (for different combinations of P-band polarizations with forest parameters) for Pinus sylvestris. It is possible however that the sign of the observed correlation is misleading and that the opposite sign would occur if the influence of other unexamined variables would be removed. Rooij (1991) suggested the influence of soil and undergrowth of young oak trees on the backscatter level.

P-band ratio HV and VV was reasonably well related with basal area and vol/Ha of Fagus sylvatica (r=+0.62 and r=+0.71). As with the optical data this can be explained by the fact that no understory, which could distort the relationship was present in stands of Fagus sylvatica.

In the Speulderbos P-band VSI showed clear relationships with dbh (r=+0.59) and basal area (r=+0.49) considering that all stands of all classes are included. However, the calculated positive correlation coefficients are not particularly high. VSI is a measure of the depolarization of the linearly polarized radar signal. VSI is high when depolarization mechanisms (e.g. scattering by cylindrical elements such as woody stems) occur (Pope et al.,1992). At a radar wavelength of 68 cm (P-band) big branches and stems act as multiple path scattering elements. This may explain the positive correlation of P-band VSI and forest parameters.

Contrary to optical data, radar data show relationships with forest parameters for all stands independent of forest class. Radar spectral variables P-band HH, P-band HV, P-band ratio HV and VV, P-band VSI and P-band BMI all show significantly high positive correlations with forest

parameters. For one species only, radar data did not give such good results as optical data.

We can conclude that for optical remote sensing, the empirical modeling approach can only be used when studying vegetations with nearly closed canopies. This is e.g. the case with the species Fagus sylvatica. Microwave data have some possibilities for estimating forest parameters independent of species. P-band data (especially P-band HV) seem to be the most promising in this respect. However one has to consider the influence of other unexamined variables, such as soil moisture content and surface roughness, on the backscatter level. Theoretical modeling will be necessary in order to interprete and generalize our observations.

6.4 Microwave backscatter modeling

The Microwave Scattering Model for Layered Vegetation (Karam et al., 1992) was used to model the interaction of microwaves with two Populus species. The output data we received from Texas represented $\sigma°$(dB) simulations in HH-, HV- and VV polarizations for an incidence angle range of 20° to 60° in steps of 5°.

In the following analysis, simulated backscatter values, $\sigma°$(dB) are compared with several sets of measured backscatter values, $\sigma°$(dB) from our database. This is done for an 18 years old Populus 'Oxford' stand and for the three ages of Populus 'Robusta'. We have to remark here that for Populus 'Robusta', in some cases theory and data of different stand ages are compared with each other. Simulated backscatter values of 9 years old Populus 'Robusta' are compared with data of 7 years old Populus 'Robusta' stands. Also in one case, simulated backscatter values of 12 years old Populus 'Robusta' are compared with data of an 11 years old Populus 'Robusta' stand.
In Table 6.5 model simulations are compared with experimental data for Populus 'Oxford' (stand PZ_8_C2).
In Appendix VII the results for Populus 'Robusta' are presented in figures. These figures give simulated (theory) and measured (data) backscatter values as a function of incidence angle for 18 years old, 12 years old and 9 years old Populus 'Robusta'.

Table 6.5 and the figures in Appendix VII show that simulated $\sigma°$(dB) values are nearly always showing a deviation of more than 1 dB from measured $\sigma°$(dB) values. This is not a good result because we had hoped that theory would not deviate more than 1 dB from the data.

Table 6.5. Comparison of model simulations with experimental data for Populus 'Oxford' (stand PZ_8_C2). The simulated backscatter values $\sigma°$(dB) for an incidence angle of 50° are compared with the measured data $\sigma°$(dB) for an incidence angle of 49.16°.

$\sigma°$(dB) values		HH	HV	VV
C-band	theory	-10.25	-17.43	-10.88
	data	-5.07	-11.66	-5.85
L-band	theory	-8.50	-15.41	-10.62
	data	-8.52	-13.15	-8.31
P-band	theory	-8.30	-15.15	-9.08
	data	-9.81	-16.42	-9.27

From the figures in Appendix VII the **angular trend** of the backscatter values can be studied. For 18 years old Populus 'Robusta'. C-band and L-band simulations show roughly the same angular trends as the data of 17, 18 and 19 years old stands. The P-band data points do not show a clear trend. For Populus 'Robusta' age 12 and 9 comparison of angular trends was not possible because only datasets containing three to four stands were available.

At **C-band**, the data are much higher than theory predicts for all ages (Appendix VII). This is particularly true for the cross-polarized (HV) backscatter which the model underestimates by 3 to 6 dB. McDonald et al. (1991) found that the Michigan Microwave Canopy Scattering Model (MIMICS) underestimated the HV-backscatter by as much as 10 dB. However they did not account for higher order scattering within the canopy. In general the effect of higher order multiple scattering on the backscatter level becomes more important as frequency increases (e.g. from L-band to C-band). This is illustrated in table 6.6. This table lists first- and second order C-band and L-band simulation results for 18 years old Populus 'Robusta'. It can be seen that for the higher frequency C-band, the backscatter level is raised considerably when second order scattering is accounted for. This is particularly true for C-band HV backscatter, which is raised almost 10 dB. Karam et al. (1992) found that second order terms had little effect on the level and trend of the like polarized signals.

Table 6.6. Simulation results for 18 years old Populus 'Robusta' up to first order and up to second order scattering at C-band and L-band. For all polarizations the simulated σ°(dB) values are given for an incidence angle of 50°.

	C hh	C hv	C vv	L hh	L hv	L vv
only first order	-12.91	-25.41	-12.50	-5.41	-18.75	-9.68
first and second order	-8.11	-16.57	-9.65	-5.15	-17.67	-9.41

In the light of these last findings we think that also higher than second order multiple scattering in the canopy might contribute significantly to the total backscatter level at C-band.

The PDF of leaves and small branches have a big influence on the backscatter level. Shifting the PDF of the leaves a little more to the vertical side might raise the VV backscatter level. From table 5.4 can be seen that small branches favor the angle between 85° and 90° (horizontal) and that their number density could be on the high side. C-band HV is in general enhanced when vertical branches interact with the soil (Amar, 1993, personal communications). It may therefore be beneficial to check the validity of the "TREE" simulation programm for the small branches.

At **L-band**, measured HH data are generally lower than theory predicts. Only for 9 years old Populus 'Robusta', simulations are in good agreement with the HH measurements (Appendix VII). Compared to C-band, scattering at L-band is less influenced by canopy constituents. Most scatterers in the canopy are small compared to the L-band wavelength. Also the larger scatterers in the diameter classes 20-40mm and 40-80mm are orientated more vertically than the smaller scatterers. Consequently the scattered field can propagate towards the forest floor. Therefore also a soil-canopy interaction term and a trunk-ground interaction term will contribute to the total backscatter level at L-band. These two terms are especially important in HH polarization (Karam et al., 1992). An understory layer of Alnus glutinosa will disturb these interaction terms. The reason for the L-band

HH data being lower than the L-band HH simulations is probably due to the fact that no understory layer was modeled.
L-band HV data are generally about 3 dB higher than L-band HV simulations. The L-band HV backscatter level is raised about 1dB when accounting for second order scattering within the canopy (table 6.5). Maybe the simulated backscatter values will rise a little when also higher than second order scattering is accounted for. L-band VV simulations seem to be in agreement with L-band VV data (Appendix VII).

At **P-band**, theory agrees to some extent with measurements for VV polarization. For 18 years old and 12 years old Populus 'Robusta', HH simulations are generally 2 to 3 dB higher than HH data. As with L-band the reason for this could be the presence of an understory layer in these stands that reduces the trunk-ground interaction term.

Modeling was also done for **Populus 'Robusta' with an understory layer of Alnus glutinosa**. The addition of one branch scatterer type and leaves in the second layer did not result in much better predictions of the backscatter levels.
At C-band, HH simulations were lowered by 1 dB at the most. At L-band, HH simulations were lowered by not more than 0.3 dB on average. At P-band, HH simulations were lowered by 0.2 dB on average.
The cross polarized backscatter levels were raised about 0.5 dB in all three bands.
At C-band, L-band and P-band, the VV polarized backscatter levels changed very little.
In general the effect of modeling the understory layer by adding one branch scatterer type and leaves to the second layer did not improve the predictions. This might indicate that the scatterer inclination distribution of the branches is important and might have to be changed in order to come closer to the real situation of forest vegetation.

In **conclusion**, when comparing the backscatter levels for Populus 'Oxford' and Populus 'Robusta' (table 6.5 and appendix VII), it can be seen that using the "TREE" simulation programm for generating the input parameters for the backscatter model does not result in much better predictions of the backscatter levels for the Populus 'Robusta' stands.

Multiple scattering processes in the forest canopy appear to have a major influence on the backscatter level, especially at C-band. The Microwave Scattering Model for Layered Vegetation does not account for higher than second -order scattering processes within the forest canopy. The simulated backscatter values would probably correspond better to the actually measured data when also these processes are taken into account.

7. CONCLUSIONS

The main objective of this study has been to investigate the possibilities for a combined (synergetic) use of optical and microwave remote sensing data for forest vegetation studies.

There are undoubtedly possibilities for a combined use for forest classification purposes. The results of the forest classifications improved considerably in most cases, using a combination of optical and microwave data. TMS8 should be one of the bands in the combination. The choice of the radar bands in the combination is dependent on forest type. Since the STEPDISC procedure does not take into account all relationships between the bands, certain important band combinations might have been overlooked. Future research could generate all possible band combinations in order to investigate if better band combinations exist.

The possibilities for a combined use for estimation of forests biophysical parameters seem limited. Both optical and microwave data showed relationships with stand age, dbh, height, basal area and vol/ha. In this study microwave P-band data showed relationships with forest parameters for all stands independent of forest class. Optical indices were highly correlated with forest parameters but only for Fagus sylvatica. The combined use of optical and microwave data did not produce additional information.

No conclusions can be drawn concerning synergy of optical and microwave remote sensing models because no optical model was available.

Our findings about the microwave model are given in section 6.4 of the results.

Part II:

Literature study on optical and microwave models

1 INTRODUCTION

Conceptually, the remote sensing of vegetation is quite simple. Develop a relationship between the vegetation parameters and its radiance as measured by a remotely located sensor, and then invert this relationship to extract the vegetation parameters from the measured radiance. However, the practical implementation of this concept has taken decades of research in developing various models, sensors, and measurement techniques, and additional research needs to be done (Goel, Norman, 1992).

There are many reasons to develop a model in the scientific field of remote sensing of vegetation. Among the more important ones are:

- to better understand and explain why we observe what we observe
- to identify those measurements that are likely to have the biggest pay-off. This is done through sensitivity analysis and by exploring parameter space through model simulations.
- to minimize the number of measurements and potential errors in measurements and to forecast the vegetation canopy behavior for internal and external parameters like wavelength, relative humidity, time, etc.
- to discover new concepts and introduce new techniques.

One can distinguish three kinds of models (Richards, 1990; Clevers, Hoekman, 1989):

(a) Empirical models

The most simple approach is the pure empirical model. This type of model is based largely upon fitting preconceived mathematical expressions to sets of data; model parameters are then found by regression. The difficulty with such an approach however, is that little information is contained on the physical basis of the matter-energy interaction and therefore little knowledge may be gained about the significance of particular scattering events. This type of model can only be of use when only a small number of sensor- and objectparameters are involved. Consequently it seems more appropriate for forest type classification than for estimation of objectparameters.

(b) Semi-empirical models

Semi-empirical models have a certain theoretical basis. Some of the physical parameters however are substituted by species or class dependent object parameters. Consequently, validation has to be performed for all species and classes, but is simpler than for physical models. As this type of model seems most suitable for practical use it is refered to as "user model".

(c) Physical models

This type of model has an analytical framework in which the models are based upon well known expressions for the reflection and backscattering coefficients. The basis is often electromagnetic theory e.g. radiative transfer approach. The radiative transfer theory consists of the radiative transfer equations which govern the electromagnetic energy propagation through scattering media. Various radar backscatter models have been based on this theory (Hsu et al., 1992).

From an interpretation perspective, it is most important that models are invertible; e.g. that they can be used with recorded image data as input, to provide biophysical and other properties as output (Richards, 1990).

2 OPTICAL MODELS FOR FOREST VEGETATION

Simple regressions of single band thematic mapper reflectance data against forest stand parameters show that strong relationships exist between spectral features and vegetation features. For example, a strong positive relationship was found by Spanner (1990) between LAI and Thematic Mapper band 4 radiance of temperate coniferous forests in the western USA and Ärdo (1992) found a strong relationship between spectral radiance in TM band 5 and stand volume of a coniferous forest area in Sweden. Results from these empirical models can be helpfull in developing semi empirical and physical models.

CLAIR model

A semi empirical model (CLAIR) may be used to estimate the LAI of a forest stand. The CLAIR model (Clevers, 1988) is a simplified reflectance model for estimating LAI. It uses a corrected infrared-reflectance for estimating LAI according to the inverse of a special case of the Mitscherlich function (Mitscherlich, 1923). Simulations with the SAIL model confirmed the potential of this simplified (semi-empirical) reflectance model for estimating LAI.
When multi-temporal analysis is required, the infrared-reflectance has to be corrected because soil moisture is not constant during the season and differences in soil moisture content greatly influence the infrared-reflectance independently of the LAI. This correction is calculated by substracting the contribution of the soil from the measured reflectance. The assumption that there is a constant ratio between the reflectances of bare soil in different spectral bands, independent of soil moisture content, enables the corrected infrared-reflectance to be calculated without knowing soil reflectance.

Input parameters:
- corrected infrared reflectance calculated with:
  - green reflectance
  - red reflectance
  - infrared reflectance
- $R\infty$ ir, asymptotically limiting value for the infrared reflectance.
- α, combination of extinction and scattering coefficients

Output:
- Leaf Area Index.

In relation to trees and forests three kinds of physical models are encountered in the remote sensing literature.

Plane parallel optical model

The first one is the plane parallel optical model. This kind of model considers the canopy consisting of one or more planar layers, containing distributed elements with given geometrical and optical properties that absorb and scatter radiation.

The Scattering Arbitrary Inclined Leave (SAIL) model (Verhoef, 1984) which is an extended version of the Suits model (Suits, 1972) is the most widely used parallel optical model. It regards the canopy as a homogeneous mixture of diffusely (Lambertian) reflecting and transmitting panels (leaves). The leaves are assumed to be arbitrarily distributed. This means that the model parameters are functions of the polar zenith angle and the azimuth angle of the leaf's upward normal. To simplify the model it is assumed that the leaf's azimuth is distributed at random. The main characteristics of the SAIL model are that agronomic variables like the leaf area index and the leaf

inclination are used as input parameters and it provides realistic angular profiles of the directional reflectance as a function of the view angle or the solar zenith angle.

Input parameters:
- leaf hemispherical reflectance
- leaf hemispherical transmittance
- LAI
- azimuthally symmetric leaf angle distribution
- view zenith angle
- solar zenith angle
- soil hemispherical reflectance
- hot spot size parameter
- fraction of diffused skylight

Output:
- directional reflectance as a function of the view angle or solar zenith angle.

Goel and Thompson (1984) showed that the SAIL model is mathematically totally invertible. This means the model can be used to estimate leaf area index and leaf angle distribution fairly accurately using only canopy reflectance data.

The SAIL model is only applicable to canopies with a homogeneous distribution of vegetation. Forests are not homogeneous and shadows cast by individual crowns will play an important role in the scene reflectance. This problem is not adressed by the SAIL model. Goel, Henderson and Pitts (1984) however showed that a two-layer SAIL model can be used to estimate the LAI of a homogeneous black spruce canopy. They concluded that for an acceptable accurate estimation, bidirectional canopy reflectance for more than 7 solar/view directions are required.

Geometrical optical model

The second kind of physical model is the geometrical-optical model. It decribes the forest as a composite of opaque, geometrical shapes, which cast shadows on the ground.

The **Otterman model** (Otterman 1984) treats, in a simplified way, the reflection of the direct solar radiation by a surface consisting of a soil-plane and protruding vertical plant elements. The vegetation is seen as a collection of randomly located vertical cylinders of variable height. The interception of the direct solar beam by these cylinders is analysed in terms of:

- the reflectances of the soil surface and the external vertical surfaces of the cylinders (Lambertian reflectance)
- the protrusion diameter parameter (sum of the products of the height times diameter of these cylinders per unit horizontal area).

Only the first reflection of the direct solar beam is computed accurately.

A comparison with the albedo measurements reported over a pine forest indicates that this simple analytic model reproduces quite well the dependence of the albedo on the solar zenith angle and the overall light trapping characteristics of such a complex surface. However the model is not applicable to open forest canopies in which trees can occur in low densities and/or are relatively large, because the trees are assumed to be small and numerous.

These problems are addressed by **Li/Strahler** (1985). They modeled low density timber stands as a collection of randomly spaced cones. Each cone is taken to be a flat Lambertian reflector, which absorbs visible light differently. Both the heights and radii of cones are assumed to be log-normally distributed. The cones are assumed to be opaque. Tree counts from pixel to pixel vary according to a given distribution, (uniform, Poisson, or Neyman). The canopy reflectance is taken to be an area-weighted sum of the reflectances of four spectral scenes:

- sunlit area of the cone
- shadowed area of the cone
- sunlit area of the ground
- shadowed area of the ground.

Input parameters:
- size of the trees
- shape of the trees
- density of the cones
- size of the pixel
- angle of illumination
- relative brightness of the cones and their background under condition of both shadowing and direct illumination.

Output:
- average brightness of a pixel and its variance.

The model can also be inverted to provide estimates of the size, shape and spacing of the conifers as cones.

Inversion input :
- pixel brightness value
- parameters describing the angle of illumination
- brightness values of the illuminated and shadowed cones and background.

The solution estimates mean height, apex angle and density of the cones. Simulations by Li / Strahler (1985) showed that the three-dimensional geometry alone can go a long way towards explaining the bidirectional reflectance function of forest canopies.
Franklin and Strahler (1988) used the model to estimate tree size and density in two bioclimatic zones in West-Afrika. They concluded that the model predicts size and density of trees over large areas of open woodland with good accuracy.
A major shortcoming of this model is that it does not take into account the interaction of radiation with vegetation elements.

Combination (parallel optical/geometrical optical)

In the SAIL model, one of the key assumptions made is that the individual foliage elements are randomly positioned. Random distribution is not a good approximation for dense crowns of widely spaced rows or widely separated individual trees. Under these conditions it usually is acceptable to assume that the foliage is distributed within the confines of many subcanopies which will obscure varying amounts of soil or understory and serve to cast shadows on the soil or understory. Each of these subcanopies can be assumed to have regular geometrical shapes like spheroids, ellipsoids, cylinders or cubes.

This representation of a canopy is used in the **T**hree dimensional **R**adiation **I**nteraction **M**odel (**TRIM**) which also accounts for the interaction of the radiation with the vegetation within each subcanopy (Goel, Grier 1987).

Here the ground is divided into a rectangular grid. In a simple version each cell contains one elliptical subcanopy. The profile of the canopy is described by a continuous function with two parameters. By varying the two parameters one can represent various stages of growth of the canopy. These parameters can also be used to calculate the percentage of ground cover in any growth stage. The model uses the canopy parameters of the SAIL model for the homogeneous canopy.
The TRIM model has one major advantage: it can represent homogeneous as well as inhomogeneous canopies. A shortcoming of the model is that it is still only applicable for canopies where the subcanopies are distributed in a regular pattern.

A model that also accounts both for the effects of shadowing and crown transmittance is the Forest Light Interaction Model (**FLIM**) (Rosema et al., 1992). Contrary to the model of Li / Strahler this model is of stochastic nature. The forest is viewed as a discontinuous canopy layer with crowns and gaps. The reflectance of this canopy is described in terms of probabilities of viewing a crown or a gap i.e. the ground. The crown reflectance is described in the same way as the reflectance of a similar homogeneous canopy. Multiple scattering is neglected and ground reflection and infinite crown reflectance are assumed to be known.

Inputparameters:
- tree density
- average tree crown horizontal area
- observation angle
- solar zenith angle
- height of the crowns
- tree crown diameter
- LAI
- extinction coefficient

Output:
- forest reflectance

Inversion:

Input parameters are:
- TM bands 3-4-5

Output:
- crown ground coverage
- crown LAI
- crown yellowness

The FLIM model gives a fair representation of actual forest-light interaction, but the verification of the model was performed with inaccurate grounddata, so the performance of the model has not been actually tested yet. More research and practical experience are required to validate this technique. An advantage of FLIM is its practical utility for image processing because it does not depend on non-image data such as leaf spectral characteristics.

3 MICROWAVE MODELS FOR FOREST VEGETATION

Various models describe the relation between the radar reflection signal and the forest- and sensorparameters. Backscatter modeling can be viewed from different starting points. Some models describe the canopy without a specific description of its components. Usually this means assuming that the canopies are continuous.

To develop scattering models information about the sources of backscattering in vegetation targets is of major importance.
Radar backscattering from forests include contributions due to:

- volume scattering in the canopy itself
- surface scattering by the underlying ground surface (or understory)
- multiple interaction involving both the canopy volume and the ground surface (Ulaby et al.,1990).

In general; major shortcomings of available backscatter models are that:

- the canopy is often treated as a continuous layer in the horizontal direction, which is valid only for closed canopies
- the canopy is often treated as having uniform properties in the vertical direction, thereby treating the crown section and the trunk section in the same way
- usually the scatterers in the crown volume are chosen to be uniform in size, shape and dielectric constant in order to simplify computations (Ulaby et al.,1990).

Using lineair regression techniques forest properties can be derived from multipolarization microwave data. Two examples are given:
Wu (1987) found that mean SAR data extracted from polygons were highly related to pine plantation biomass. The results suggested their potential application in estimating pine plantation biomass.
Beaudoin (1992) found that P-band backscatter was strongly related to forest ground parameters. The HH return was found physically related to both trunk and crown biomass, whereas VV returns and especially HV returns were found tightly linked to crown biomass and unaffected directly by environmental parameters such as soil moisture, ground local slope and presence of an understory bush layer.
Inversion of the empirical model type is quite simple. However this model can only be used when a small number of object parameters is involved.

CLOUD-model

A semi-empirical model which assumes the vegetation canopy to be an (homogeneous) electric layer is the water cloud model (Attema, Ulaby, 1978). The CLOUD-model describes the relationship between backscatter and plant water. The CLOUD-model is based on the assumption that vegetation can be modeled adequately as a water cloud. The cloud exists of identical spheres with a uniform and random orientation. Through inversion, information on biomass and plant water content may be obtained.

MULTILEVEL model

In this physical model a forest stand is modeled as a collection of scatter planes. For example four

levels six meters apart to model a forest stand with a heigt of 24 meters (Hoekman, 1990). Through inversion the model provides information about the vertical distribution of the backscattering sources.

EOM and FUNG model

Contrary to the previous two models the model of Eom and Fung explicitly describes the effects of vegetation structure and orientation. This physical model which is based on an exact solution of the radiative transfer equation assumes scattering to be dominated by the leaves. Vegetation is modeled as a layer of leaves above a rough ground surface. The leaves are modeled as a random layer of dielectric (ellipsoid) discs. A second version of the model has been developed for conifers where the needles are modelled as a collection of dielectric ellipsoides. Through inversion the model may provide information about:

- volume scattering
- ground surface scattering attenuated by vegetation
- surface volume interaction (Eom,Fung, 1984).

MIMICS

The Michigan Microwave Canopy Scattering Model (MIMICS 1) is a physical model based on a first order solution of the radiative transfer equation for a tree canopy comprising a crown layer, a trunk layer and a rough surface ground boundary. First order scattering involves single scattering by each region and double scattering by pairs of regions. This means that no processes involving multiple scattering (e.g. triple scattering) are included in MIMICS 1. The crown is modeled in terms of distributions of dielectric cylinders (representing needles and /or branches) and discs (representing leaves), and the trunks are treated as dielectric cylinders of uniform diameter. The following scattering mechanisms are accounted for in MIMICS 1:

- foliage volume scattering
- scattering from the trunks and branches
- scattering from the woody matter followed by surface scattering
- surface scattering from the forest floor
- scattering from the foliage followed by surface scattering.

The input parameters needed can be divided in geometrical parameters and dielectric parameters. The model is intended for use in the 0.5-10 GHz region at incidence angles of more than 10°. Limitations of MIMICS 1 are that only single scattering is accounted for and that the canopy has to be closed.

A Microwave Scattering Model for Layered Vegetation

This physical model developed by Karam et al. (1992) is based on the second order solution of the radiative transfer equation. This means that multiple scattering within the canopy and between the ground and the canopy are accounted for. The canopy is modeled as a two-layered medium above a rough surface. The upper layer is the crown containing leaves, stems and branches. The crown layer consists of several groups of scatterers, namely, the leaves and a few different sizes of branches. Scatterers belonging to the same group are identical in size. The lower layer is the trunk region modeled as randomly positioned cylinders with preferred orientation distribution above a rough soil surface. The Kirchhoff model under scalar approximation is used to represent the scattering properties of the rough soil surface (Ulaby et al., 1984).

The major advantages of this model are:

- first and second -order scattering within the canopy is accounted for
- the model accounts for the surface roughness in the canopy-soil interaction terms
- it allows many branch sizes and their orientation distributions
- it is valid over a wide frequency range for both deciduous and coniferous vegetation.

The previous two physical models were both focused on the prediction of σ°(dB) values as a funtion of object parameters. They are noninvertable, which means that it is not possible to estimate object parameters from the measured backscatter values. However sometimes analytical techniques allow inversion of rather complex models that are driven by many parameters. Combining the microwave data with optical data may offer better possibilities for inversion.

REFERENCES

Ardö, J., 1992, Volume Quantification of Coniferous Forest Compartments using Spectral Radiance recorded by Landsat Thematic Mapper. International Journal of Remote Sensing, vol.13, no.9.

Attema, E.P.W. and F.T. Ulaby, 1978, Vegetation Modelled as a Water Cloud. Radio Science, vol.13, pp.357-364.

Baker, J.R., and P.L. Mitchell, 1992, The UK element of the MAESTRO-1 campaign, International Journal of Remote Sensing, vol.13, no.9, pp.1593-1608.

Blanchard, L.E. and O. Weinstein, 1980, Design Challenges of the Thematic Mapper, IEEE Transactions on Geoscience and Remote Sensing, vol.18, no.2, pp.146-160.

Butera, M.K., 1986, A Correlation and Regression Analysis of Percent Canopy Closure versus TMS Spectral Response for Selected Forest Sites in the San Juan National Forest, Colorado. IEEE Transactions on Geoscience and Remote Sensing, vol.24, no.1.

Campbell, J.B. 1987, Introduction to Remote Sensing, Guilford Press, New York.

Chahine, M.T. 1983, Interaction Mechanisms within the Atmosphere, in: Manual of Remote Sensing, 2nd edition.

Clevers, J.G.P.W. 1988, The Derivation of a Simplified Reflectance Model for the Estimation of Leaf Area Index. Remote Sensing of Environment, vol.25, pp.53-69.

Clevers, J.G.P.W. and D. Hoekman, 1989, Modelvorming en Synergie; optische en microgolf remote sensing, deelrapport 1: voorstudie, BCRS. report no.89-23, 82p.

Curran, P.J. 1983, Problems in the Remote Sensing of Vege-tation Canopies for Biomass Estimation: In Fuller, R.M. Ecological Mapping from Ground, Air and Space, Institute of Terrestrial Ecology, Symposium no. 10, Cambridge.

Curran, P.J. 1985, Principles of Remote Sensing, Longman Inc., New York.

Dillon, W.R. and M. Goldstein, 1984, Multivariate analysis, Wiley & Sons, New York.

Dottavio, C.L., 1981, Effect of Forest Canopy Closure on Incoming Solar Radiance, Proc. 1981 Machine Processing of Remotely Sensed Data Symp., West Lafayette, pp.375-383.

Droesen W.J., D.H. Hoekman, H.J.C. van Leeuwen, J.J. van der Sanden, B.A.M. Bouman, D. Uenk, M.A.M Vissers and G.G. Lemoine, 1990, MEASTRO 89 Ground Data Collection Horsterwold/Speulderbos/Flevoland (NL). Final Report. Agric. Univ. Wageningen, the Netherlands.

Franklin, J., 1986, Thematic Mapper Analysis of Coniferous Forest Structure and Composition. International Journal of Remote Sensing, vol.7 no.10, pp.1287-1301.

Franklin, J. and A.H. Strahler, 1988, Invertible Canopy Reflectance Modeling of Vegetation Structure in semi-arid Woodland.IEEE Transactions on Geoscience and Remote Sensing, vol.26, no.6.

Goel, N.S. and T. Grier, 1987, Estimation of Canopy Parameters for Inhomogeneous Vegetation Canopies from Reflectance Data III. TRIM: A Model for Radiative Transfer in Heterogeneous Three-dimensional Canopies. Remote Sensing of Environment.

Goel, N.S., K.E. Henderson and D.E. Pitts, 1984, Estimation of Leaf Area Index from Bidirectional Spectral Reflectance Data by Inverting a Canopy Reflectance Model. Proceedings of the International Symposium Machine Processing of Remotely Sensed Data, pp.339-347.

Goel, N.S. and J.M. Norman, 1992 Biospheric Models, Measurements and Remote Ssensing of Vegetation. ISPRS Journal of Photogrammetry and Remote Sensing, 47 pp.163-188.

Goel, N.S. and R.L. Thompson, 1984, Inversion of Vegetation Canopy Reflectance Models for Estimating Agronomic Variables.IV. Total Inversion of the SAIL Model. Remote Sensing of Environment, vol.15, pp.237-253.

Groot, J., 1991, Introduction to Radar Polarimetry, Technical Report FEL-91-B122, TNO-FEL, The Hague.

Hildebrandt, G., H.J. Stibig, and M. Schardt, 1988, Classification of Intensively Managed Forests in Germany by Spaceborn Remote Sensing. Proceedings of the IUFRO Subject Group 4.02.05 Meeting, Helsinki, Finland.

Hoekman, D.H., Radar Remote Sensing Data for Applications in Forestry. Thesis. Wageningen, 1990.

Hsu, C.C., H.C. Han, R.T. Shin, J.A. Kong, A. Beaudoin, and T. Le Toan, 1992, Radiative Transfer Theory for Polarimetric Remote Sensing of Pine Forest. Proceedings of IGARSS '92 Symposium, Houston, Texas, May 26-29, 1992, vol.II, pp.1129-1131.

Karam, M.A., A.K. Fung, R.H. Lang and N.S. Chauhan, 1992, A Microwave Scattering Model for Layered Vegetation. IEEE Transactions on Geoscience and Remote Sensing, vol.30, no.4, pp.767-784.

Leckie, D.G., 1990, Synergism of Synthetic Aperture Radar and Visble/Infrared Data for Forest Type Discrimination. Photogrammatic Engineering & Remote Sensing, vol.56, no.9, pp1237-1246.

Le Toan, T., A. Beaudoin, J. Riom and D. Guyon, 1991, Relating Forest Parameters to SAR Data. Proceedings of IGARSS '91 Symposium, Espoo, Finland, June 3-6, 1991, vol.II, pp.689-692.

Li, X. and A.H. Strahler, 1985, Geometrical-Optical Modeling of a Conifer Forest Canopy. IEEE Transactions on Geoscience and Remote Sensing, vol.23, no.5, pp.906-919.

Lillesand, T.M., 1987, Remote Sensing and Image Interpretation, 2nd edition, John Wiley & Sons Inc. New York.

McDonald, K.C., M.C. Dobson and F.T. Ulaby, 1991, Modeling Multi-Frequency Diurnal Backscatter from a Walnut Orchard. IEEE Transactions on Geoscience and Remote Sensing, vol.29, no.6, pp.852-863.

Mitscherlich, E.A., 1923, Bodenkunde für Land- und Forstwirte, Verlagsbuchhandlung Paul Parey, Vierte Auflage, Berlin.

Otterman, J. 1984, Albedo of a Forest Modeled as a Plane dense Protrusions. Journal of Climate Applied and Meteorology, vol.23, no.2, pp.297-307.

Oza, M.P. and V.K. Srivastava, 1989, Relationship between Landsat MSS Data and Forest Tree Parameters, International Journal of Remote Sensing, vol.10, no.11, pp.1813-1819.

Peterson, D.L., W.E. Westman, N.J. Stephenson, V.G. Ambrosia, J.A. Brass, M.A. Spanner, 1986, Analysis of Forest Structure using Thematic Mapper Simulator Data, IEEE Transactions on Geoscience and Remote Sensing, vol.24, no.1, pp.113-120.

Pope, O.P., J.M. Rey-Benayas, J.F., Paris, 1992, Radar Remote Sensing of Forest and Wetland Ecosystems in the Central American Tropics. Draft 11-12-1992. To be submitted to Remote Sensing of Environment.

Popella, A. and M. Schardt, 1988, Comparison of TM, SIR-B and Simulated Radar Images in Particular Consideration of Forest Classification, ISPRS, Kyoto.

Rees, W.G., 1990, Topics in Remote Sensing: Physical Principles of Remote Sensing, University Press, Cambridge.

Richards, J.A., P.W. Woodgate, A.K. Skidmoore, 1987, An explanation of enhanced radar backscattering from flooded forests. International Journal of Remote Sensing, vol.8, no.7, pp.1093-1100.

Richards, J.A., 1990, Radar Backscatter Modeling of Forests: a Review of current Trends. International Journal of Remote Sensing, vol.11, pp.1299-1312.

Richardson, A.J., C.L. Wiegand, 1979, Distinguishing vegetation from soil background information. Photogrammetric Engineering and Remote Sensing, 43, pp.1541-1552.

Rooij, W.W.L. van, 1991, Radar in forestry - With an analysis of P-band polarimetric radar data of the Sprielder forest, Report September 1991, Wagenigen Agricultural University.

Rosema, A., J.J. Borgesius, H. Noorbergen and W. Verhoef, 1992, A New Forest Light Interaction Model in Support of Forest Monitoring. Remote Sensing of Environment, vol.42, pp.23-41.

Sader, S.A., 1987, Forest Biomass, Canopy Structure and Species Composition Relationships with Multipolarization L-band Synthetic Aperture Radar Data, Photogrammetric Engineering and Remote Sensing, vol.53, no.2, pp.193-202.

Sadowski, F.G., J.A. Sturdevant, W.H. Anderson, P.H. Seevers, J.W. Feuquay, L.K. Balick, F.A. Waltz and D.T. Lauer, 1985. Early Results of Investigations of Landsat 4 Thematic Mapper and Multiscanner Applications. In: Proceedings of Landsat-4 Science Characterization Early Results Symposium. February 22-24, 1983. Greenbelt, Maryland.

Sanden, J.J. v/d, 1988, Spectral Seperation of Coniferous Forest Species in Landsat-5 Thematic Mapper Data., Agricultural University Wageningen, The Netherlands.

SAS Institute Inc., 1989, SAS/STAT Users's Guide, Version 6, 4th ed., Cary, NC, 1673 pp.

Schardt, M. 1990, Verwendbarkeit von Thematic Mapper-Daten zur Klassifizierung von Baumarten und Natürlichen Altersklassen, Deutsche Forschungsanstalt für Luft- und Raumfahrt, Oberpfaffenhofen.

Skidmore, A.K., P.W. Woodgate and J.A. Richards, 1986, Classification of the Riverina Forests of south east Australia using co-registered Landsat MSS and SIR-B Radar Data. Symposium on Remote Sensing for Resources Developement and Environmental Management, Enschede.

Spanner, M.A., L.L. Pierce, D.L. Peterson and S.W. Running, 1990, Remote Sensing of Temperate Coniferous Forest Leaf Area Index; The Influence of Canopy Closure, Understory Vegetation and Background Reflectance., International Journal of Remote Sensing vol.11, no.1, pp.95-111.

Suits, G.H. 1972, The Calculation of Directional Reflectance of a Vegetation Canopy. Remote Sensing of Environment, vol.2, pp.117-126.

Swain, P.H. and S.M. Davis, Remote Sensing: The Quantitative Approach. New York: McGraw-Hill, 1978, p.386.

Thunnissen, H.A.M., M.N. Jaarsma and O.F. Schoumans, 1992, Landcover Inventory in the Netherlands using Remote Sensing: Application in a Soil and Groundwater Vulnerability Assessment System. International Journal of Remote Sensing, vol.13, no.9.

Tucker, C.L., 1978, A Comparison of Satellite Sensor Bands for Vegetation Monitoring, Photogrammetric Engineering and Remote Sensing, vol.44, no.11, pp. 1369-1380.

Tucker, C.J., 1979, Red and photographic infrared linear combination for monitoring vegetation. Remote Sensing of Environment, vol.8, pp.127-150.

Ulaby, F.T. and C Elachi (editors). Radar Polarimetry for Geoscience Applications. Artech House, Norwood, 1990.

Ulaby, F.T., D. Held, M.C. Dobson, M.C. McDonald and T.B.A. Senior, 1987. Relating Polarization Phase Difference of SAR Signals to Scene Properties. IEEE Transactions on Geosciense and Remote Sensing, vol.25, no.1 pp.83-92.

Ulaby, F.T., R.K. Moore and A.K. Fung, Microwave Remote Sensing: Active and Passive, vol II. New York: Addison-Wesley, 1984.

Ulaby, F.T., K. Sarabandi, K. McDonald, M. Whitt and M.C. Dobson ,M.C., 1990, Michigan Microwave Canopy Scattering Model. International Journal of Remote Sensing, vol.11, pp.1223-1253.

Verhoef, W., 1984, Light Scattering by Leaf Layers with Application to Canopy Reflectance Modeling: The SAIL Model. Remote Sensing of Environment., vol.16, 125-141.

Zoughi, R., L.K. Wu, R.K. and Moore, 1986, Identification of Major Backscattering Sources in Trees and Shrubs at 10 Ghz. Remote Sensing of Environment, vol.19, no.3, pp.269-290.

Zyl, J.J. van, 1989, Unsupervised classification of scattering behaviour using radar polarimetry data, IEEE Transactions on Geoscience and Remote Sensing, vol.27, no.1, pp.36-45.

Zyl, J.J. van, 1990, Calibration of Polarimetric Radar Images using only Image Parameters and Tihedral Corner Reflector Responses, IEEE Transactions on Geoscience and Remote Sensing, vol.28, no.3, pp.337-349.

Zyl, J.J. van, R. Corande, Y. Lou, T. Miller and K. Wheeler, 1992, The NASA/JPL three-frequency polarimetric AIRSAR system. Proceedings of IGARSS '92 Symposium, Houston, Texas, May 26-29, 1992, vol.I, pp.649-651.

Appendix I. Within forest class variances

OPTICAL DATA HORSTERWOLD									
VARIANCE									
	Acer ps.	Fagus	Fraxinus	Picea	Pinus n.	Populus	Quercus	Salix	
TMS1	0.98	0.92	0.82	0.43	0.71	2.28	4.53	1.75	
TMS2	1.67	1.44	1.19	0.77	2.22	3.52	6.86	2.33	
TMS3	3.58	1.11	1.81	2.42	2.20	5.96	11.30	2.35	
TMS4	4.06	0.85	1.57	2.64	3.46	5.25	10.20	1.86	
TMS5	2.05	0.26	0.67	1.05	1.89	2.75	4.49	0.95	
TMS6	7.97	7.18	20.13	8.71	6.31	26.97	44.60	26.13	
TMS7	22.97	20.06	54.30	22.94	17.05	52.75	115.33	72.74	
TMS8	16.19	15.62	41.58	16.51	13.32	42.92	82.51	59.44	
TMS9	3.28	3.07	11.16	2.49	4.00	20.16	7.06	15.23	
TMS10	1.01	0.38	0.90	0.71	1.92	3.62	2.34	1.28	
TMS11	0.83	0.03	0.06	0.67	0.84	1.17	4.14	0.26	
TMS12	3.49	0.16	0.28	2.94	3.55	4.92	17.79	1.34	
OPTICAL DATA SPEULDERBOS									
VARIANCE									
	Fagus	Pseudots.	Pinus sy.	Quercus	Larix k.				
TMS 1	0.15	0.42	0.63	0.74	0.41				
TMS 2	0.59	0.51	1.47	1.17	0.67				
TMS 3	0.77	1.25	1.50	1.17	0.78				
TMS 4	0.52	0.81	1.79	1.27	0.61				
TMS 5	0.26	0.46	0.87	0.58	0.23				
TMS 6	4.59	35.56	10.27	3.82	3.01				
TMS 7	20.57	83.53	25.93	8.24	5.34				
TMS 8	20.43	73.12	25.05	8.84	4.04				
TMS 9	2.24	11.49	16.07	6.67	1.30				
TMS 10	0.27	1.05	3.08	1.12	0.24				
TMS 11	0.30	1.01	1.75	0.55	0.13				
TMS 12	1.27	4.07	7.59	2.29	0.55				
RADAR DATA HORSTERWOLD									
VARIANCE									
	Acer ps.	Fagus	Fraxinus	Picea	Pinus n.	Populus	Quercus	Salix	
C-HH	0.67	0.11	0.36	0.17	0.13	0.58	0.49	0.16	
C-HV	0.43	0.13	0.09	0.19	0.07	0.48	0.54	0.22	
C-VV	0.67	0.17	0.33	0.65	0.15	0.56	1.07	0.33	
L-HH	2.30	0.21	1.39	0.08	0.23	2.01	3.35	0.26	
L-HV	2.40	0.09	1.26	0.61	0.21	3.21	5.79	0.20	
L-VV	2.88	0.22	1.64	0.44	0.13	2.52	6.45	0.19	
P-HH	2.13	0.66	5.75	4.71	0.10	5.23	11.53	2.38	
P-HV	1.15	0.59	4.86	2.41	0.47	4.30	5.70	1.24	
P-VV	4.73	1.19	3.71	1.75	0.20	3.63	8.50	3.00	
RADAR DATA SPEULDERBOS									
VARIANCE									
	Fagus	Pseudots.	Pinus sy.	Quercus	Larix k.				
C-HH	2.53	0.24	0.16	0.11	0.05				
C-HV	3.40	0.30	0.19	0.08	0.08				
C-VV	2.56	0.16	0.31	0.11	0.13				
L-HH	0.18	0.12	0.17	0.24	0.08				
L-HV	0.08	0.36	0.30	0.16	0.28				
L-VV	0.10	0.23	0.35	0.18	0.36				
P-HH	1.27	0.56	0.22	0.53	0.55				
P-HV	0.25	1.33	0.28	0.17	0.15				
P-VV	0.09	0.41	0.51	0.25	0.77				

Appendix II. Pooled within canonical structure

SPEULDERBOS

OPTICAL

Pooled Within Canonical Structure

	CAN1	CAN2	CAN3	CAN4
TMS1	0.1689	0.0174	-0.097	0.158
TMS2	0.0368	0.0821	0.0169	0.2088
TMS3	0.0734	-0.061	0.0138	0.3353
TMS4	-0.002	0.1284	0.0724	0.378
TMS5	0.0688	0.1217	-0.085	0.3435
TMS6	0.5066	-0.404	-0.17	-0.141
TMS7	0.5732	-0.407	-0.136	-0.243
TMS8	0.5866	-0.376	-0.136	-0.229
TMS9	0.5999	0.031	-0.108	0.0523
TMS10	0.3716	0.2978	-0.099	0.2986
TMS11	-0.147	0.124	0.0024	0.0604
TMS12	-0.144	0.1187	-0.002	0.0886

RADAR

Pooled Within Canonical Structure

	CAN1	CAN2	CAN3	CAN4
C-hh	0.2756	0.1156	-0.362	-0.098
C-hv	0.2701	-0.006	-0.271	0.1492
C-vv	0.1441	0.142	-0.208	0.1983
L-hh	0.4673	0.1435	0.5863	-0.417
L-hv	0.0914	-0.203	0.5344	-0.448
L-vv	-0.188	-0.363	0.5002	-0.452
P-hh	0.2528	0.4423	0.2925	-0.251
P-hv	-0.117	0.0928	0.7772	-0.077
P-vv	-0.219	0.3583	0.4013	-0.475

COMBINATION

Pooled Within Canonical Structure

	CAN1	CAN2	CAN3	CAN4
TMS1	0.1081	0.0242	0.0154	0.1016
TMS2	0.0206	0.0641	0.0346	0.0698
TMS3	0.0408	-0.004	0.0234	0.1977
TMS4	-0.008	0.1052	0.0546	0.1198
TMS5	0.0446	0.1049	-0.005	0.1153
TMS6	0.3202	-0.252	0.0497	0.2314
TMS7	0.3609	-0.269	0.0969	0.2057
TMS8	0.3693	-0.251	0.107	0.2024
TMS9	0.3771	0.0021	0.1889	0.1599
TMS10	0.2351	0.1858	0.1394	0.0973
TMS11	-0.091	0.0819	-0.04	-0.064
TMS12	-0.089	0.0819	-0.043	-0.049
C-hh	-0.194	-0.072	0.036	0.1722
C-hv	-0.179	0	0.1407	0.1781
C-vv	-0.097	-0.099	0.1011	0.0959
L-hh	-0.325	0.0132	0.077	-0.408
L-hv	-0.064	0.1919	-0.064	-0.281
L-vv	0.1276	0.2638	-0.168	-0.218
P-hh	-0.186	-0.218	0.0015	-0.324
P-hv	0.0798	-0.004	-0.016	-0.489
P-vv	0.1285	-0.188	-0.255	-0.391

HORSTERWOLD

OPTICAL

Pooled Within Canonical Structure

	CAN1	CAN2	CAN3	CAN4
TMS1	0.0774	-0.0175	-0.0517	0.0161
TMS2	0.0054	-0.0502	0.0164	0.0299
TMS3	0.0122	-0.0518	-0.129	0.0657
TMS4	-0.019	-0.0411	-0.0071	0.0154
TMS5	0.0231	-0.0385	-0.0235	0.0315
TMS6	0.3507	-0.0221	-0.5118	-0.018
TMS7	0.4606	0.0445	-0.5448	-0.12
TMS8	0.4925	0.0359	-0.5245	-0.111
TMS9	0.4736	0.1097	-0.1196	0.2317
TMS10	0.2725	0.0865	0.0109	0.1914
TMS11	-0.102	0.3807	0.0675	0.2363
TMS12	-0.099	0.3853	0.0632	0.2487

RADAR

Pooled Within Canonical Structure

	CAN1	CAN2	CAN3	CAN4
C-hh	0.421	0.2595	-0.1351	0.1741
C-hv	0.3375	0.5453	0.0415	-0.009
C-vv	0.3737	0.2014	-0.1434	0.2651
L-hh	-0.25	0.3293	-0.0723	0.3173
L-hv	-0.177	0.2955	-0.0856	-0.022
L-vv	-0.142	0.1448	0.1035	0.0276
P-hh	-0.124	0.3519	0.2132	0.3565
P-hv	-0.161	0.1537	-0.023	0.0879
P-vv	-0.062	0.1404	0.2476	0.3402

COMBINATION

Pooled Within Canonical Structure

	CAN1	CAN2	CAN3	CAN4
TMS1	0.0585	0.0261	0.0085	0.03
TMS2	0.0056	-0.0015	-0.0119	-0.024
TMS3	0.0206	-0.0335	-0.0148	0.0296
TMS4	-0.01	-0.0183	-0.0107	-0.025
TMS5	0.0199	0.0036	-0.0133	-0.002
TMS6	0.2894	0.0432	0.0273	0.2705
TMS7	0.3676	0.0945	0.0883	0.3207
TMS8	0.3896	0.115	0.0908	0.3022
TMS9	0.3291	0.257	0.0983	0.1938
TMS10	0.1787	0.1805	0.0757	0.0728
TMS11	-0.118	0.0617	0.1533	0.1713
TMS12	-0.116	0.0631	0.1521	0.1833
C-hh	0.179	-0.3738	0.1944	-0.066
C-hv	0.1055	-0.346	0.4545	-0.173
C-vv	0.1634	-0.3314	0.1434	-0.031
L-hh	-0.19	0.0667	0.1919	-0.081
L-hv	-0.129	0.0582	0.181	-0.215
L-vv	-0.083	0.095	0.1438	-0.037
P-hh	-0.127	-0.0069	0.2946	0.0715
P-hv	-0.096	0.091	0.1081	-0.103
P-vv	-0.038	0.0489	0.2031	0.153

Appendix III. Confusion matrix STEPDISC for the Speulderbos

CONFUSION MATRIX SPEULDERBOS

optical Percentage classified into SOORT

From SOORT	Fagus sy	Pseudos	Pinus syl	Quercus	Larix kae	Total
Fagus sylvatica	100	0	0	0	0	100
Pseudostuga menz.	0	80	20	0	0	100
Pinus sylvestris	0	10	75	0	15	100
Quercus robur	9.09	0	0	90.91	0	100
Larix kaempheri	0	0	0	0	100	100

radar Percentage classified into SOORT

From SOORT	Fagus sy	Pseudos	Pinus syl	Quercus	Larix kae	Total
Fagus sylvatica	100	0	0	0	0	100
Pseudostuga menz.	0	80	10	0	10	100
Pinus sylvestris	0	10	85	0	5	100
Quercus robur	0	0	0	100	0	100
Larix kaempheri	0	20	10	0	70	100

combination Percentage classified into SOORT

From SOORT	Fagus sy	Pseudos	Pinus syl	Quercus	Larix kae	Total
Fagus sylvatica	100	0	0	0	0	100
Pseudostuga menz.	0	70	0	0	30	100
Pinus sylvestris	0	0	85	10	5	100
Quercus robur	9.09	0	0	90.91	0	100
Larix kaempheri	0	0	0	0	100	100

Appendix IV. Confusion matrix STEPDISC for the Horsterwold

CONFUSION MATRIX HORSTERWOLD

optical Percentage classified into SOORT

From SOORT	Acer p	Fagus	Fraxinu	Picea a	Pinus n	Sec. Ai	Sec. Ai	Sec. Tc	Quercu	Salix tir	Total
Acer pseudoplatanus	80	0	10	0	0	0	0	0	10	0	100
Fagus sylvatica	0	100	0	0	0	0	0	0	0	0	100
Fraxinus exelsior	10	0	60	0	0	0	0	20	10	0	100
Picea abies	0	0	0	90.91	9.09	0	0	0	0	0	100
Pinus n.n.	0	0	0	0	100	0	0	0	0	0	100
Sec. Aigeiros	0	0	3.03	0	0	71.21	6.06	16.67	3.03	0	100
Sec. AigXTac.	3.7	0	0	0	0	3.7	55.56	14.81	3.7	18.52	100
Sec. Tac.	0	0	5.26	0	0	31.58	21.05	26.32	5.26	10.53	100
Quercus robur	36.36	0	27.27	0	0	0	0	0	27.27	9.09	100
Salix tinaarloo	10	0	0	0	0	0	30	20	10	30	100

radar Percentage classified into SOORT

From SOORT	Acer p	Fagus	Fraxinu	Picea a	Pinus n	Sec. Ai	Sec. Ai	Sec. Tc	Quercu	Salix tir	Total
Acer pseudoplatanus	60	0	10	0	0	10	0	0	20	0	100
Fagus sylvatica	0	90	0	0	0	0	0	0	0	10	100
Fraxinus exelsior	20	0	60	0	0	10	0	0	10	0	100
Picea abies	0	0	0	100	0	0	0	0	0	0	100
Pinus n.n.	0	0	0	0	100	0	0	0	0	0	100
Sec. Aigeiros	6.06	3.03	15.15	3.03	0	40.91	1.52	6.06	3.03	21.21	100
Sec. AigXTac.	11.11	0	3.7	3.7	0	0	51.85	11.11	18.52	0	100
Sec. Tac.	5.26	0	0	0	0	10.53	21.05	63.16	0	0	100
Quercus robur	9.09	27.27	9.09	0	0	0	9.09	0	45.45	0	100
Salix tinaarloo	10	20	0	0	0	10	0	0	0	60	100

combination Percentage classified into SOORT

From SOORT	Acer p	Fagus	Fraxinu	Picea a	Pinus n	Sec. Ai	Sec. Ai	Sec. Tc	Quercu	Salix tir	Total
Acer pseudoplatanus	90	0	0	0	0	0	0	0	0	10	100
Fagus sylvatica	0	100	0	0	0	0	0	0	0	0	100
Fraxinus exelsior	0	0	60	0	0	0	0	0	30	10	100
Picea abies	0	0	0	100	0	0	0	0	0	0	100
Pinus n.n.	0	0	0	0	100	0	0	0	0	0	100
Sec. Aigeiros	0	0	4.55	0	0	53.03	3.03	7.58	0	31.82	100
Sec. AigXTac.	0	0	0	0	0	3.7	62.96	22.22	7.41	3.7	100
Sec. Tac.	0	0	5.26	0	0	10.53	31.58	52.63	0	0	100
Quercus robur	27.27	0	27.27	0	0	0	9.09	0	36.36	0	100
Salix tinaarloo	10	0	0	0	0	30	10	0	0	50	100

Appendix V. Confusion matrix CANDISC for the Speulderbos

CONFUSION MATRIX SPEULDERBOS

optical Percentage classified into SOORT

From SOORT	Fagus sy	Pseudos	Pinus syl	Quercus	Larix kae	Total
Fagus sylvatica	100	0	0	0	0	100
Pseudostuga menz.	0	80	20	0	0	100
Pinus sylvestris	0	0	95	0	5	100
Quercus robur	9.09	0	0	90.91	0	100
Larix kaempheri	0	0	0	0	100	100

radar Percentage classified into SOORT

From SOORT	Fagus sy	Pseudos	Pinus syl	Quercus	Larix kae	Total
Fagus sylvatica	100	0	0	0	0	100
Pseudostuga menz.	0	100	0	0	0	100
Pinus sylvestris	0	0	90	5	5	100
Quercus robur	0	0	0	100	0	100
Larix kaempheri	0	10	0	0	90	100

combination Percentage classified into SOORT

From SOORT	Fagus sy	Pseudos	Pinus syl	Quercus	Larix kae	Total
Fagus sylvatica	100	0	0	0	0	100
Pseudostuga menz.	0	100	0	0	0	100
Pinus sylvestris	0	0	100	0	0	100
Quercus robur	0	0	0	100	0	100
Larix kaempheri	0	10	0	0	100	100

Appendix VI. Confusion matrix CANDISC for the Horsterwold

CONFUSION MATRIX HORSTERWOLD

optical Percentage classified into SOORT

From SOORT	Acer p	Fagus	Fraxinu	Picea a	Pinus n	Sec. Ai	Sec. Ai	Sec. Tc	Quercu	Salix tir	Total
Acer pseudoplatanus	80	0	20	0	0	0	0	0	0	0	100
Fagus sylvatica	0	100	0	0	0	0	0	0	0	0	100
Fraxinus exelsior	20	0	40	0	0	10	0	10	20	0	100
Picea abies	0	0	0	90.91	9.09	0	0	0	0	0	100
Pinus n.n.	0	0	0	0	100	0	0	0	0	0	100
Sec. Aigeiros	0	0	1.52	0	0	66.67	4.55	19.7	0	7.58	100
Sec. AigXTac.	0	0	3.7	0	0	0	59.26	14.81	0	22.22	100
Sec. Tac.	0	0	10.53	0	0	21.05	36.84	15.79	0	15.79	100
Quercus robur	9.09	0	27.27	0	0	0	0	0	63.64	0	100
Salix tinaarloo	10	0	0	0	0	10	10	0	0	70	100

rador Percentage classified into SOORT

From SOORT	Acer p	Fagus	Fraxinu	Picea a	Pinus n	Sec. Ai	Sec. Ai	Sec. Tc	Quercu	Salix tir	Total
Acer pseudoplatanus	60	0	40	0	0	0	0	0	0	0	100
Fagus sylvatica	0	80	0	0	0	0	0	0	0	20	100
Fraxinus exelsior	20	0	80	0	0	0	0	0	0	0	100
Picea abies	0	0	0	100	0	0	0	0	0	0	100
Pinus n.n.	0	0	0	0	100	0	0	0	0	0	100
Sec. Aigeiros	0	1.52	3.03	0	0	78.79	0	1.52	9.09	6.06	100
Sec. AigXTac.	0	0	0	0	0	7.41	59.26	14.81	18.52	0	100
Sec. Tac.	0	5.26	0	0	0	10.53	10.53	73.68	0	0	100
Quercus robur	0	0	0	0	0	9.09	18.18	9.09	63.64	0	100
Salix tinaarloo	0	30	0	0	0	0	0	0	0	70	100

combination Percentage classified into SOORT

From SOORT	Acer p	Fagus	Fraxinu	Picea a	Pinus n	Sec. Ai	Sec. Ai	Sec. Tc	Quercu	Salix tir	Total
Acer pseudoplatanus	80	0	20	0	0	0	0	0	0	0	100
Fagus sylvatica	0	100	0	0	0	0	0	0	0	0	100
Fraxinus exelsior	30	0	70	0	0	0	0	0	0	0	100
Picea abies	0	0	0	100	0	0	0	0	0	0	100
Pinus n.n.	0	0	0	0	100	0	0	0	0	0	100
Sec. Aigeiros	0	0	0	0	0	86.36	1.52	7.58	0	4.55	100
Sec. AigXTac.	0	0	0	0	0	0	70.37	22.22	0	7.41	100
Sec. Tac.	0	0	0	0	0	10.53	15.79	68.42	0	5.26	100
Quercus robur	18.18	0	0	0	0	0	9.09	0	72.73	0	100
Salix tinaarloo	0	0	0	0	0	10	0	0	10	80	100

Appendix VII. Figures with simulated and measured σ°(dB) values as a function of incidence angle for 18, 12 and 9 years old Populus 'Robusta'.

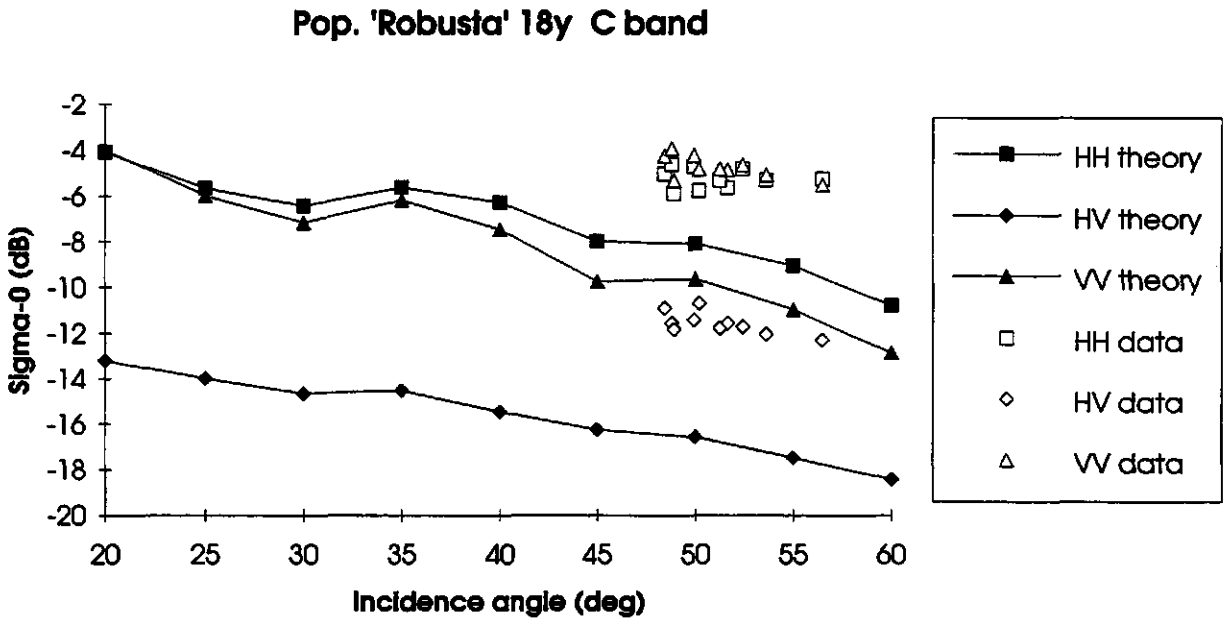

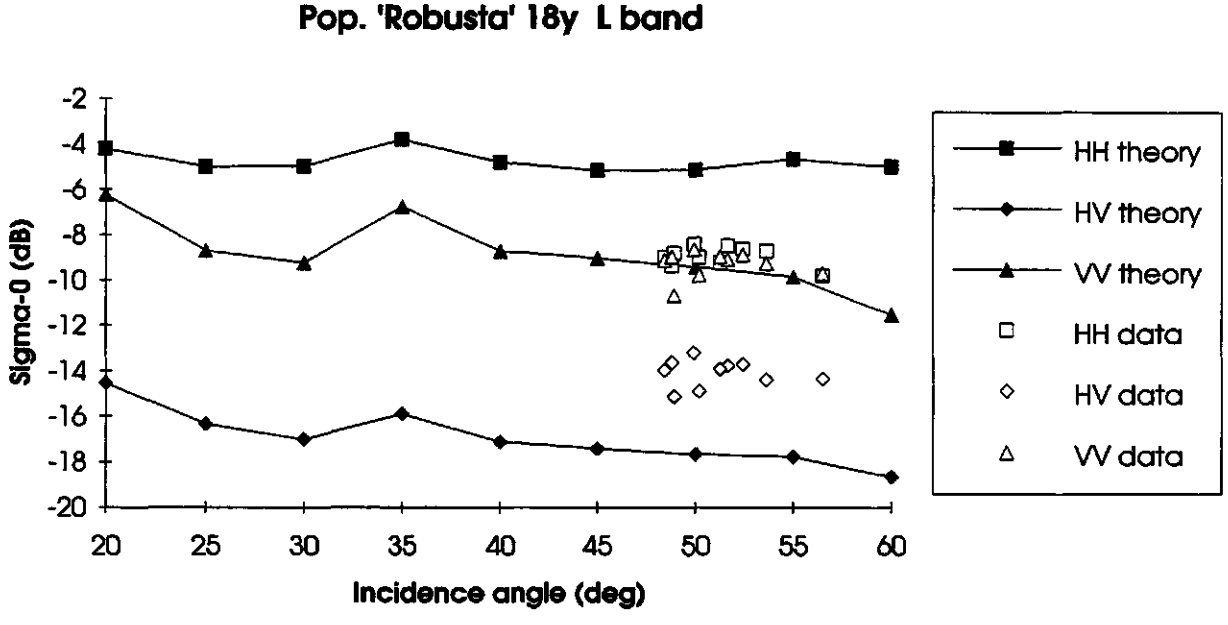

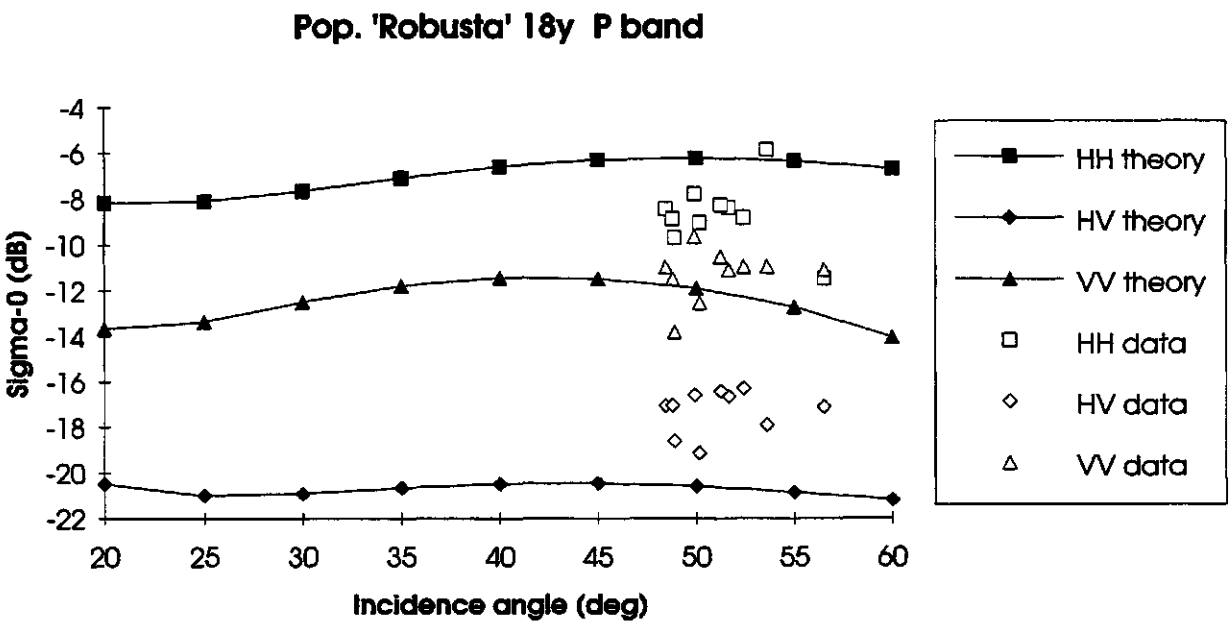
Pop. 'Robusta' 18y P band
Sigma-0 (dB)
-4
-6
-8
-10
-12
-14
-16
-18
-20
-22
20
25
30
35
40
45
50
55
60
Incidence angle (deg)
HH theory
HV theory
VV theory
HH data
HV data
VV data

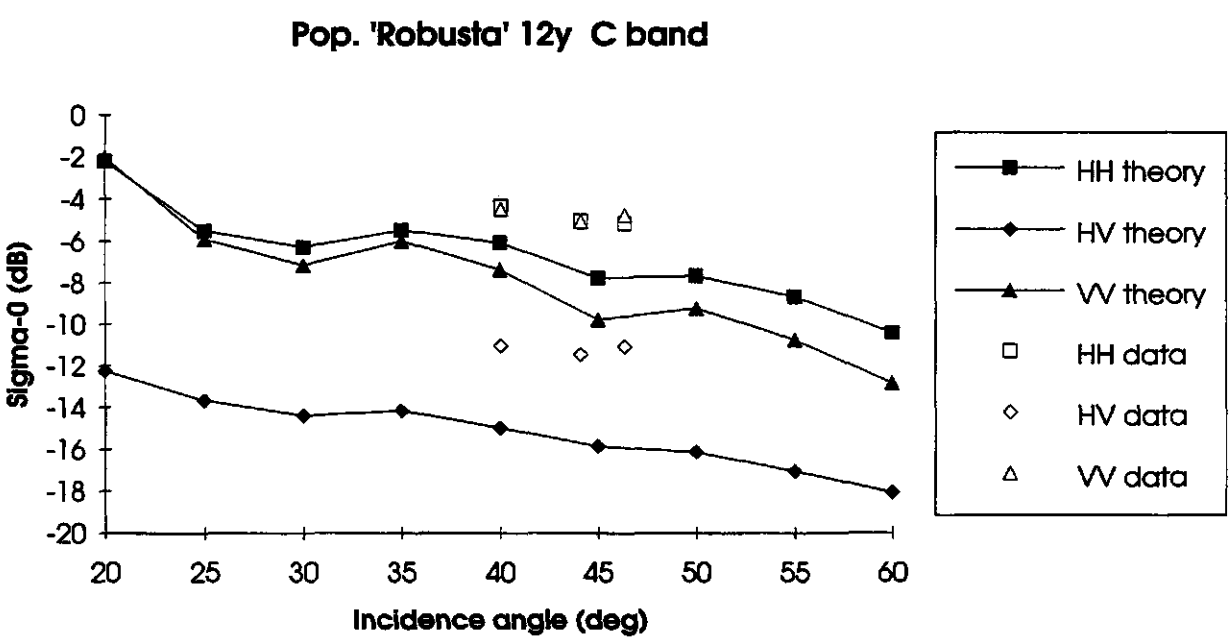
Pop. 'Robusta' 12y C band
Sigma-0 (dB)
0
-2
-4
-6
-8
-10
-12
-14
-16
-18
-20
20
25
30
35
40
45
50
55
60
Incidence angle (deg)
HH theory
HV theory
VV theory
HH data
HV data
VV data

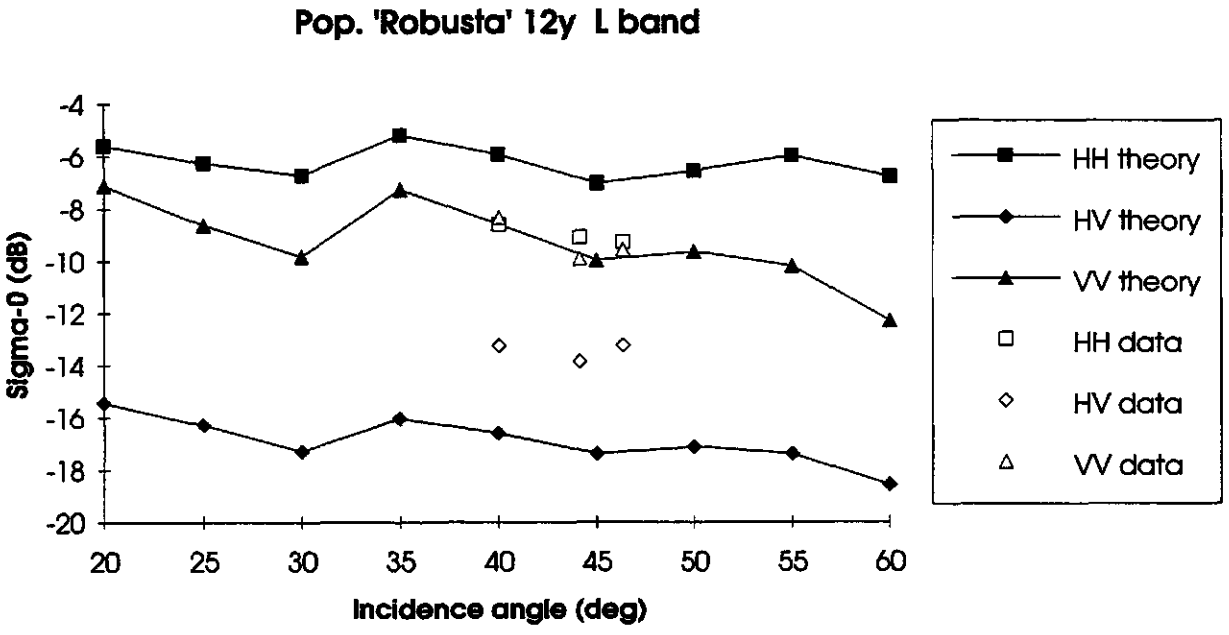
Pop. 'Robusta' 12y L band
Sigma-0 (dB)
-4
-6
-8
-10
-12
-14
-16
-18
-20
20
25
30
35
40
45
50
55
60
Incidence angle (deg)
HH theory
HV theory
VV theory
HH data
HV data
VV data

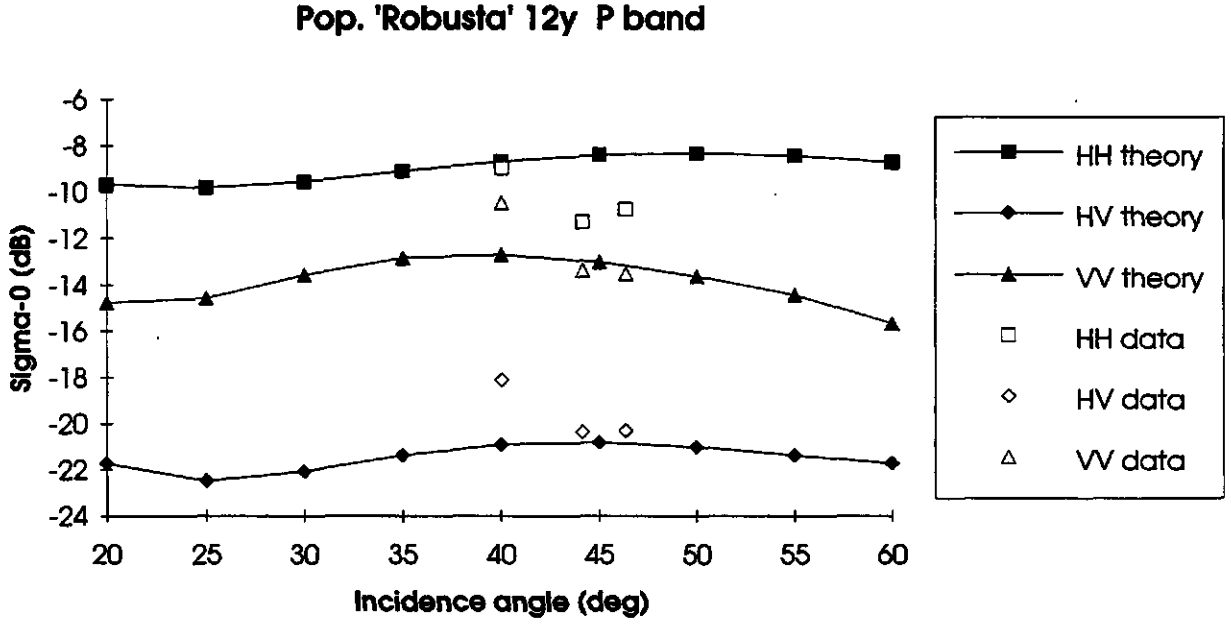
Pop. 'Robusta' 12y P band
Sigma-0 (dB)
-6
-8
-10
-12
-14
-16
-18
-20
-22
-24
20
25
30
35
40
45
50
55
60
Incidence angle (deg)
HH theory
HV theory
VV theory
HH data
HV data
VV data

Pop. 'Robusta' 9y C band

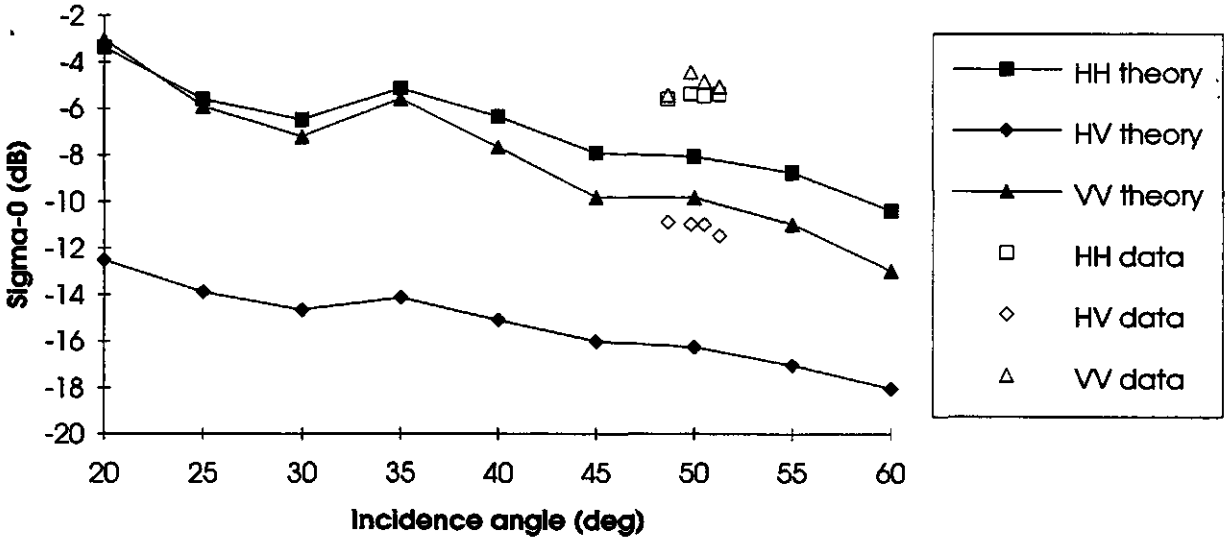

Pop. 'Robusta' 9y L band

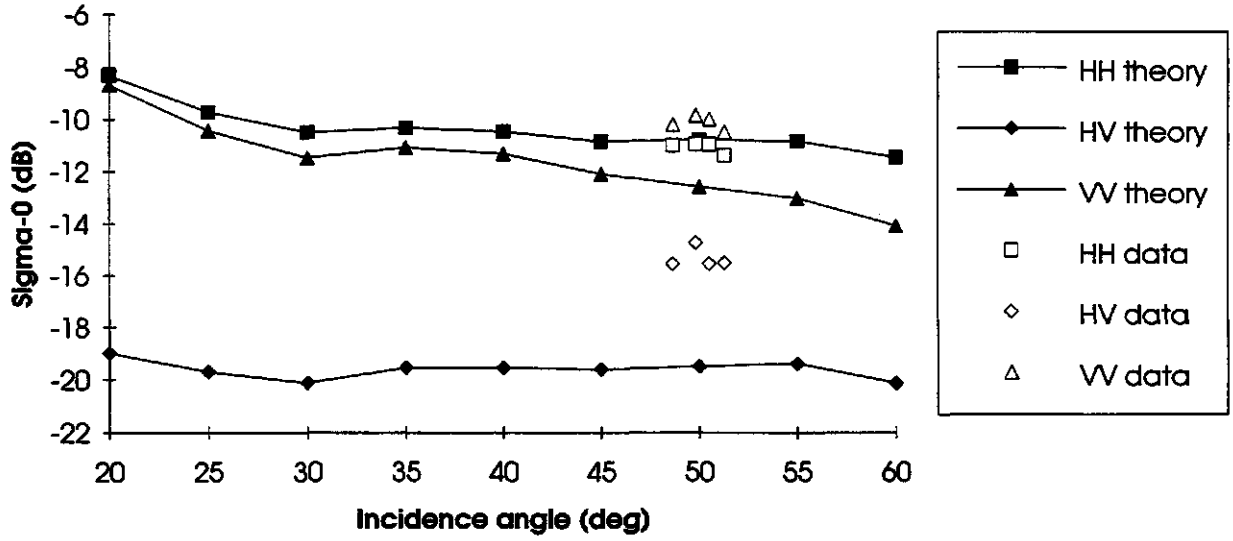

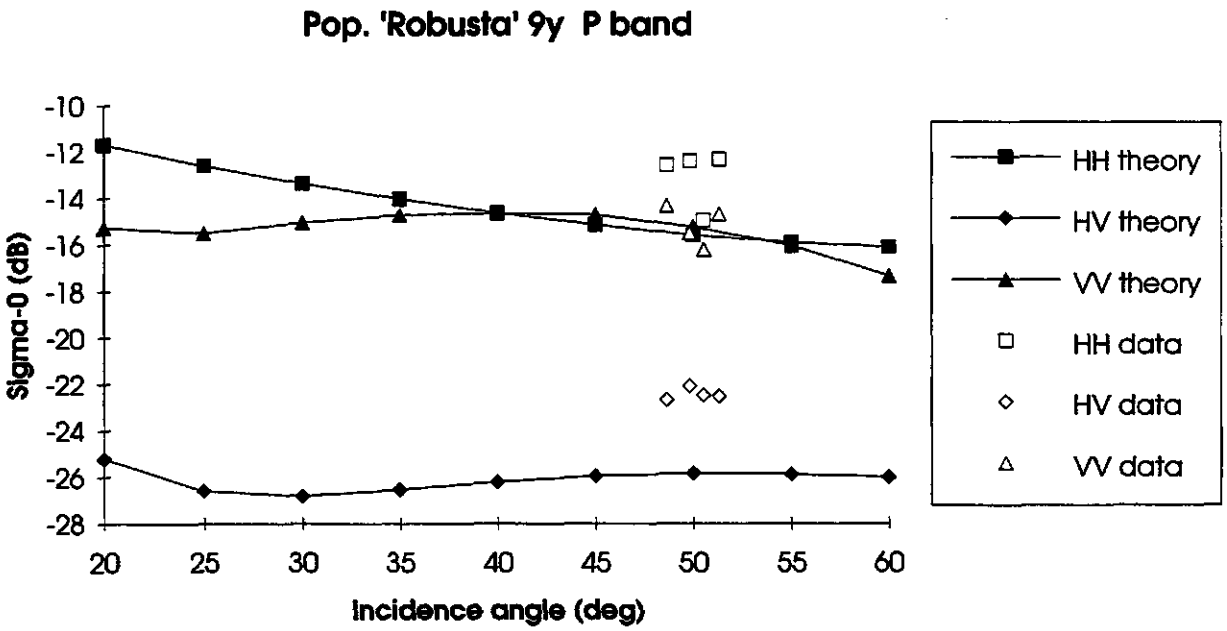
Pop. 'Robusta' 9y P band
Sigma-0 (dB)
-10
-12
-14
-16
-18
-20
-22
-24
-26
-28
20
25
30
35
40
45
50
55
60
Incidence angle (deg)
HH theory
HV theory
VV theory
HH data
HV data
VV data

NAAMSWIJZIGING

Met ingang van 28 januari 1992 is de naam van de vakgroep Hydrologie, Bodemnatuurkunde en Hydraulica gewijzigd in Waterhuishouding.

Inlichtingen zijn verkrijgbaar bij het secretariaat van de vakgroep:
telefoon : 08370 - 82293/82778
telefax : 08370 - 84885
Vakgroep Waterhuishouding
Landbouwuniversiteit
Nieuwe Kanaal 11
6709 PA Wageningen

For further information please contact the secretariat of the department:
telephone : 31 - 8370 - 82293/82778
telefax : 31 - 8370 - 84885
Department of Water Resources
Agricultural University
Nieuwe Kanaal 11
6709 PA Wageningen
The Netherlands

OVERZICHT VERSCHENEN RAPPORTEN

Nr	Auteur(s) + titel	Prijs (Hfl)
1.	Promes, P.M. 1990. De problematiek van de koppeling van grondwatermodellen en openwatermodellen.	*
2.	Kors, A.G. en P.M. Promes, 1990. Gebruikershandleiding voor het openwatermodel LYMPHA.	*
3.	Dommerholt, A. en P.M.M. Warmerdam (redaktie), 1990. Verslag van de buitenlandse excursie naar Münsterland, het Ruhrgebied en de Eifel. 4 t/m 7 september 1989.	*f* 14,00
4.	Simunek, J. 1990. Analysis of soil survey data of the Hupselse Beek.	*f* 14,00
5.	Dirksen, C. 1990. Unsaturated hydraulic conductivity.	*f* 19,50
6.	Boiten, W. 1990. Afvoerrelatie V-vormige vistrap.	*
7.	Dam, J.C. van, J.N.M. Stricker en P. Droogers, 1990. From one-step to multi-step. Determination of soil hydraulic functions by outflow experiments.	*f* 21,00
8.	Boiten, W. 1990. Advies debietmeetstation Oude Diep te Echten.	*
9.	Promes, P.M. 1990. De koppeling van het grondwatermodel GELDYM-MUST en het openwatermodel LYMPHA. Model TRIGON.	*
10.	Amerongen, F. van, R. Dijksma en J.M. Schouwenaars, 1990. Hydrologisch onderzoek in het hoogveengebied De Engbertsdijksvenen. (Verslag van de belangrijkste resultaten en verzamelde gegevens in de periode 1987-1989).	*f* 24,50
11.	Moene, A.F. 1990. The addition of retention data derived from pedotransfer functions in one-step outflow optimization.	*f* 21,00

* Voor inlichtingen over dit rapport dient u zich te wenden tot de opdrachtgever.

Nr	Auteur(s) + titel	Prijs (Hfl)
12.	Boiten, W., 1991. Afvoeren Nieuwe Ley te Goirle.	*
13.	Schaaf, S. van der en C.J. de Vries, 1991. Integraal waterbeheer Ede. Deelrapport ontwatering.	*
14.	Boiten, W., 1991. Meetadvies afvoerbepaling via twee suatiesluizen.	*
15.	Schaaf, S. van der, 1991. Gevolgen van de aanleg van de rondweg S-25 bij Veenendaal en daarmee verband houdende ingrepen voor de waterhuishouding van Hel en Blauwe Hel.	*
16.	Verhoef, A. en R.A. Feddes, 1991. Preliminary review of revised FAO radiation and temperature methods.	f 24,50
17.	Voet, P. van der en J.P.M. Witte, 1991. Redesign DEMGEN: Hydrologische schematisering van PAWN-district 29 (Noordwest Veluwe) met een geografisch informatiesysteem. Een haalbaarheidsonderzoek.	*
18.	Boiten, W., A. Dommerholt en L.J.J. Dijkhuis, 1991. Hydrologisch meetplan waterschap Lits en Lauwers.	*
19.	Bier, G., D. van der Hoek, S. van der Schaaf (red.) en T.J. Spek, 1992. Kwel en natuurontwikkeling in het Binnenveld tussen de Neder-Rijn en Veenendaal. Deel 1: Tekst, Deel 2: Bijlagen.	f 50,00
20.	Uijlenhoet, R., 1992. A simple surface radiation budget model for a point in snow covered mountainous terrain.	f 31,00
21.	Brorens, B.A.H.V., 1992. Water resource system training model "WATSYS". User's manual.	f 21,00
22.	Vries, C.J. de, 1992. Hydrologische gegevensbestanden in de Gelderse Vallei, het Binnenveld en het proefgebied de Veenkampen. Gegevens voor het modelleren van proefgebied de Veenkampen met het niet-stationaire grondwaterstromingsmodel SIMGRO.	f 16,50
23.	Vries, C.J. de, 1992. Stedelijk grondwaterbeheer. Het optimaliseren van het grondwater-meetnet van de gemeente Ede.	*
24.	Vermulst, J.A.P.H., 1992. Redesign DEMGEN: Een voorstel tot groepering van grondwatertrappen.	*
25.	Vermulst, J.A.P.H., 1992. Redesign DEMGEN: Toetsing van de hydrologische schematisatie op afvoeren van de Schuitebeek.	*
26.	Stricker, J.N.M. (editor), 1992. Urban/rural application of weather radar for flow forecasting. Proceedings of the informal CEC-workshop in Wageningen, december 1990.	f 25,00
27.	Boiten, W., 1992. Northern Tunisia Water Resource Management Project. Report of a preappraisal mission for the World Bank, april 26 - may 4, 1992.	*
28.	Dommerholt, A. en P.M.M. Warmerdam (redaktie), 1992. Verslag van de buitenlandse excursie naar het Ruhrgebied en de Harz. 18 tot en met 22 mei 1992.	f -,-
29.	Dommerholt, A., 1992. Afwijkingen in gemeten waterstanden. Waterstandsmetingen met peilbuis en intake pipe.	f 13,50
30.	Boiten, W., 1992. Vertical gates for distribution of irrigation water.	f 10,00
31.	Vissers, M.A.M. en J.J. van der Sanden, 1992. Groundtruth collection for the JPL-SAR and ERS-1 campaign in Flevoland and the Veluwe (NL) 1991.	*

Nr	Auteur(s) + titel	Prijs (Hfl)
32.	Ignar, S. en J.J. Bogardi, 1993. Rainfall-runoff model for design flood computation with variable parameters.	*f* 10,50
33.	Maren, G. van en C. Varekamp, 1993. Combining optical and microwave remote sensing data of forest vegetation. MAC Europe 1991.	*f* 25,00


PAPIER MET
MILIEUKEURMERK